Value-added Bioproducts Development from Lignocellulosic Biomass

by

Mi Li

A dissertation submitted to the Graduate Faculty of
Auburn University
in partial fulfillment of the
requirements for the Degree of
Doctor of Philosophy

Auburn, Alabama
December 13, 2014

Keywords: Lignocellulosic biomass, enzymatic hydrolysis,
lactic acid, gluconic acid, cellulose nanocrystals

Approved by

Maobing Tu, Chair, Associate Professor of Forestry
Yoon Y. Lee, Uthlaut Family Professor of Chemical Engineering
Steven E. Taylor, Professor of Biosystems Engineering
Oladiran Fasina, Professor of Biosystems Engineering
Xinyu Zhang, Associate Professor of Polymer and Fiber Engineering

Abstract

Alternative fuels and chemicals from renewable biomass can be used to reduce U.S. dependence on foreign oil, increase national energy security, and address environmental challenges. While renewable biomass can be used for the production of biofuels and value-added bioproducts, the key impediment to commercialization is the lack of a cost-effective process for converting biomass into biofuels. Therefore, development of value-added bioproducts from lignocellulosic biomass is critically needed for biofuels development. The production of lactic acid and acrylic acid from biomass hemicellulose can generate extra revenue for the biorefinery process, which can grow the bio-based industries potentially and make the biofuels production economically viable.

Pretreatment is required to disrupt the cellulose-lignin matrix in lignocellulose and enhance the accessibility to digestive enzymes, but residual lignin and xylan may decrease the efficiency of enzymatic hydrolysis. However, the interactions between lignin/xylan and cellulolytic enzymes are not very well understood. My initial work was therefore concerned with quantifying and correlating the residual lignin/xylan content with enzymatic hydrolysis rates and yields. It was found that a higher residual xylan (9.7%) in organosolv pretreated Sweetgum (OPSG) resulted in a slower initial hydrolysis rate (1.19 g/L/h), and a higher amount of residual lignin (18.6%) in organosolv pretreated Loblolly Pine (OPLP) resulted in a lower final hydrolysis yield of glucan (76.4%). A more accurate fundamental understanding of the roles of xylan and lignin in limiting the enzymatic hydrolysis has been developed showing that the initial

hydrolysis rate is dominated by the xylan content whereas the final hydrolysis yield is controlled by lignin content.

The catalytic conversion of hemicellulose sugars to lactic acid under alkaline conditions was investigated. It was observed that the kinetics of sugars degradation under aqueous alkaline condition followed a pseudo-first-order reaction based on the overall interconverted isomers. The yields of lactic acid from each sugar in 0.5 M NaOH at 60 ℃ were 55% (fructose), 46% (glucose), 38% (mannose), and 35% (xylose). Meanwhile, we found that $Ba(OH)_2$ significantly increased the yield of lactic acid from xylose from 33 to 46%. In addition, the production of gluconic acid and xylonic acid was studied by microbial fermentation with *Gluconobacter oxydans* ATCC621. The presence of xylonic acid resulted in strong inhibition of glucose and xylose fermentation, which can be alleviated by addition of $CaCO_3$.

Finally, cellulose nanocrystals (CNCs) were prepared from sulfuric acid (H_2SO_4) and hydrochloric acid (HCl) hydrolysis of Avicel and filter paper and characterized for the development of potential piezoelectric materials. The H_2SO_4 treated CNCs (H_2SO_4-CNCs) and HCl treated CNCs (HCl-CNCs) were characterized and compared based on their morphology, thermo-stability, and surface charge. The H_2SO_4-CNCs isolated from Avicel and filter paper resulted in a different lytropic phase behavior indicated by their birefringence patterns. Time domain NMR was used to analyze the interaction of water molecules with CNCs. Three locations of water molecules were identified in the CNCs. In addition, the CNCs with negatively charged groups strongly impeded the enzymatic hydrolysis. Finally, chemical modifications with acetic anhydride (Ac_2O) and polyisobutylene succinic anhydride (PIBSA) were carried out to improve the dispersibility and compatibility of CNCs.

Acknowledgments

Special thanks to my advisor, Dr. Maobing Tu, for his guidance and mentorship in my research in the past four years. Dr. Tu has expanded my scientific thinking dramatically and challenged me consistently and intellectually on my research work. He helped me develop some important transferrable skills in my study such as critical thinking, hypothesis development, detail-oriented observation, data analysis, report writing, and effective presentation. His strong support, encouragement, and passion has shaped my future career as an independent scientist. I am also grateful to my committee members, Dr. Steven Taylor, Dr. Yoon Lee, Dr. Oladiran Fasina, and Dr. Xinyu Zhang for strengthening my background in Chemistry, Chemical Engineering, Polymer Science, and Biorefinery Technology. Their support and suggestions have improved my research work and enhanced my confidence significantly. I would have never been able to finish my projects and dissertation without the guidance, encouragement, and help from my committee members. I offer my sincere appreciation for their exemplification to scientific work which will be beneficial to the rest of my career.

I am also indebted to Dr. Yonnie Wu at the Mass Spectrometry Laboratory in the Department of Chemistry and Biochemistry, Dr. Brian Via, Mr. David Mills, and Mr. Christian Brodbeck at the Center for Bioenergy and Bioproducts, Dr. Thomas Elder at the USDA-Forest service, Dr. Sushil Adhikari in Biosystem Engineering, and Dr. Tom Gallagher in Forestry, Dr. Allan E. David and Dr. Virginia A. Davis in Chemical Engineering, for their numerous support and discussions for my research project.

I would like to thank my fellow researchers and good friends Patrick Bass, Jackson Rucker Staggers, Liang Wei, Anshu Shrestha, William Chaplow, Dongxu Cao, Alexander Haywood, Jie Zhong, Peng Cheng, Suan Shi, Jing Li, Chenhuan Lai, Ray Xu, Daihui Zhang, Jamarius Carvin, Pixiang Wang, Zhizhi Sheng, Rui Xie, Zhiqiang Shi, Hao Shi, Xiaofei Wang, Yang Huang, Victoria Fang, Ifedolapo Mofoluwasayo Fasina, George Cheng, and those in Dr. Brian Via's group. My research would not be completed without their friendship and support.

I want thank Dr. Rob Martin and his family, the Booths, the Walkers, and the Smiths for their fellowship and help to make my studies and family lives joyful and blessed!

Lastly, I am particularly grateful to my wife Jun Xiao, daughter Mia Li, and my immediate family for their endless love, trust, support, and encouragement.

Table of Contents

List of Tables

List of Figures

List of Abbreviations

AFEX	Ammonia fiber explosion
AGU	Anhydroglucose units
ARP	Ammonia recycle percolation
AFM	Atomic force microscopy
BET	Brunauer–Emmett–Teller theory
BG	Beta-glucosidase
$Ca(OH)_2$	Calcium hydroxide
$CaSO_4$	Calcium sulfate
CBH	Cellobiohydrolases
CMC	Carboxymethylated cellulose
CNCs	Cellulose nanocrystals
DAPI	4',6-diamidino-2-phenylindole
DI	Deionized
DW	Dry weight
EG	Endoglucanases
FITC	Fluorescein isothiocyanate
FP	Filter paper
FTIR	Fourier transform infrared spectroscopy
GA	Gluconic acid
GC	Gas chromatography

GDH	Glucose dehydrogenase
HCl	Hydrochloric acid
HPLC	High performance liquid chromatography
H_2SO_4	Ionic liquids
KGA	Keto-gluconic acid
LC-MS	Liquid chromatography-mass spectrometry
MCC	Microcrystalline cellulose
NaAc	Sodium acetate
NaBr	Sodium bromide
NaClO	Sodium hypochlorite
NaOH	Sodium hydroxide
NH_4OH	Ammonium hydroxide
NMR	Nuclear magnetic resonance
OD	Optical density
OPLP	Organosolv pretreated Loblolly Pine
OPSG	Organosolv pretreated Sweetgum
ppm	Parts per million
PIBSA	Polyisobutylene succinic anhydride
SEM	Scanning electron microscope
SHF	Separate hydrolysis and fermentation process
SSCF	Simultaneous saccharification and co-fermentation process
SSF	Simultaneous saccharification and fermentation process
TEMPO	2,2,6,6-tetramethyl-1-piperidine oxoammonium salt
TRITC	Tetramethylrhodamine isothiocyanate

TGA	Thermal gravity analysis
TSC	Thiosemicarbazide
XA	Xylonic acid
XRD	X-ray diffraction
XDH	Xylose dehydrogenase

Chapter 1 Introduction

1.1 Background—biofuels and value-added bioproducts development

Due to the finite supply of fossil fuel resources, availability as an energy source and industrial products will eventually be depleted in the near future at current consumption rates. In this regard, lignocellulosic materials have been considered as a credible and alternative raw material to petroleum for the reasons associated with energy security, diversity, and sustainability (Hoekman 2009; Huber et al. 2005; Huber et al. 2004).

Lignocellulosic materials (or lignocellulosic biomass), such as woody biomass, are mainly composed of cellulose, hemicellulose, and lignin. Cellulose and hemicellulose are polymers of carbohydrates built from monosaccharides such as glucose, xylose, and mannose. Lignin is a polymer of complex aromatic alcohols. Generally, two main technical platforms are used to convert lignocellulosic materials into desired products: biochemical platform and thermochemical platform. Analogous to petroleum refineries, biorefinery integrates the biomass conversion processes, technologies, and equipment to energy usually called biofuels and valuable chemicals called bioproducts or biomaterials (**Figure 1-1**). Lignocellulosic biomass is superior to other feedstock due to two major reasons: (1) it has no competition with food based biomass; and (2) it shows the desired physical and chemical properties suitable for production, harvest, handling, storage, and transportation.

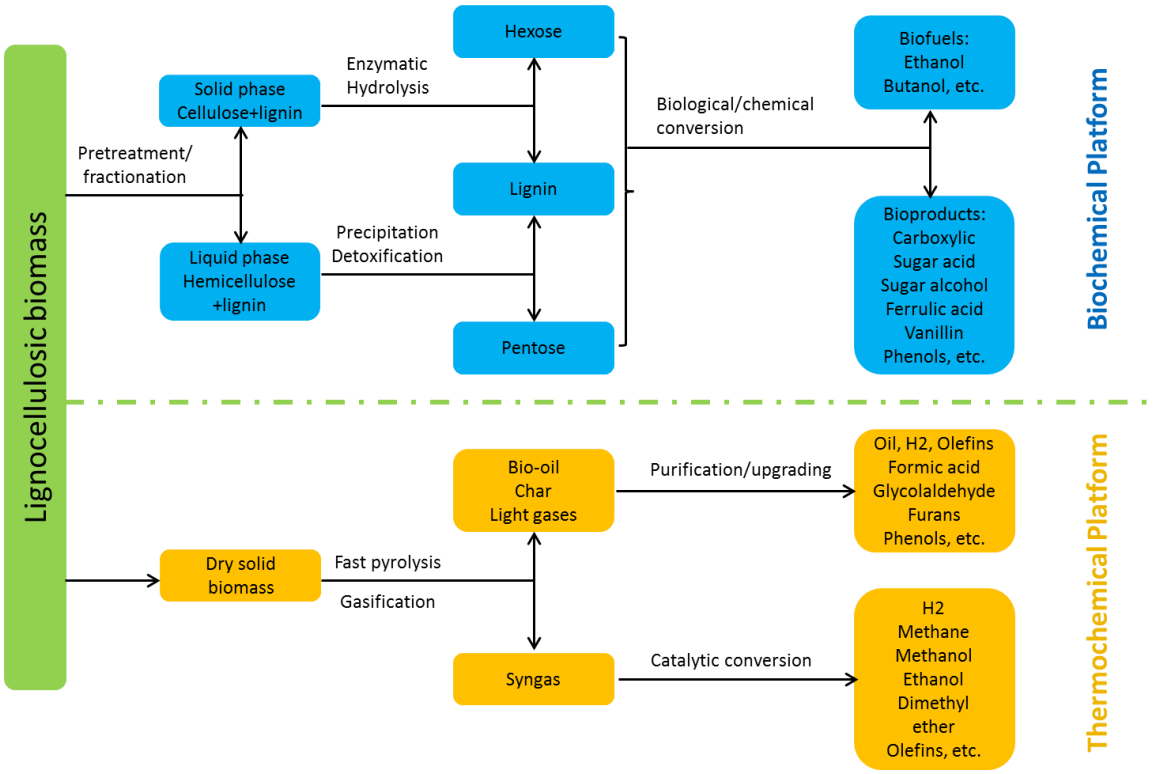

Figure 1-1. Schematic of biorefinery from lignocellulosic biomass.

1.2 Lignocellulosic biomass

1.2.1 Morphology and ultrastructure of lignocellulosic biomass

Wood has a complex hierarchical structure giving rise to its special mechanical and physical properties (**Figure 1-2**). Generally, wood is divided into softwoods (gymnosperms such as conifers) and hardwoods (angiosperms such as deciduous or broad-leaf trees). The common wood species found in the southern United States include pine, fir, spruce, sweetgum, aspen, birch, oak, willow, poplar, and blackwood (Bergman et al. 2010). Wood depending on crown, trunk, or root is composed of different anatomical tissues. These tissues are ultimately made of a variety of different wood cells with different roles.

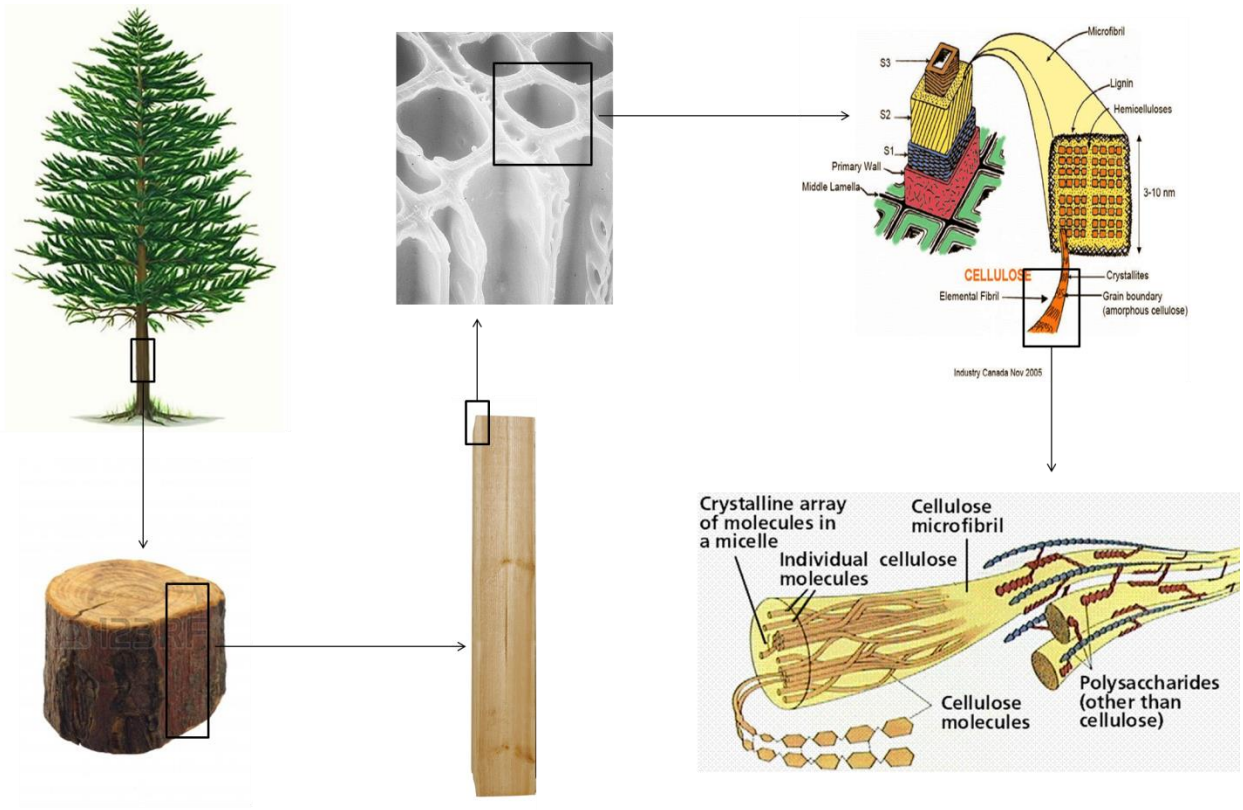

Figure 1-2. A hierarchical view of wood structure (Purves et al. 1994).

Wood is composed of axial and radial cell system in high order (**Figure 1-3A**). The wood structure and cell types are typically schemed in the tangential, radial, and transverse sections. These cells are usually oriented in parallel to the tree trunk (90-95%). About 5-10% of the cells are arranged in radial directions. In the transverse section, wood is composed of bark, cambium, sapwood, heartwood, and pith. The growth rings separate the sapwood and heartwood annually. The sapwood and heartwood varies on status of parenchyma cells. The sapwood contains living parenchyma cells helpful for water transportation whereas the heartwood includes dead cells (usually darker in color) and accumulated extractives resulting in less permeablility and more durability.

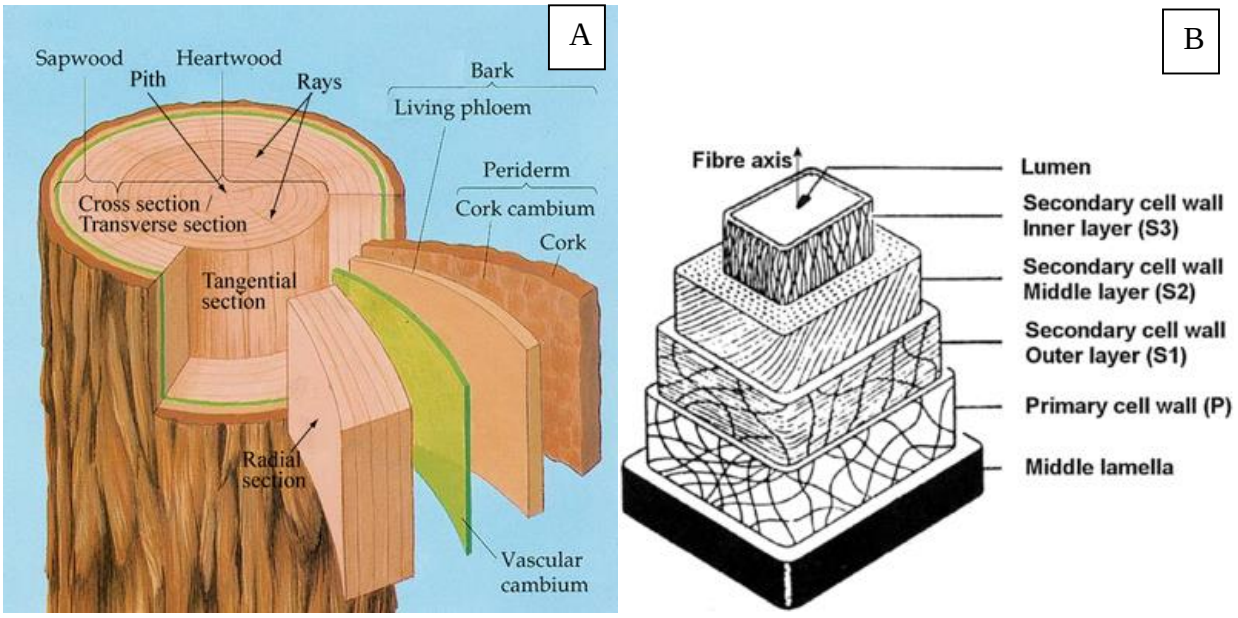

Figure 1-3. Sectional view of a tree trunk (A) (Greer et al.) and ultrastructure of a cell wall (B) (Nieminen et al. 2013).

The ultrastructural architecture of a wood cell wall is better observed under electron microscopy. A typical structure of the tracheid cell wall is composed of the middle lamella (ML), primary wall, secondary wall layers, warty layer, and lumen (**Figure 1-3B**). The ML region separating the cell wall is rich in lignin content. The cell wall is mainly comprised of cellulose microfibrils. The orientation of these fibrils varies depending on the layer.

1.2.2 Lignocellulosic biomass chemistry

The precise chemical composition of lignocellulosic materials varies on the types of species, sources, and even parts of a given tree. In general, the woody biomass is mainly composed of cellulose (40-50%), hemicellulose (15-30%), lignin (16-35%) and a small amount of extractives (1-5%) (Fengel and Wegener 1989; Pettersen 1984) (**Table 1**). Besides these major compositions, the wood cell wall also contains pectin and glycoprotein extension which glue the cellulose microfibrils in a crisscross network and hemicellulose (Monica Ek 2009). Cellulose and

hemicellulose are polymers of carbohydrates and their building blocks are monosaccharides such as glucose, xylose, and mannose. Lignin is a polymer of complex aromatic alcohols. All these components are bundled in a recalcitrant form.

Table 1. Chemical composition in woody biomass.

Chemical Composition	Softwood (%)	Hardwood (%)
Cellulose	40-50	40-50
Hemicelluloses	18-25	20-30
Lignin	23-33	16-25
Extractives	1-5	1-2
Inorganic (ashes)	0.2-0.5	0.2-0.5

Cellulose

Cellulose is an almost inexhaustible carbohydrate from the plant kingdom (Klemm et al. 2005). In general, cellulose is a fibrous, rigid, water-insoluble substance with fascinating structure and properties. From a structural point of view, cellulose is a carbohydrate polymer comprised of repeating β-D-glucopyranose molecules. The repeating units are covalently linked through β-1,4-glucoside bonds between the equatorial OH group at C4 and C1 position (Klemm et al. 2005). In fact, cellulose is composed of repeating dimer corkscrewing two anhydro-D-glucose unites (AGU) 180 °with respect to each other (**Figure 1-4**) (Habibi et al. 2010). The two adjacent AGU units define the dimer— cellobiose. The degree of polymerization (DP) is expressed as a number of constituent AGU suggesting the chain length of cellulose, usually 300-1700 in wood pulp (Klemm et al. 2005). Each cellulose chain possesses one reducing end and one nonreducing end. The nonreducing end is featured with a glucose unit ending with C4-OH group whereas the reducing end is terminated with a hemiacetal group at the C1 position.

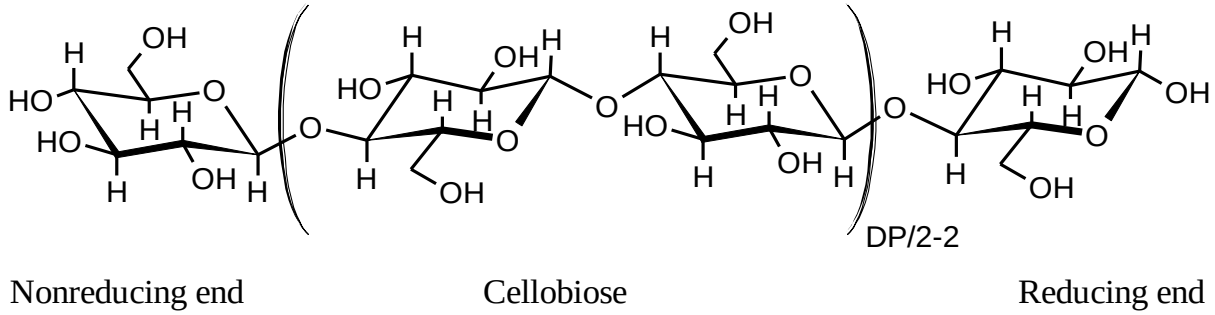

Figure 1-4. The primary molecular structure of cellulose (DP: degree of polymerization).

The secondary structure of cellulose essentially gives rise to cellulose as a biological and technically interesting bio-polysaccharide. There are three hydroxyl groups on each of the AGU rings at positions C2 and C3 (secondary) as well as C6 (primary). When the AGU pyranose rings displayed in a $^4C_1$ chair conformation, all the H atoms on the ring point vertically away from the plane (axial), while the OH groups are parallel to the plane (equatorial). As a result, a single cellulose chain with a glycosidic bond is stabilized by the intramolecular hydrogen bonds between the O6' and O2-H and between the O5 and O3'-H (**Figure 1-5**). Likewise, a cellulose sheet is formed by the intermolecular hydrogen bonds between O3 and O6-H on the neighboring chain (**Figure 1-5**). This supramolecular structure with parallel chains as mentioned here is called cellulose I. The triclinic and monoclinic unit cell stabilized by the intra- and intermolecular hydrogen bonds define the tightly packed cellulose crystallites structure Iα and Iβ, respectively (Monica Ek 2009). However, these hydrogen bonds and the orientation of individual cellulose chain can vary on the respective source and post-treatment (Monica Ek 2009), which gives rise to six inter-convertible cellulose polymorphs, namely, I, II, III_I, III_{II}, IV_I, and IV_{II} (Habibi et al. 2010).

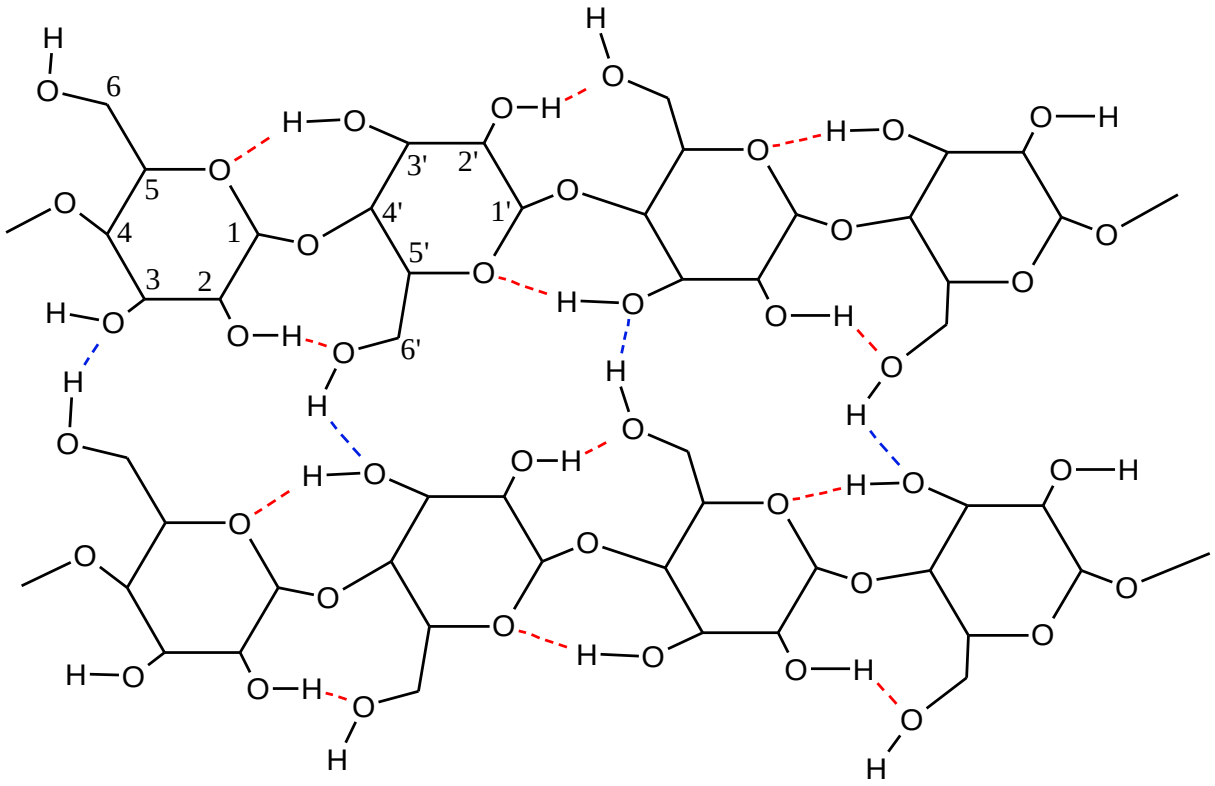

Figure 1-5. A top view of cellulose sheet structure stabilized by intra- and inter-molecular hydrogen bonds.

Cellulose II, with more thermodynamically stable supramolecular structure, can be formed from cellulose I by mercerization and regeneration (Habibi et al. 2010). Cellulose II differs from cellulose I in that the hydroxyl group at C6 rotates and changes the hydrogen-bonding network. As a result, every second chain has an opposite polarity to the next (in an antiparallel arrangement) which leads to one more hydrogen bond per AGU molecule. The polymorphs III and IV are similar to cellulose II and I, respectively (Monica Ek 2009).

From the shape of the fibril, cellulose is bio-synthesized in a hierarchical organization within the cell wall. The cellulose chains bundle together with lateral dimension from low to high as elementary fibril (1.5-3.5 nm), microfibril (10-30 nm), and microfibrillar bands (100 nm

or more) usually called as macrofibrils or cellulose fibers (**Figure 1-6**). In higher plant, typically, elementary fibril is comprised of 36 individual cellulose chains.

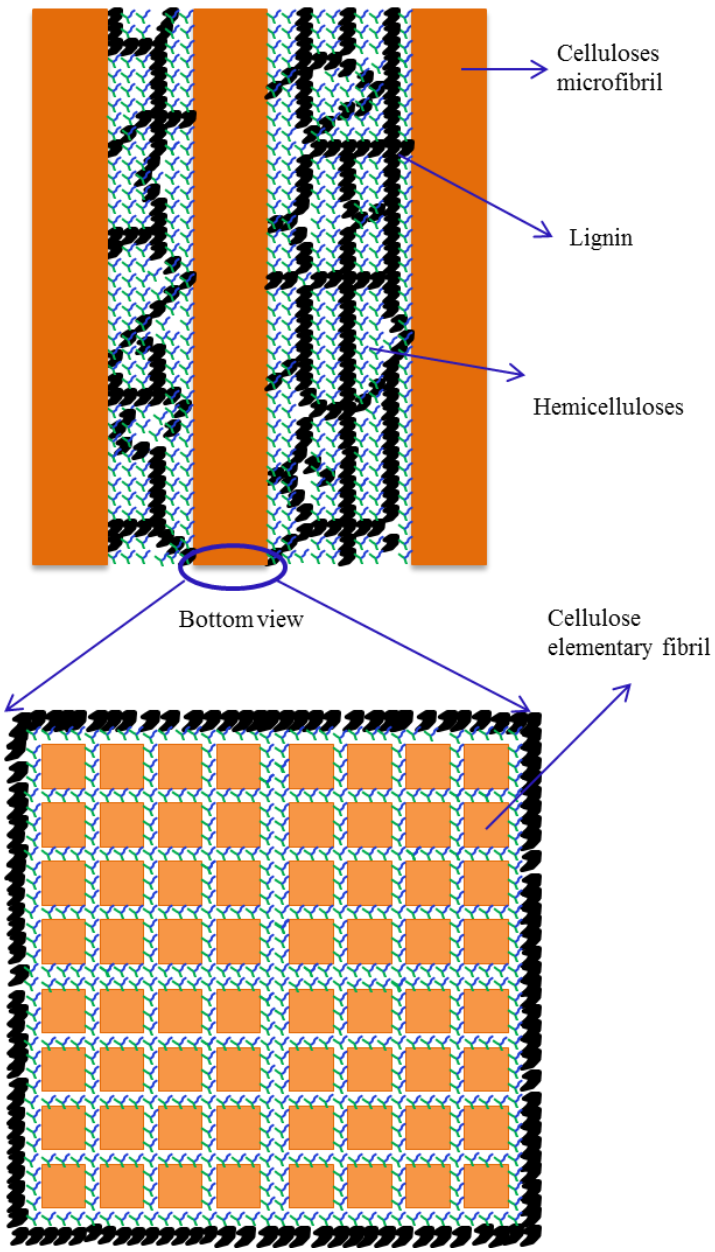

Figure 1-6. Biopolymer arrangement in a wood cell wall.

Hemicelluloses

Although hemicelluloses work as structural carbohydrates like cellulose, hemicelluloses actually represent a distinct and separate group of cell wall polysaccharides (Monica Ek 2009).. They are tightly associated with cellulose and lignin and account for 20-35 wt% of the dry mass. Unlike cellulose, hemicelluloses generally occur in the form of hetero-polysaccharides with branches and result in a lower DP of approximately 100-200. Typically, six types of hemicelluloses are found in wood including galactoglucomannan, glucomannan, arabinoglucuronoxylan, arabinogalactan, glucuronoxylan, and glucomannan from linking mannose, xylose, galactose, glucose, and arabinose molecules. These subunits are bonded together in the woody biomass primarily through β-*O*-4 linkages (Kocurek 1984). Other linkages such as 1→2, 1→4, and 1→6 glycosidic bonds are branched off from the backbone.

A

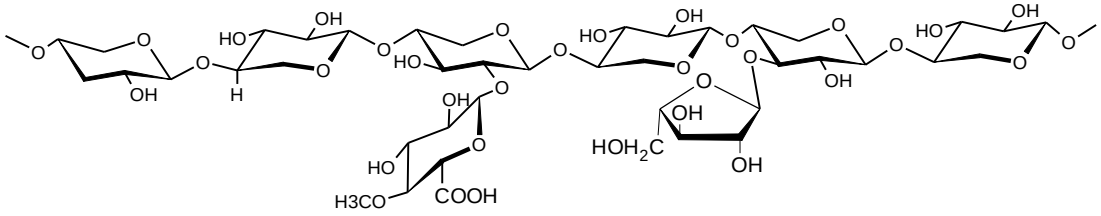

-->4)-β-D-Xyl*p*-(1-->4)-β-D-Xyl*p*-(1-->4)-β-D-Xyl*p*-(1-->4)-β-D-Xyl*p*-(1-->4)-β-D-Xyl*p*-(1-->4)-β-D-Xyl*p*-(1-->

2 — 1 α-D-4-OMe-Glc*p*A

3 — 1 α-L-Ara*f*

B

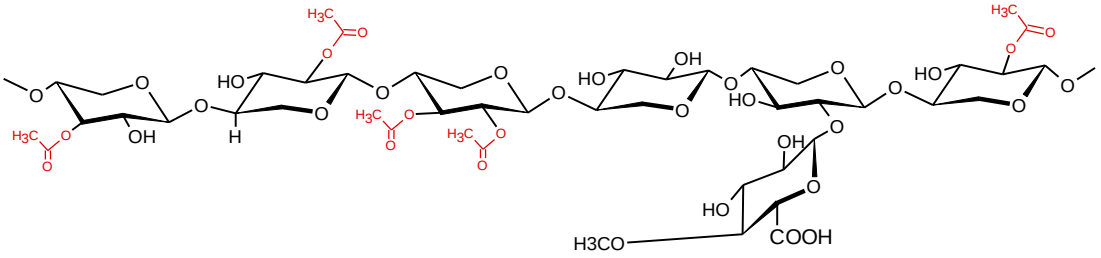

-->4)-β-D-Xyl*p*-(1-->4)-β-D-Xyl*p*-(1-->4)-β-D-Xyl*p*-(1-->4)-β-D-Xyl*p*-(1-->4)-β-D-Xyl*p*-(1-->4)-β-D-Xyl*p*-(1-->

3 Ac; 2 Ac; 3 Ac, 2 Ac; 2 — 1 α-D-4-OMe-Glc*p*A; 2 Ac

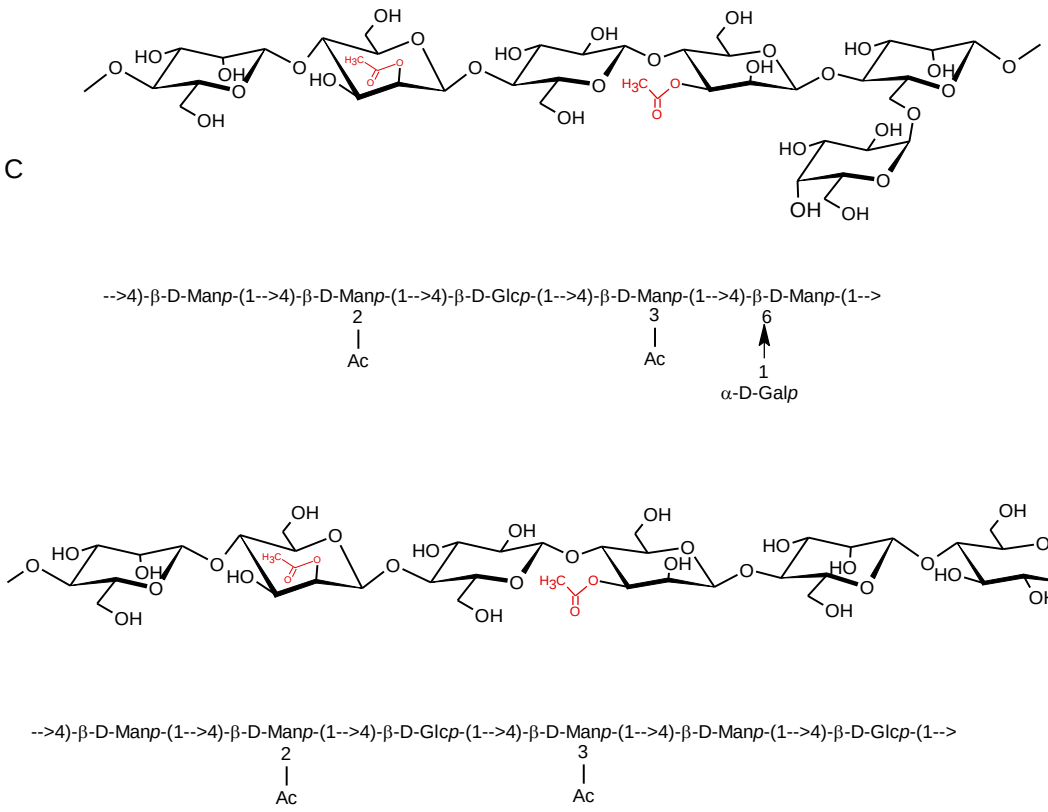

Figure 1-7. Structure of hemicelluloses in softwood and hardwood. A: arabino-4-*O*-methylglucuronoxylan; B: glucuronoxylan; C: galactoglucomannan; and D: glucomannan.

The structures of hemicelluloses present in softwood and hardwood are quite different. Softwood is mainly composed of partially acetylated galactoglucomannan and small proportions of arabino-(4-*O*-methylglucurono)xylan; whereas hardwood is mostly comprised of partially acetylated (4-*O*-methylglucurono)xylan and a small amount of glucomannan. The composition of hemicelluloses also varies by cell wall layer and by location within the tree. The chemical structures of xylan and mannan in softwood and hardwood are illustrated in **Figure 1-7**.

Lignin

Lignin is another abundant biopolymer filling up the space between cellulose microfibrils and hemicellulose like a phenolic plastic (Monica Ek 2009). It has a complex structure with a

mixture of aromatic and aliphatic monomers. In contrast to cellulose and hemicellulose, lignin forms a three-dimensional connection randomly that linked by ether (C-O-C) and carbon (C-C) bonds. Three common monomers present in lignin polymer are *p*-coumaryl alcohol, coniferyl alcohol, and sinapyl alcohol (**Figure 1-8**). There are also other monolignols (lignin monomers) founded including coniferaldehydes, acetylated coniferyl alcohols, and ferulic acid (Monica Ek 2009).

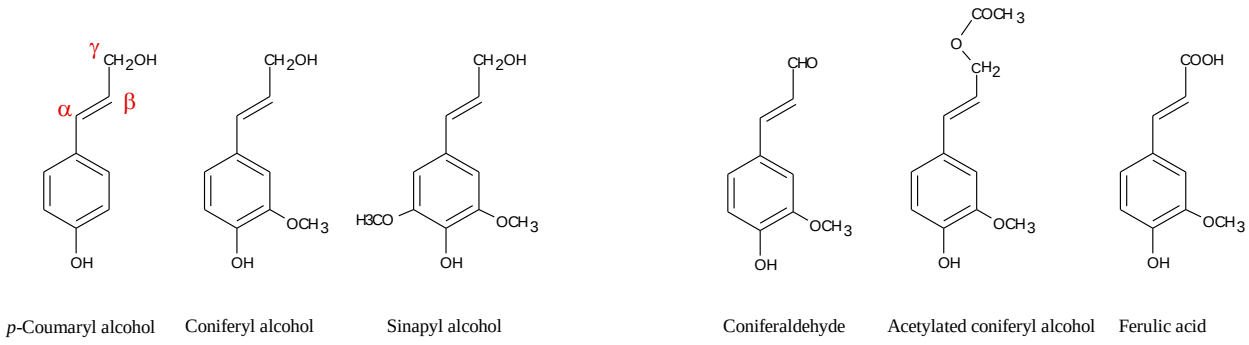

Figure 1-8. Building blocks (monomers) for lignin.

The softwood and hardwood lignins differ in their proportions of these building blocks. Softwood lignin (also called guaiacyl lignin) is mainly composed of coniferyl alcohol and may possess a small amount of *p*-coumaryl alcohol. In contrast, hardwood lignin (also called syringyl-guaiacyl lignin) consists of approximately equal amount of both coniferyl and sinapyl alcohols. The grass lignin is polymer of all the three monolignols.

Extractives

Wood extractives are chemical compounds extracted from wood with organic solvents. Extractives are mainly composed of fats, fatty acids, esters, sterols, terpenoids, and waxes. They vary with the solvent and method used.

1.3 Biochemical conversion of lignocellulosic biomass to fuels and chemicals

The bioconversion of lignocellulosic biomass to fuels and chemicals involves three main steps: an initial pretreatment step to disrupt the recalcitrant structure of lignocellulosic biomass and make cellulose accessible to hydrolytic enzymes; an enzymatic hydrolysis step thereafter to hydrolyze the carbohydrate polymers to fermentable monosaccharides, and finally a fermentation (anaerobic or aerobic) step to convert monomeric sugars to biofuels and chemicals, as depicted in the flow chart (**Figure 1-9**).

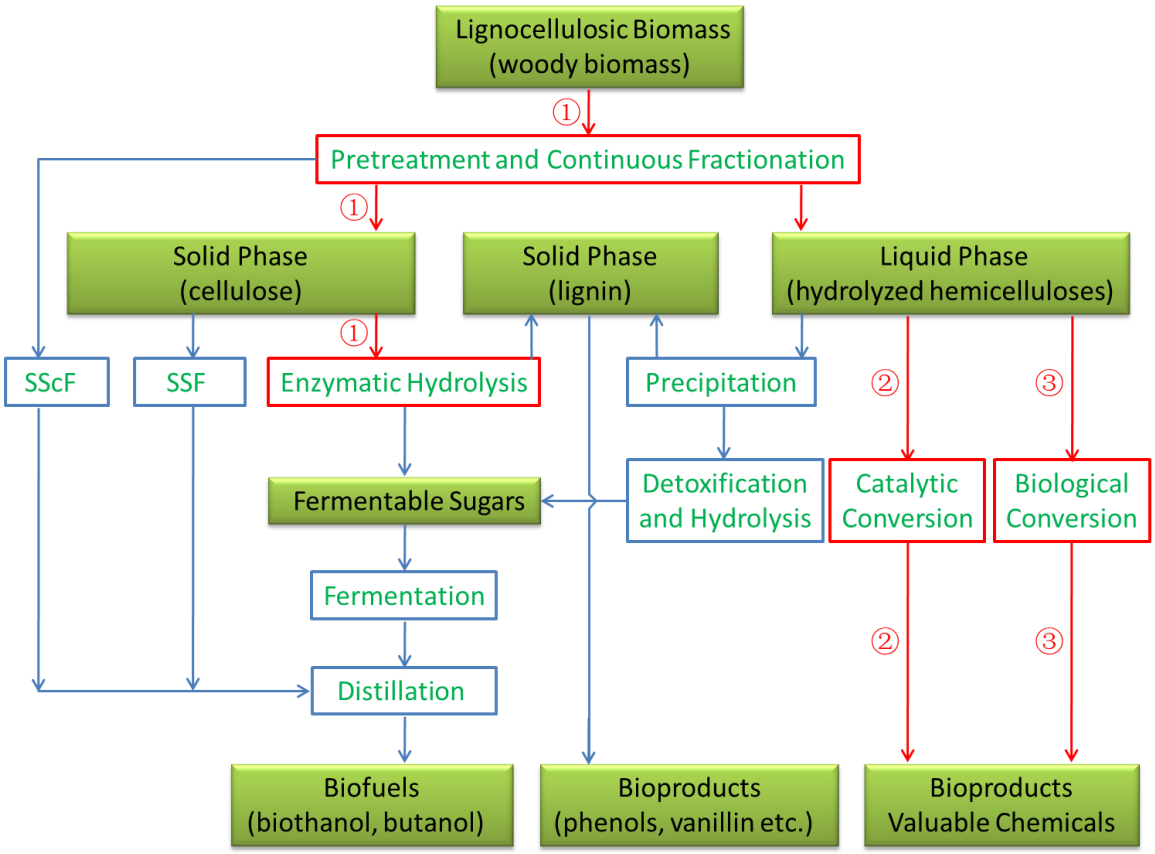

Figure 1-9. Biochemical conversion of lignocellulosic biomass to biofuels and chemicals.

The pretreatment partially separates hemicelluloses and lignin from cellulose that improves the enzyme accessibility to cellulose significantly. After pretreatment, the biomass is

fractionated into a solid part rich in cellulose (hydrolysate) and a liquid part rich in solubilized hemicellulose sugars (prehydrolysate). In separate hydrolysis and fermentation process (SHF), the hydrolysate and prehydrolysate are fractionated prior to the next conversion. In a simultaneous saccharification and co-fermentation process (SSCF), the hydrolysate and prehydrolysate are subjected to hydrolysis and fermentation simultaneously without fractionation. The sustainable products, biofuels, bioproducts, and value-added chemicals are separated and collected at the end of the biochemical conversion stream.

1.3.1 Pretreatment and fractionation of lignocellulosic biomass

The production of biofuels and biobased chemicals from renewable lignocellulosic biomass is accomplished by hydrolyzing carbohydrate polymers into their soluble components followed by the fermentation to desired end products. The bottle neck of this bioconversion process lies within the break-down of the recalcitrant structure in lignocellulose (Himmel et al. 2007a). A desired pretreatment process must (a) maximize the enzymatic convertibility or promote effective conversion to available carbohydrates; (b) minimize loss of sugars; (c) maximize the production of other valuable co-products, e.g. lignin; (d) minimize the toxicity to enzymes and/or microorganisms; (e) minimize the operational cost in energy, chemicals, and capital equipment; (f) be scalable to industrial size; and (g) minimize solid-waste residues (Agbor et al. 2011; Lynd 1996; McMillan ; Mosier et al. 2005; Taherzadeh and Karimi 2008; Zhu and Pan 2010a). So far, none of the pretreatment technologies have satisfied these listed criteria completely.

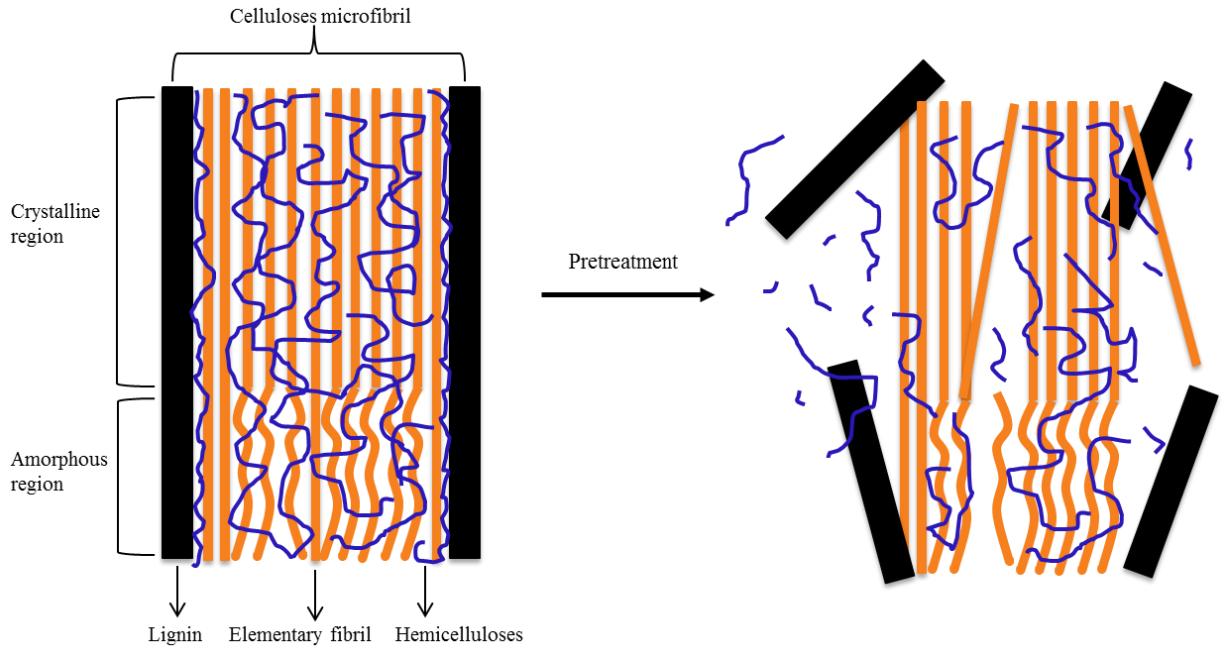

Figure 1-10. Schematic of pretreatment on lignocellulosic material (HSU et al. 1980; Mosier et al. 2005).

During the pretreatment process, cellulose, hemicellulose, and lignin are somehow fractionated as a result of disrupting the physical barrier and crystalline structure (**Figure 1-10**). A variety of pretreatment methods have been investigated in the past decades, such as physical (mechanical comminution), thermal-chemical (pyrolysis), physic-chemical (steam explosion, AFEX, and CO_2 explosion), chemical (ozonlysis, acid hydrolysis, alkaline hydrolysis, oxidative delignification, organosolv process), and biological pretreatment (Agbor et al. 2011; Brodeur et al. 2011; Chum et al. 1988; McMillan ; Mosier et al. 2005; Sun and Cheng 2002; Wyman et al. 2005; Zhao et al. 2009; Zhu and Pan 2010a). These pretreatment methods result in different biomass fractionation by the extent of lignin removal, enzyme accessibility, and fermentation efficiency (**Table 2**). Some of the popular pretreatment methods and their effects on decomposition of the lignocellulosic biomass and on the downstream steps are categorized and discussed in the following.

Table 2. The effect of chemical pretreatments on biomass fractionation and downstream steps.

Pretreatment	Chemical used	Reaction condition	Main effects	Pros	Cons
Comminution	Physical pretreatment	Mechanical operation	Reduce cellulose crystallinity	Structure little-changed	High energy needed; slow
Steaming or steam explosion (STEX)	Auto-hydrolysis (acetic acid)	180-210 ℃ 1-10 min	Partial hydrolysis of hemicellulose; redistribution of lignin on fibers; fractionation of fibers	Surface area increased; structure little-changed; fast operation	Limited removal of lignin; little disrupt of crystallinity
Liquid hot water	Auto-hydrolysis (hydrothermolysis)	160-230 ℃ 10-30 min	Removal of hemicelluloses and some lignin	No chemicals added; no neutralization needed; particle size insensitive	Limited disrupt of crystallinity; limited lignin removal; lignin structure altered
Acid hydrolysis	H_2SO_4 (0.3-3% w/w) SO_2/HCl/HNO_3/H_3PO_4	140-180 ℃ 10-60 min	Removal of hemicelluloses	Enhanced susceptibility	Corrosiveness; degradation products; neutralization needed
Ammonia freeze/fiber explosion (AFEX)	NH_3 H_2O (5-15%)	90-100 ℃ 5-10 min	Cleavage of lignin; partially depolymerization of cellulose and hemicellulose; less degradation products	Ammonia recyclable; little degradation products; high solid operation	Limited lignin removal; not well on softwood; Chemical cost
Lime	$CaCO_3$/NaOH	85-150 ℃; 1 h - days	Removal of lignin;	Low temperature; high delignification	Longer time; irrecoverable salts; biomass size sensitive
Wet oxidation	H_2O_2 (1-5%)	180-200 ℃ 5-15 min	Removal of lignin; partial degradation of lignin; solubilization and oxidation of some hemicelluloses	Enhanced susceptibility	Much inhibitory
Ozonolysis	O_3	20-30 ℃ 5-15 min	Degrade lignin and hemicelluloses	Effective delignification; less toxic products	Chemical cost
Organosolv	Alcohol (40-60%)/ organic acids (HCOOH, peracids)	100-250 ℃ 30-60 min	Removal of lignin and some hemicelluloses (extracted out)	Isolate high quality lignin; removal of hemicellulose ; solvent recyclable	Some toxic; extra washing process; solvent cost
Biological	Fungi	20-30 ℃ days	Degradation of lignin and hemicelluloses; partial degradation of cellulose	Low energy requirement; mild condition; enzymatic hydrolysis step partially skipped	Very slow

Irradiation

Lignocelluloses are disrupted by irradiation under an electron beam (Kumakura et al. 1982). Irradiation can be beneficial by accelerating the crushing effect on the biomass resulting in reduced particle size and enhanced efficacy of subsequent enzymatic hydrolysis.

Steam explosion

The steam explosion pretreatment is often coupled with a dilute acid. Chipped biomass is treated with saturated steam in a pressure vessel at high temperature (160-260°C) and is suddenly reduced to atmospheric pressure by explosion (Brownell et al. 1986). The explosive process disrupts the biomass crystallinity and increased the pore sizes of biomass (Brownell et al. 1986; Grous et al. 1986).

Hydrothemolysis

Hydrothermolysis is carried out in a reactor using pressurized hot water (190-250 ℃) that disrupts lignin barrier, dissolves hemicellulose, and eventually increases enzymes accessibility (Allen et al. 1996; Hörmeyer et al. 1988; Negro et al. 2003). A treatment of 4-10 min has a good solubilization of biomass at 50% and a hemicellulose recovery at 80%. The fractionated biomass exhibited a small amount of toxicity by HMF and furfural (< 1 g/L) and presented 72% of the theoretical ethanol yield in the process of SSF (Suryawati et al. 2009). However, the autohydrolysis occurs in this process due to the presence of acetic acid, formic acid, or uronic acid from hemicelluloses.

Steam explosion with catalyst

This is the same pretreatment method modified by adding an acid as a catalyst (Brodeur et al. 2011; Eklund et al. 1995). The diluted acid improves the solubilization of hemicelluloses as well as the digestibility of cellulose with a reduced treatment time and temperature. Moreover, less inhibitory compounds were formed when hemicelluloses were removed (Ballesteros et al.).

Ammonia fiber explosion/expansion (AFEX)

The biomass is rapidly depressurized after saturation with liquid anhydrous ammonia under high pressures and moderate temperatures (60-100 ℃) (Lau et al. 2010; Teymouri et al. 2005). Variables such as retention time (5-40 min) and ammonia loading amount (ca. 1 kg/kg DW) were chosen and varied with feedstock type (Alizadeh et al. 2005; Chundawat et al. 2007). The ammonia gas swells the biomass and disrupts the linkages between lignin, hemicellulose, and cellulose giving rise to more accessible sites for enzymes (Dien et al. 2008). However, the mild treatment condition and less sugar degradation are offset by the extra steps in recycling the chemicals.

Ammonia recycle percolation (ARP)

In contrary to AFEX, aqueous ammonia (5-15%) is used to percolate biomass at higher temperature (140-210 ℃) with longer retention time at a certain flow rate (ca. 5 mL/min) (Kim and Lee 2005; Kim et al. 2006). ARP outperformed AFEX with higher delignification and removal of hemicelluloses. An increased cellulose fraction is retained with the ARP method, but it is not cost-effective due to the energy input and liquid loading plus the similar issues associated with AFEX process.

Supercritical fluid (SCF)

SCF pretreatment is a process in which lignocellulosic biomass is penetrated by the coexistent state of a gas as a liquid above the critical temperature and pressure (Kim and Hong 2001; Sawan 1998). This supercritical fluid (CO_2, NH_3, or CO_2 and H_2O) overcomes the mass transfer limitations in other pretreatments by its special diffusivity and viscosity (Brunner 2005; Chou 1987; Sawan 1998).

Acid pretreatment

Treatment of lignocelluloses with diluted or concentrated acid to break the matrix of biomass is mostly investigated and nearly commercialized in a wide variety of biomass types. (Digman et al. 2010; Wyman et al. 2009; Xu et al. 2009) Pretreatment with H_2SO_4 is a preferred choice, while other acids, HCl (Wang et al. 2010), H_3PO_4 (Zhang et al. 2007), HNO_3 (Brink 1993; Brink 1994), HAc (Xiao and Clarkson 1997), and TFA (Marzialetti et al. 2008) have also been studied to remove the hemicelluloses and improve the enzymatic hydrolysis. The pretreatment of lignocelluloses with concentrated acids (30-70%) at low temperature (40°C) or diluted acids (0.5-2%) at high temperature (100-200°C) is possible (Wyman 1996). Concerns with concentrated acids are equipment corrosion, operation safety, and gypsum wastes from neutralization. At elevated temperature (130-210 ℃), diluted acids (0.1-1% H_2SO_4) significantly improves the cellulose hydrolysis by almost 100% hemicellulose removal. Other advantages of this method include hydrolyzing hemicellulose to fermentable sugars and dissolving lignin with minimal degradation (Carrasco et al. 1994). A combination of diluted acid with $ZnCl_2$ was reported to lead to a high enzymatic hydrolysis yield (93%) (Azzam 1987). However, the drawbacks such as corrosion, toxicity and production of inhibitory compounds (phenolic

compounds, HMF and furfural) to fermentation has prohibited the use of the acid pretreatment method (Pienkos and Zhang 2009; Xie 2014).

Alkaline pretreatment

Alkaline pretreatment refers to the use of bases, such as NaOH (Sun et al. 1995), KOH (Weil et al. 1997), $Ca(OH)_2$ (Park et al. 2010a), NH_4OH (Teymouri et al. 2005), Na_2CO_3 (Vaccarino et al. 1987), or $NaHCO_3$ (Wang et al. 2005) for the biomass treatment. It removes lignin efficiently and part of the hemicelluloses by breaking the ester and glycosidic bonds, and decrystallizes the cellulose for the enhancement of enzymes accessibility. Lime and NaOH were extensively used to delignification and dissolution of hemicelluloses. A result of 60% delignification and 80% removal of hemicellulose was found by treating wheat straw with 1.5% NaOH at 20°C for 144 h (Sun et al. 1995). Lime is superior to other alkaline in cost. The alkaline pretreatment temperature is less severe but requires longer treatment time and higher base concentration. In addition, alkaline involved pretreatment alters the structures of lignin (Cheng et al. 2010).

Alkaline peroxide pretreatment

Lignocelluloses were soaked in H_2O_2 containing water at pH 11-12 by NaOH at room temperature for 24 h. A high yield of enzymatic hydrolysis on pretreated wheat straw (97%) (Saha and Cotta 2006) and rice hulls (96%) (Saha and Cotta 2007) were achieved by means of alkaline peroxide pretreatment method. Moreover, no degraded compounds such as HMF and furfural were detected in this process. Another advantage to alkaline pretreatment is that the basic structure of lignin was mostly retained (Mishima et al. 2006).

Organosolv pretreatment

Lignocellulosic materials were pretreated in a large amount of aqueous-organic liquid system with or without added catalysts (HCl or H_2SO_4) at 100-250 ℃ (Zhao et al. 2009). The organosolv pretreatment process disrupts the lignin-carbohydrate matrix and dissolves the lignin and part of the hemicelluloses, leaving the cellulose as a solid. Organosolv pretreatment is attractive due to less pollution, easier solvent recycling, better component fractionation, and a higher hydrolysis yield (Zhao et al. 2009). Dry lignin, aqueous hemicellulose syrup, and relatively pure cellulose, were separated and utilized at the end of this process (Duff and Murray 1996). A number of organic solvents were used including methanol (Chum et al. 1988), ethanol (López et al. 2006), acetone (Araque et al. 2008), ethylene glycol (Thring et al. 1990), THF alcohol (Zhao et al. 2009), glycerol (Sun and Chen 2008). These low-molecular-weight alcohols (methanol and ethanol) are favored for their low cost and easy recovery associated with their low boiling points. The high boiling point solvents increase the degree of delignification due to higher operating temperature but lower cellulose yield. Other organic compounds, organic acids, peracetic acid (PAA), dioxane, phenol, NMMO, ethylenediamine were investigated (Zhao et al. 2009). Unlike other pretreatment methods for woody biomass, organosolv pretreatment requires no significant particle size reduction because high cellulose digestibility is still obtainable (> 90%) and this reduces the energy consumption (Agbor et al. 2011). The organosolv pretreated substrates exhibited very good enzymatic hydrolysis yields. However, the high cost and solvent removal step are main disadvantages for the method.

Wet oxidation

In the wet oxidation process, oxygen or air is used to oxidize the compounds in water. A reduction of biomass size and addition of Na_2CO_3 are required before the pretreatment at ca. 200 ℃ for 10 to 30 min (Brodeur et al. 2011). Wet oxidation is good at removing lignin and solubilizing hemicellulose (Banerjee et al. 2009).

Green solvents

Pretreatment of lignocellulosic biomass operated in the ionic liquids that dissolve a number of biomass types at mild processing conditions (Brodeur et al. 2011). The mixture of solvents with high polarities, high thermal stabilities with low vapor pressures, salts with small anion and large cation interrupt the hydrogen bonding of cellulose giving rise to good enzyme accessibility (Zhu et al. 2006).

In summary, both physical and biological processes are overall cost ineffective compared to the chemical method, though they possess some intrinsic advantages. Relatively, the chemical and physicochemical methods are more efficient at the disruption of the recalcitrant structure of lignocellulosic biomass. Organosolv pretreatment with H_2SO_4 is a preferred method; it provides overall efficiency in terms of biomass fractionation, solvent recovery, component degradation, and operating conditions.

1.3.2 Enzymatic hydrolysis of pretreated biomass

Pretreatment process disrupts the recalcitrant structure, fractionates the main component, and enhances biomass digestibility for downstream processes. However, the key issue of the biorefinery has not been addressed until the carbohydrates of lignocellulose are decomposed into fermentable sugars. In the enzymatic hydrolysis stage, a mixture of cellulolytic and

hemicellulolytic enzymes are used to digest the carbohydrates under mild conditions (pH 4.5-5.0 at 40-50 ℃) and to liberate the monosaccharides ready for fermentation. The commonly used hydrolases include exo-1,4-β-D-glucanases (CBH), endo-1,4-β-D-glucanases (EG), 1,4-β-D-glucosidases (BG), endo-1,4-β-D-xylanases, 1,4-β-D-xylosidases, endo-1,4-β-D-mannanases, and 1,4-β-D-mannosidases (**Table 3**) (Jorgensen et al. 2007).

Table 3. Common enzymes used for hydrolyzing biomass carbohydrates.

Group	Name	Abbreviation	Cleavage point
cellulolytic	exo-1,4-β-D-glucanases	CBH	process along the cellulose chain
	cellobiohydrolases	EC 3.2.1.91	cleave cellobiose units from the end
	endo-1,4- β-D-glucanases	EG EC 3.2.1.4	cut glycosidic bond randomly in the cellulose chain
	1,4- β-D-glucosidases	BG	hydrolyze cellobiose to glucose
		EC 3.2.1.21	cleave glucose unit from cellooligosaccharides
hemicellulolytic	endo-1,4- β-D-xylanases	EC 3.2.1.8	hydrolyze internal bond in the xylan chain
	1,4- β-D-xylosidases	EC 3.2.1.37	cut xylose from xylooligosaccharides at the non-reducing end
	endo-1,4- β-D-mannanases	EC 3.2.1.78	hydrolyze internal bond in the mannan chain
	1,4- β-D-mannosidases	EC 3.2.1.25	cut mannose from xylooligosaccharides at the non-reducing end

These hydrolases could work synergistically to cleave polysaccharides into monosaccharides by creating new accessible sites for each other and relieving product inhibition (**Figure 1-11**) (Eriksson et al. 2002; Väljamäe et al. 2003). Typically, three steps, namely, transportation of enzymes from bulk solution to the substrate surface, adsorption of the enzymes to the substrates, hydrolysis of the polysaccharides into subunits, and desorption of enzymes and

products back to the bulk solution, are involved in the process of enzymatic hydrolysis (Walker and Wilson 1991). As a result, biomass sugars are released by hydrolyzing the cellulose and hemicellulose. The efficiency of biomass hydrolysis is restricted by many factors including (1) end products inhibition (glucose and cellobiose are inhibitory to BG and CBH, respectively); (2) non-productive binding of enzyme onto lignin and unproductive binding onto cellulose; (3) accessibility obstacles caused by lignin and hemicelluloses; and (4) denaturation and loss of enzymatic activity due to mechanical shear and proteolytic activity (Jorgensen et al. 2007).

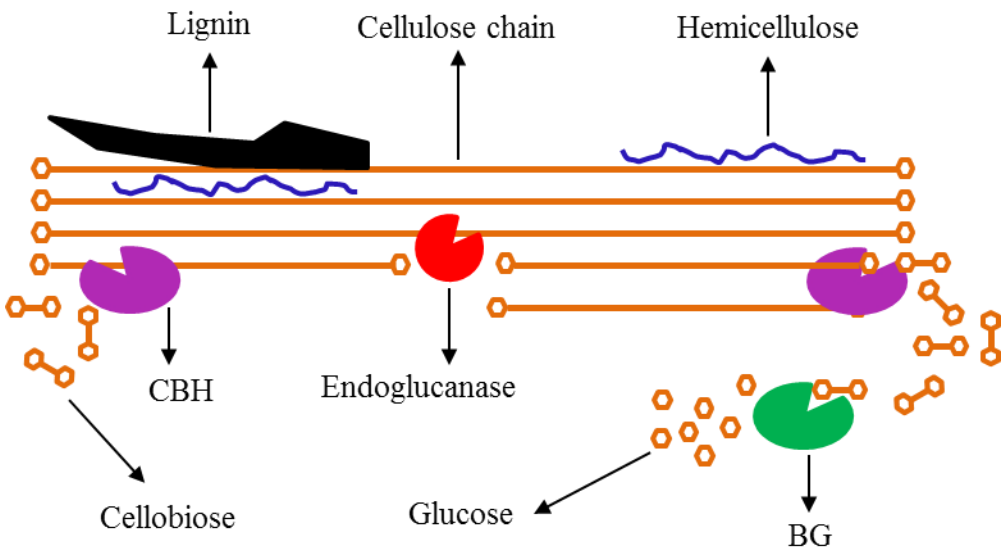

Figure 1-11. Schematic of biomass hydrolysis by synergism between cellulolytic enzymes.

In the past few decades, a significant amount of effort has been put into improving the efficiency of enzymatic hydrolysis. It is superior than acid hydrolysis for having low corrosion, mild operation conditions, high hydrolysis yield, and negligible inhibitory byproducts (Taherzadeh and Karimi 2007). However, the intrinsic problems associated with enzymatic hydrolysis are long hydrolysis time (Tengborg et al. 2001), expensive catalyst (Sheehan and Himmel 2001), and end-product inhibition (Linde et al. 2007). Strategies to enhance enzyme

performance include optimization of enzyme composition, addition of the surfactant, immobilization and recycling of enzymes, sequential hydrolysis and fermentation (SHF), simultaneous saccharification and fermentation (SSF), non-isothermal simultaneous saccharification and fermentation (NSSF), simultaneous saccharification and co-fermentation (SSCF), and consolidated bioprocessing (CBP) (Jorgensen et al. 2007; Taherzadeh and Karimi 2007).

1.3.3 Microbial fermentation

Depending on the type of lignocellulosic materials used, the monomeric sugars released after pretreatment and hydrolysis in the hydrolysate primarily include both hexose (glucose, mannose, galactose, fucose, and rhamnose) and pentose sugars (xylose and arabinose) (Keshwani and Cheng 2009). The theoretical yields of bioethanol from one ton hexose and pentose are 155 and 154 gallons, respectively (Ibraheem and Ndimba 2013).

A number of parameters have to be considered for evaluating the microbial fermentation performance: temperature range, pH range, alcohol tolerance, growth rate, productivity, osmotic tolerance, specificity, yield, genetic stability, and inhibitor tolerance (Balat 2011). For hexose fermentation, *Saccharomyces cerevisiae* and *Zymomonas mobilis* are frequently used for their elaborate uptake and consumption system preference for glucose (van Maris et al. 2006). *S. cerevisiae* turns out robust in the fermentation of lignocellulosic hardrolysates. The bacteria, *Z. mobilis* and *E. coli*, outperformed yeasts by their rapid fermentation rates (Hamelinck et al. 2005) and higher bioethanol yields (Gunasekaran and Raj 1999). But these strains are not able to ferment pentose. The commonly used xylose metabolism strains are *Candida shehatae*, *Pichia stipites*, and *Candia prapsilosis*. Genetically modified *Z. mobilis* and *E. coli* show their

advantages on bioethanol production. Some thermophilic anaerobic bacteria, *Thermoanaerobacter ethanolicus, Clostridium thermohydrosulfuricum, Thermoanaerobacter mathranii, Thermoanaerobium brockii, and Clostridium thermosaccharolyticum,* have also been studied for their performance as bioethanol producers (Balat 2011). Recently, interests have been drawn to butanol production by *Clostridium acetobutylicum* and *C. beijerinckii* as (Dahman 2012; Qureshi and Ezeji 2008). However, an efficient and rapid fermentation process for the biomass hydrolysates is still not a reality because a variety of inhibitory compounds associated with the pretreatment process seriously retards the microbial growth and biofuels production.

1.4 Cellulose-derived materials

The abundant biopolymer—cellulose, ca. 1.5×10^{12} tons annual production, is not only a source for biofuels but also for environmentally friendly bioproducts (Klemm et al. 2005). Historically, commodities such as textiles, ropes, canvas, paper, etc. are produced from natural cellulose fibers. The utilization of cellulose has been extensively expanded from the traditional energy sources, building materials (timber), and clothing to the fields of sustainable materials, nanocomposites, and medical and life-science devices by the novel research on nanocrystalline cellulose (also called cellulose nanocrystals) in the past two decades (Klemm et al. 2011). The intrinsic mechanical properties, reinforcing capabilities, abundance, and relatively high strength and stiffness at low density advance the tremendous potential of nanocrystalline cellulose.

1.4.1 Cellulose nanocrystals (CNCs) preparation

CNCs are the isolated crystalline cellulose with one dimension in the nanometer range (usually 3-30 nm in width), also being described as nanocrystalline cellulose (Klemm et al. 2011),

crystallites, cellulose nanowhiskers (Eichhorn 2011), cellulose nanofibers (Eichhorn et al. 2010), rod-like cellulose microcrystals. CNCs inherit the important properties from cellulose including fiber morphologies, mechanical properties, hydrophilicity, and wide chemical-modification capacity.

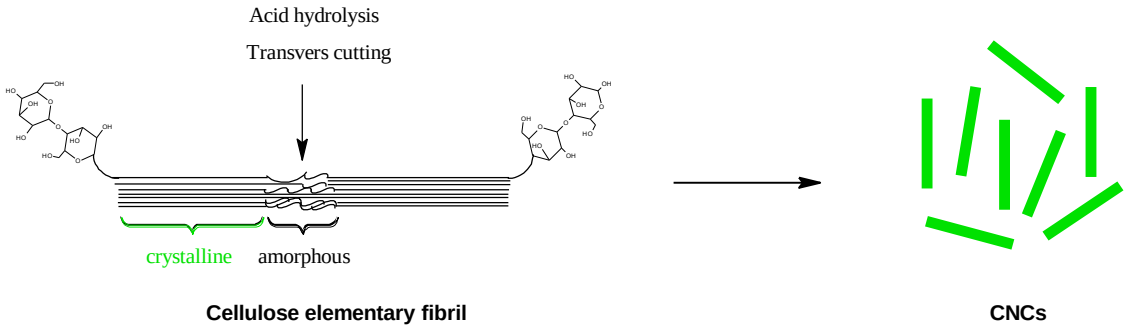

Figure 1-12. Schematic of CNCs production by acid hydrolysis.

CNCs are isolated from cellulose by treatment with strong acids (**Figure 1-12**). The acids hydrolyze the amorphous region of cellulose with a transvers cutting whereas the crystalline region is highly resistant to acid attack (Habibi et al. 2010). The acid treatment eventually leads to the removal of disordered cellulose microfibril parts and leaves the rod-like cellulose nanocrystals intact. Typically, strong acids, H_2SO_4 (Bondeson et al. 2006; Dong et al. 1998), HCl (Araki et al. 1998; Araki et al. 1999), H_3PO_4 (Camarero Espinosa et al. 2013), HBr (Sadeghifar et al. 2011), and mixed acids (Wang et al. 2008), are used to hydrolyze cellulosic material under strictly controlled conditions of temperature, time, and acid-to-solid ratio. The resulting suspension of CNCs is subjected to successive wash with centrifugation. A dialysis against distilled water with certain molecular weight cut-off removes free acids and other small molecules. The morphology and dimensions of CNCs vary highly on the isolation techniques and cellulosic sources (**Table 4**). Cotton, Avicel, and wood cellulose yield rod aspect ratio of 20-40,

whereas algal, bacterial, and tunicate cellulose generate larger dimensions with comparable aspect ratio.

Table 4. Dimensions of CNCs from various cellulose sources (Habibi et al. 2010).

Source	Length (nm)	Cross section (nm)
Algae (*Valonia*)	>1000	10-20
Bacterial cellulose	100-1000	5-50
Cotton	100-300	5-15
Cotton linter	100-500	6-30
Avicel	200-300	20-30
Ramie	50-250	5-10
Sisal	100-500	3-6.5
Tunicate	~1000	10-30
Softwood	100-200	3-5
Hardwood	140-150	4-5

The type of acids used in the CNCs preparation highly impacts the surface functionalities: HCl or HBr hydrolyzed CNCs particles are weakly charged whereas H_2SO_4 treatment results in negatively charged CNCs by the introduction of sulfate groups. A stable colloidal suspension is formed due to the repulsive electrostatic force between particles. The studies of the strengthening effect and optical properties of CNCs opens up a very promising application in nanocomposites, paper making, coating additives, security papers, food packaging, and gas barriers (Klemm et al. 2011).

1.4.2 CNCs surface modification

The new generation of cellulose based materials requires more on the properties, functionality, durability, and uniformity (Moon et al. 2011). However, owing to the natural hydrophilicity and polymerization, the utilization of CNCs is impeded in hydrophobic and non-polar media (Habibi 2014). With the presence of three hydroxyl groups on each AGU and the reducing end, the CNCs possess wide possibility for chemical surface modification. Three strategies are frequently used to modify the surface of cellulose nanoparticles (**Table 5**): (1) physical adsorption of molecules; (2) chemical modification with small molecules; and (3) polymer grafting. These modifications are necessary, even unavoidable, to adapt the interfacial properties of nanocellulose substrates and extend their use to highly sophisticated applications (Habibi 2014).

Physical adsorption, also referred as non-covalent modification, mostly define the adsorption of molecules or macromolecules onto the CNCs surface by electrostatic forces. Chemical modification primarily involves the chemical reaction between coupling agent and the hydroxyl or hemiacetal groups on CNCs. Polymer grafting is distinguished with chemical modification as the grafting agents used are usually large molecular weight with steric hindrance.

Table 5. The frequently used reagents for CNCs modification.

Reaction	Cellulose nanoparticles	Reagent
		Physical adsorption
Non-covalent	(CMC-MF)	cationic polyelectrolytes
		polyethyleneimine (Wågberg et al. 2008) poly(allylamine hydrochloride) (Wågberg et al. 2008) poly(diallyldimethylammonium chloride) (Wågberg et al. 2008)
	H_2SO_4-CNCs	anionic surfactant
		phosphoric ester of polyoxyethylene (9) nonylphenyl ether (Heux et al. 2000) phosphoric ester of ethoxylated nonylphenol (Bondeson and Oksman 2007)
	HCl-CNCs	nonionic surfactant
		sorbitan monostearate (Kim et al. 2009)
		Chemical modification
Esterification	Cellulose, CNCs	H_2SO_4 (Dong et al. 1998), acetic anhydride (Kim et al. 2002), acetyl chloride (Mukherjee et al. 2013), acetic acid (Braun and Dorgan 2008), vinyl acetate (Sèbe et al. 2013) alkenyl succinic anhydride (Yuan et al. 2006) palmitoyl acid (Berlioz et al. 2009) butyric, iso-butyric, hexanoic anhydride (Missoum et al. 2012)
Etherification	Cellulose, CNCs	monochloroacetic acid (Rácz et al. 1996) epoxypropyltrimethylammonium chloride (Hasani et al. 2008)
Silylation	Bacterial cellulose	alkyldimethylchlorosilanes (Habibi 2014)
Oxidation	Cellulose	TEMPO and NaOCl/NaBr (Isogai et al. 2011)
Urethanization	CNCs, MFC	isocyanates (Habibi 2014)
Amidation	Oxidized CNCs	amine (Habibi 2014)
Click chemistry	Alkyne-activated CNCs	azides and imidazolium bromide (Habibi 2014)
		Polymer grafting
Grafting onto	CNCs	amine-ended polymers (Harrisson et al. 2011) polypropylene maleic anhydride (Felix and Gatenholm 1991)
Grafting from	CNCs	ring opening polymerization (ROP) (Habibi 2014) atom transfer radical polymerization (ATRP)

1.4.3 CNCs-derived materials development

The potential and ideal nanoparticles—cellulose nanocrytals (CNCs) is of significant interests and possesses high reinforcement properties, high aspect ratio, low density, and functionalizability (Moon et al. 2011).

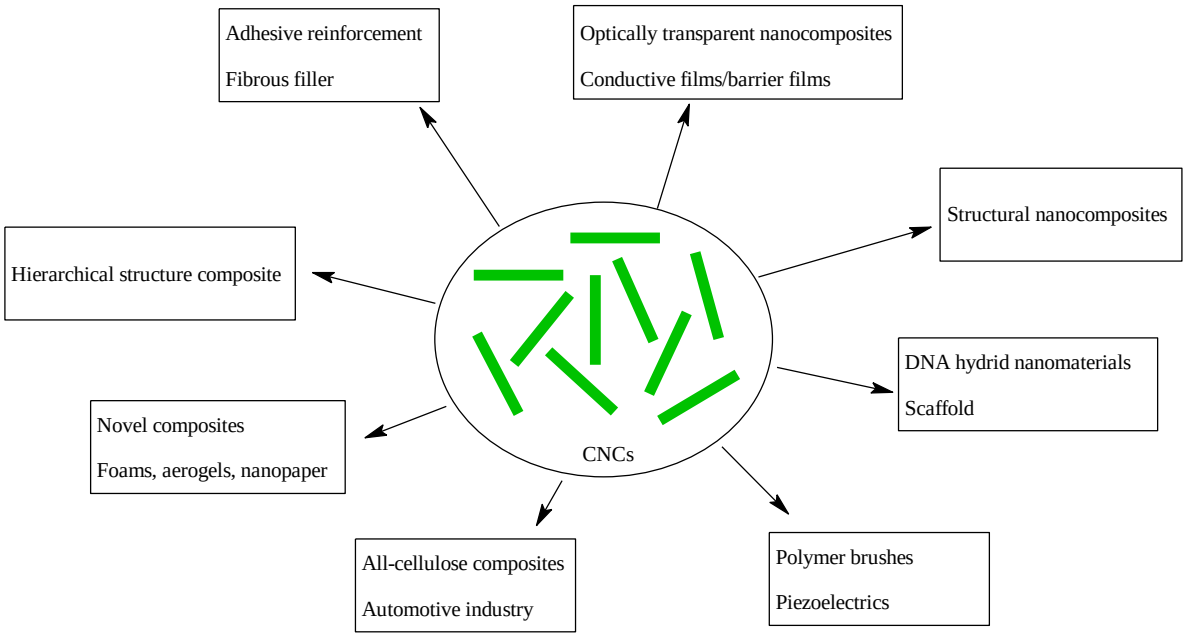

Figure 1-13. Development of CNCs-based engineered materials.

A variety of cellulose sources have been used for production of CNCs through acid hydrolysis: wood, plant, tunicate, algae, and bacterial cellulose (Habibi et al. 2010). Sulfuric acid is most frequently used to produce CNCs as it introduces a negative sulfate group on the particle surface resulting in a more stable suspension by the electrostatic repulsion force (Habibi 2014). The special properties such as nanoscale dimensions, unique morphology, low density, and mechanical strength etc. impart CNCs potential applications in the nanocomposites and neat films (**Figure 1-13**) (Eichhorn et al. 2010; Moon et al. 2011). However, the application and compatibility of CNCs to polymer matrix are limited by the high number of hydroxyl groups and

hydrophilicity. Hence, the surface chemical modification of CNCs is required to adapt the interfacial properties of CNCs or balance their hydrophilicity-hydrophobicity as aforementioned (Habibi 2014; Missoum et al. 2013).

1.5 Research objectives

With the background being said, the main objectives of this research include:

Organosolv pretreatment of woody biomass is promising and efficient in terms of breaking the matrix, delocalizing lignin, and enhancing the accessibility of enzymes. It is well-known that the residuals – lignin and xylan – on the pretreated substrates affect the efficiency of enzymatic hydrolysis negatively. How each of these two residuals associate with the enzymatic hydrolysis, especially quantitatively related to the hydrolysis rate and yield, remains unclear. So, this study attempted to correlate the content of lignin and xylan with the woody biomass hydrolysis rate and yield using Novozyme 22C.

Hemicellulose accounts for 20-30% of the woody biomass and it is readily hydrolyzed into monomeric sugars (glucose, xylose, and mannose) during the process of pretreatment. These sugars with small molecular weight in the prehydrolysate were not fully utilized. One option is to biologically convert them into bioethanol or other useful chemicals to add values to the bioconversion platform. However, the presence of large amount of degraded compounds is inhibitory to this biological conversion without detoxification. Hence, the second objective of this study was trying to chemically convert the hemicellulose sugars into valuable chemicals such as lactic acid. Aqueous alkaline solution was used to catalyze the low molecular

carbohydrates to lactic acid. The catalytic conversion kinetic was studied and the efficiency by different alkali was compared.

Apart from the lactic acid production, gluconic acid and xylonic acid can be produced from hemicellulose sugars through microbial fermentation. The oxidation of glucose and xylose quantitatively to gluconic and xylonic acid respectively by *Gluconobacter oxydands* provides additional values to the utilization of lignocelluloses. It has been observed that the *G. oxydands* metabolize glucose and xylose in different pathways. However, few studies illustrated the different fermentation profiles on the two common hemicellulose sugars. Therefore, we targeted to use simple batch fermentation to confirm the metabolism pathways and to investigate the effect of pH and end products inhibition on the production of gluconic acid and xylonic acid.

The cellulose nanocrystals (CNCs) isolated from cellulose by acids treatment showed potential application in engineered materials. Nevertheless, the intrinsic hydrophilicity of cellulose restricts its compatibility in non-polar solvent. In order to balance the hydrophilicity-hydrophobicity of CNCs and enhance its interfacial compatibility with other materials, critical surface modification is required to improve their properties. Thus, the final objective of this study was to investigate the effect of different type of acid treatments and the source of cellulose on the chemical, optical, and thermal properties of CNCs. In addition, CNCs were chemically modified by grafting hydrophobic molecules or polymer to extend its compatibility and application.

Chapter 2 Distinct roles of residual xylan and lignin in limiting enzymatic hydrolysis of organosolv pretreated biomass

2.1 Background

The biochemical conversion process consists of multiple stages converting biomass to fermentable sugars for the production of advanced biofuels (such as butanol and terpenes). Biomass feedstock is first pretreated and then subjected to enzymatic hydrolysis with subsequent microbial fermentation (or simultaneous saccharification and fermentation) of sugars to alcohols or terpenes by yeast or bacteria (Ezeji et al. 2007; McAndrew et al. 2011; Peralta-Yahya et al. 2011; Yu et al. 2011). The recalcitrant structure of cellulose and its close association with the lignin and hemicellulose matrix make it highly resistant to enzymatic hydrolysis (Himmel et al. 2007b). Therefore, lignocellulosic substrates must either be physically or chemically pretreated to improve the accessibility to enzymes for hydrolysis (Kumar and Wyman 2009a). Various pretreatment methods including steam explosion, dilute acid, hot water, ammonia fiber expansion (AFEX) and organosolv processes are currently being assessed for their ability to improve enzymatic hydrolysis (Lau et al. 2010; Wyman et al. 2011). Among these pretreatment processes, organosolv pretreatment has shown good potential for producing lignocellulosic substrates from hybrid poplar and lodgepole pine with high digestibility (Pan et al. 2006; Tu et al. 2007b). However, the residual xylan in organosolv pretreated biomass was still an important factor affecting the glucan digestibility significantly (Chum et al. 1988). Furthermore, residual lignin also plays an important role in limiting enzymatic hydrolysis of cellulose although lignin content is often low in the organosolv pretreated substrates (Pan et al. 2005). Pan et al.(Pan et al. 2005) found a strong correlation (R^2=0.91) between the residual lignin content and the final hydrolysis yield for four organosolv pretreated substrates from softwood. As a result, the

amounts of residual xylan and lignin are two important factors limiting enzymatic hydrolysis, although other factors (such as crystallinity, acetyl group, pore size and surface area accessibility) have been suggested to affect the initial hydrolysis rate and extent of enzymatic hydrolysis as well (Arantes and Saddler 2011; Laureano-Perez et al. 2005; Zhu et al. 2010).

It is typically accepted that lignin limits the enzyme accessibility to elementary cellulose fibril by wrapping the cellulose and hemicellulose within microfibrils (Fengel and Wegener 1989; Zhang and Lynd 2004; Zhu et al. 2008). Pretreatment generally disrupts the close association of lignin to microfibrils. However, the high lignin content in pretreated substrates still affects the enzymatic hydrolysis due to physical blockage and non-productive binding between enzyme and lignin (Berlin et al. 2005; Qing et al. 2010; Tu et al. 2009). Previously, we have suggested using surfactants to reduce non-productive binding and improve enzymatic hydrolysis of steam exploded lodgepole pine (Tu et al. 2009). Lignin removal generally is thought to be able to increase the ultimate hydrolysis yield, not the hydrolysis rate (Zhu et al. 2008). Hemicellulose removal (especially xylan removal) can increase the initial hydrolysis rate significantly (Grohmann et al. 1989; Ohgren et al. 2007). Xylanase supplementation has been suggested to reduce effects of xylan on enzymatic hydrolysis of pretreated biomass and improve the final hydrolysis yield (Ohgren et al. 2007; Zhang et al. 2011). Since most of xylan in biomass is highly acetylated, deacetylation has been found to greatly improve the cellulose accessibility and the hydrolysis rate (Chen et al. 2012; Kumar and Wyman 2009b; Labbe et al. 2012). However, few studies have focused on quantitatively distinguishing the distinct roles of residual xylan and lignin in limiting the enzymatic hydrolysis.

In this chapter, we used ethanol organosolv pretreatment to fractionate Loblolly Pine (*Pinus taeda*) and Sweetgum (*Liquidambar styraciflua*) under the same condition. The resultant substrates with different xylan and lignin contents were used to distinguish the effects of residual xylan and lignin on the enzymatic hydrolysis of pretreated substrates. Scanning electron microscopy (SEM) was used to characterize the cell wall disruption and surface properties of pretreated biomass. Langmuir adsorption isotherm was used to characterize enzyme affinity to the pretreated substrates and the initial hydrolysis rate. Quantitative information on enzymatic hydrolysis was evaluated based on the initial hydrolysis rate and the final hydrolysis yield. The correlation between the amount of residual xylan and the initial hydrolysis rates, and the correlation between the amount of residual lignin and the final hydrolysis yields were established. Effects of residual xylan and lignin on ethanol yields were also compared on pretreated softwood and hardwood in the simultaneous saccharification and fermentation (SSF) process.

2.2 Materials and methods

Woody biomass and pretreatment methods

Loblolly pine and Sweetgum wood chips were collected from the Forest Products Laboratory at Auburn University. The initial moisture content of these wood chips was approximately 9.0 wt%. Wood chips were ground by a Wiley mill (Thomas Scientific, Philadelphia, PA), and the wood powder between 20-40 mesh was collected for the chemical composition analysis. The wood chips was reduced to an average size of $1.0 \times 2.0 \times 0.3$ cm^3 (L ×W ×H) by a Waring commercial blender (Dynamics Corporation of America, New Hartford, CT) prior to the organosolv pretreatment. Organosolv pretreated Loblolly pine (OPLP) and Sweetgum (OPSG) were prepared in a 4 L Parr batch reactor (Parr Instrument Co., Moline, IL)

as previously described (Tu et al. 2009). Briefly, wood chips (400 g) were loaded into reactor (7:1 liquor/solid ratio) and treated at 170 ℃ for 60 min with 65% ethanol and 1.1% (w/w) sulfuric acid. After pretreatment the slurry was fractionated into a solid fraction and liquid fraction (prehydrolysate) by filtration. The prehydrolysate was collected and stored at 4 ℃ for later use, while the solid materials (200 g) were homogenized with a blender (Qster, Milwaukee, USA) for 30 seconds and washed with aqueous water (600 mL) at room temperature. The chemical composition of original raw biomass and pretreated biomass was listed in **Table 6.**

SEM analysis of untreated and pretreated substrates

SEM analysis of raw biomass (40 mesh), OPLP and OPSG substrates was performed with a field emission scanning electron microscopy (JEOL 7000F) operated at 20.0 KV. The samples were coated with a thin gold layer (50 nm) using PELCO SC-6 Sputter Coater.

Chemical analysis of raw biomass and pretreated substrates

The extractives content of raw biomass and pretreated substrates (wood powders, 20-40 mesh) was determined using acetone extraction according to the standard method as described previously (Sluiter et al. 2011). The lignin and carbohydrate composition of Loblolly Pine were determined using the extractive-free samples according to National Renewable Energy Laboratory protocol (Ruiz and Ehrman 1996). A Shimadzu (LC-20A) HPLC system consisting of degasser, autosampler, LC-20AD pump and RID-10A detector coupled with a 300 mm × 7.8 mm i.d., 9 μm, Aminex HPX-87P column, with a 30 mm × 4.6 mm i.d. guard column of the same material(Bio-Rad, Hercules, CA) was used to separate and quantitate individual sugars. Water was used as the mobile phase at an isocratic flow rate of 0.6 mL/min to separate sugars, and the

temperature of column was maintained at 85 ℃ during the elution. The chemical composition of biomass was determined in duplicates.

Cellulase enzymes and enzymatic hydrolysis

Commercial cellulase (Novozyme 22C) was obtained from Novozymes (Franklinton, NC). The enzyme activity of the Novozyme 22C (100 FPU/mL) was determined using Whatman No. 1 filter paper as the substrate and the β-glucosidase activity (343 IU/mL) of Novozyme 22C was determined using *p*-nitrophenyl-β-D-glucoside (PNPG) as a substrate. Multifect Pectinase (~1,660 IU/mL, 24 mg/mL protein) and Multifect Xylanase (~25,200 IU/mL, 13.4 mg/mL protein, according to Dien et al.(Dien et al. 2008)) were used as accessory enzymes (Genencor International, Palo Alto, CA) for the enzymatic hydrolysis of pretreated substrates.(Dien et al. 2008) Cellulase from *Trichoderma reesei* ATCC 26921 was obtained from Sigma–Aldrich (St. Louis, MO) for the cellulase adsorption isotherm determination. The enzymatic hydrolysis was carried out in duplicates.

Enzymatic hydrolysis of OPLP and OPSG were carried out in 100 mL of 50 mM sodium citrate buffer (pH 4.8) at a 2% consistency (w/w glucan) as previously described (Tu et al. 2007a). The reaction mixture of pretreated biomass and enzyme was incubated at 45 ℃ with shaking at 150 rpm. The cellulase loading was 10 or 20 FPU/g glucan. No extra β-glucosidase enzyme was added into the reaction due to the sufficient β-glucosidase activity in the Novozyme 22C. Samples were taken from the reaction at various time intervals (2, 5, 8, 12, 24, 48 and 72 h) and centrifuged to remove the insoluble material (solid precipitate). The glucose and xylose contents were measured by HPLC with the same Aminex HPX-87P column. The glucose or xylose yield (%) of the substrates was calculated from the released glucose or xylose content, as

a percentage of the theoretical sugars available in the pretreated substrates. Initial hydrolysis rate (r) was calculated based on the released sugars in the first five or six hour of enzymatic hydrolysis of substrates ($\boldsymbol{r = (C_t - C_0)/t}$, where C_0 and C_t and are the sugar concentrations at 0 and t h respectively). For the pectinase and xylanase supplementation, the enzymatic hydrolysis was carried out with 10 FPU of Novozyme 22C per gram of glucan, and Multifect Pectinase or Multifect Xylanase were added into the reaction mixture based on the protein content at 3.6 mg/g glucan and 2.7 mg/g glucan as previously described (Dien et al. 2008)**.** The protein content in the supernatant was measured by the Bradford assay using bovine serum albumin (BSA) as the protein standard.

Yeast strain, culture medium and SSF process

Saccharomyces cerevisiae (Baker's yeast) was grown in a YPG liquid medium composed of 10 g/L yeast extract, 20 g/L peptone and 20 g/L glucose at 30 ℃. Simultaneous saccharification and fermentation (SSF) was performed (with 10 or 20 FPU/g glucan of Novozyme 22C) in 50 mM citrate buffer with pretreated OPLP and OPSG substrates (2% w/w glucan) at 37 ℃ and 180 rpm for 96 h. The initial yeast inoculation was 2.0 g/L. Samples were taken and analyzed by HPLC for sugars and ethanol determination with a 300 mm × 7.8 mm i.d., 9 μm, Aminex HPX-87H column, with a 30 mm × 4.6 mm i.d. guard column of the same material (Bio-Rad, Hercules, CA). Ethyl xyloside in SSF samples was analyzed by an Ultra Performance LC Systems (Waters, Milford, MA) coupled with a quadrupole time-of-flight mass spectrometer with electrospray ionization (ESI) in the positive ESI-MS operated by the Masslynx software (V4.1). Sample was directly injected into the ESI source at a flow rate of 50μL/min with a mobile phase of 100% acetonitrile (ACN) or 50% ACN in water. The ion source voltages were

set at 3 KV for positive and negative ion mode acquisitions, respectively. The sampling cone was set at 37 V and the extraction cone was at 3 V. In both the positive and negative ion modes the source and desolvation temperature was maintained at 120 ℃ and 225 ℃, respectively with the desolvation gas flow at 200 L/h.

Cellulase adsorption isotherm

Cellulase adsorption on organosolv pretreated substrates was performed at 4 ℃ in 50 mM citrate buffer (pH 4.8) as described previously **(Tu et al. 2007a).** Cellulase C2730 (from *Trichoderma reesei* ATCC 26921, 44 mg protein/mL, Sigma-Aldrich, St. Louis, MO) was used to determine the adsorption isotherm, Novozyme 22C was not used due to the high β-glucosidases in this cellulase mixture. A range of enzyme concentrations from 0.01 mg/mL to 2.0 mg/mL were added in 50 mM citrate buffer (pH 4.8) with the substrates suspended at 2% consistency (based on glucan). The mixture was incubated at 4 ℃ for 2 h to reach equilibrium. The protein content in the supernatant was determined for the free cellulase by Bradford assay using bovine serum albumin (BSA) as the protein standard. The adsorbed cellulase was calculated by taking the difference between the initial cellulase content and free cellulase content in the supernatant. The classical Langmuir adsorption isotherm was applied to the cellulase adsorption on OPLP and OPSG in solution. In this case, the surface concentration of adsorbed enzymes (Γ) was given by the equation

$$\Gamma = \frac{\Gamma_{max} KC}{1 + KC}$$

where Γ_{max} is the surface concentration of protein at full coverage (mg/g substrate), *K* is the Langmuir constant (mL/mg), and *C* is the free protein concentration in the bulk solution (mg/mL).

2.3 Results and discussion

2.3.1 Chemical composition of organosolv pretreated biomass

The chemical composition of untreated Loblolly Pine (softwood) and Sweetgum (hardwood) were compared in **Table 6**. The carbohydrates (cellulose and hemicellulose) represented approximately 63.3 wt% in Loblolly Pine and 63.4 wt% in Sweetgum. The total lignin content was higher in softwood (28.7 wt%) than that in hardwood (25.8 wt%). These results were in agreement with previous reports on the composition of pine and Sweetgum.(Frederick et al. 2008; Sievers et al. 2009; Wei et al. 2011; Zhu and Pan 2010b) After organosolv pretreatment, the lignin content in OPLP substrate was 18.6%, which was twice that of OPSG substrate (9.0%). The solid yields were 53.8% (Loblolly Pine) and 58.7% (Sweetgum). The carbohydrate portion of the OPLP and OPSG substrates was composed mainly of glucan with similar content, but xylan content (9.7%) was much higher in hardwood OPSG substrate than that in softwood OPLP substrate (2.9%). The mannan content was reduced from 12.2% to 4.5 % in OPLP.

Table 6. Chemical composition of untreated and organosolv pretreated biomass.

Compositions	Untreated Loblolly pine (%)	Untreated Sweetgum (%)	OPLP substrate (%)	OPSG substrate (%)
Acetone extractives	1.64 ±0.08	0.99 ±0.09	8.53 ±0.19	8.47 ±0.21
Acid-insoluble lignin	28.48 ±0.04	23.56 ±0.28	18.38 ±0.17	8.16 ±0.03
Acid-soluble lignin	0.26 ±0.03	2.24 ±0.02	0.23 ±0.06	0.87 ±0.03
Glucan	41.33 ±0.49	41.19 ±0.73	63.32 ±1.24	69.80 ±1.78
Xylan	6.34 ±0.13	16.18 ±0.50	2.93 ±0.79	9.74 ±0.53
Galactan	2.16 ±0.09	1.87 ±0.32	NA	NA
Arabinan	1.30 ±0.11	0.83 ±0.11	0.90 ±0.21	NA
Mannan	12.17 ±0.39	3.33 ±0.49	4.50 ±0.59	3.01 ±0.28
Total	93.69	90.20	98.79	100.05

2.3.2 SEM analysis of untreated, pretreated, and hydrolyzed biomass

SEM can reveal surface morphology of plant cell wall of pretreated biomass (Donohoe et al. 2008; Jung et al. 2010; Kristensen et al. 2008). The SEM images of raw biomass and pretreated biomass (**Figure 2-1A-D**) indicated that the bound fibers in biomass were liberated or separated after organosolv pretreatment. Organosolv pretreatment is a process similar to pulping, by which the biomass is reduced into a fibrous mass. It ruptures the bonds between fibers within biomass. Furthermore, we observed considerable amount of spherical droplets covering the cell wall surface in OPLP (**Figure 2-1C**). On the contrary, very few droplets could be seen from the cell wall surface of OPSG (**Figure 2-1D**). The diameter of these droplets was from 0.2 μm to 10 μm. Previously, these droplets on plant cell wall of pretreated biomass were found to contain lignin by FTIR and NMR analysis (Donohoe et al. 2008). These lignin droplets tended to coalesce together probably due to the hydrophobicity of the lignin. The lignin droplets re-

dispersed on the surface of plant cell wall depending on the pretreatment methods. Dilute acid pretreatment produced numerous lignin droplets on the surface of pretreated corn stover (Donohoe et al. 2008), while limited amount of lignin droplets displayed on substrates from the ethanol organosolv process. This occurred probably because the organic solvent washed out the lignin droplets that precipitated on the surface of pretreated biomass and some lignin re-precipitated on the surface of organosolv pretreated biomass when washed with water. Fewer lignin droplets on OPSG could be caused by the lower lignin in raw biomass and hardwood lignin being easier to break down. For the structural changes, we observed the rupture of fibers and cracks on the surface fibers in OPLP, but not in OPSG. The surface of OPSG was much smoother than that of OPLP. After enzymatic hydrolysis (72h), residues of OPLP and OPSG were also examined by SEM (**Figure 2-1E-F**). More packed and uniform lignin was shown in OPSG residues (**Figure 2-1F**) and more un-hydrolyzed big particles (20-50 μm) were shown in OPLP residues (**Figure2-1E**).

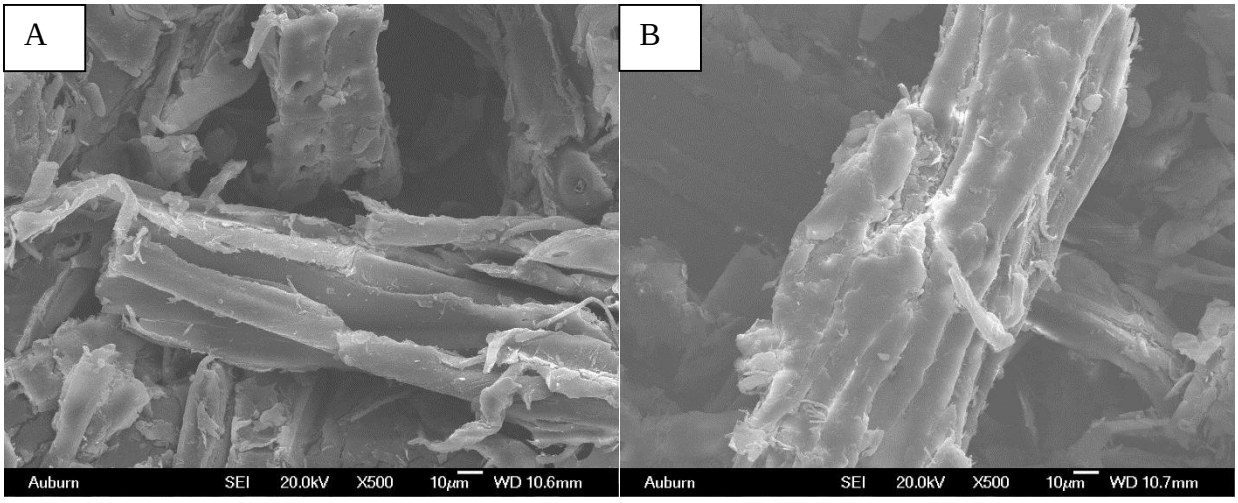

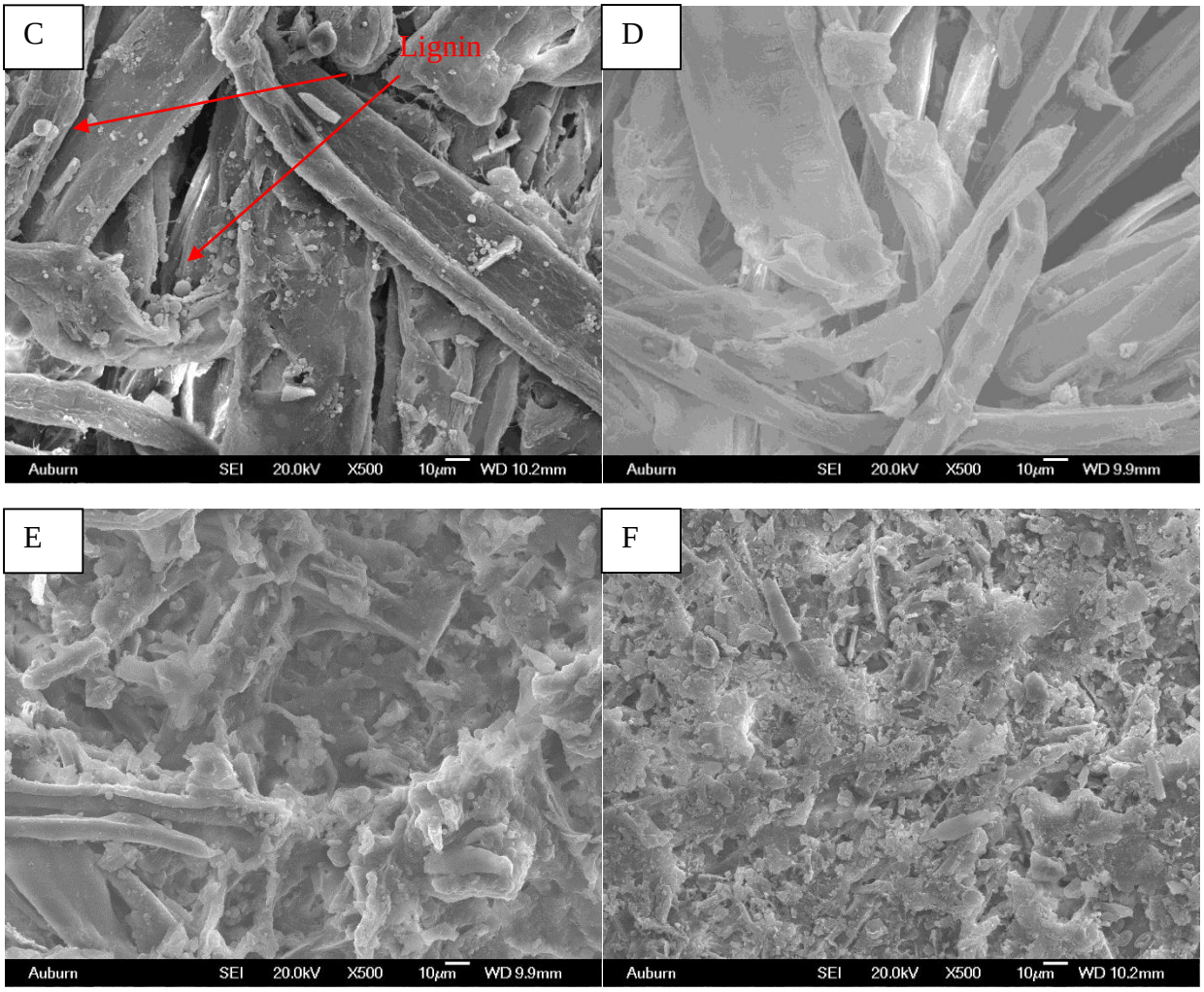

Figure 2-1. SEM images of the original Loblolly Pine (A), Sweetgum (B), OPLP (C), OPSG (D), and enzymatic hydrolyzed OPLP (E) and OPSG (F) after 72 h.

2.3.3 Effects of residual xylan and lignin on enzymatic hydrolysis of pretreated biomass

The effects of residual xylan and lignin on enzymatic hydrolysis of OPLP and OPSG substrates using Novozyme 22C were first examined (**Figure 2-2**). The glucan-to-glucose yield reached 60% on OPLP, and 89% on OPSG under the 10 FPU of enzyme loading per gram of glucan. When we increased the enzyme loading to 20 FPU, the glucose yield of OPLP increased significantly to 81%, and the OPSG substrate was almost completely hydrolyzed. The hydrolyzability of OPSG substrate was found to be much better as compared to the OPLP

substrate, probably because of higher residual lignin content (19%) in the softwood OPLP substrate (**Table 6**). However, when we examined the glucan hydrolysis curve, the hydrolysis yield of OPLP was higher than that of OPSG in the initial phase (12 h). The initial hydrolysis rate (1.00 or 1.45 g/L/h) of glucan was higher in OPLP than that (0.68 or 1.19 g/L/h) in OPSG under 10 or 20 FPU, although the amount of residual lignin was higher in OPLP. This indicated the residual lignin unlikely play a significant role in the initial hydrolysis of organosolv pretreated biomass. Interestingly, we observed the residual xylan in OPSG substrate (9.7%) was three-fold higher than that in OPLP substrate (2.9%), which could limit the initial enzymatic hydrolysis. It suggested that the residual xylan in pretreated substrate affected the initial hydrolysis rate more than the residual lignin. As for the xylose yield of enzymatic hydrolysis of OPLP and OPSG substrates (**Figure 2-2B**), the softwood OPLP substrates showed lower xylose yield (43%) than hardwood OPSG substrate (87%) after 72 h under 10 FPU of enzyme loading. Increasing the enzyme loading to 20 FPU resulted in higher xylose yields in OPLP substrate (66%) and OPSG substrate (~100%). The higher amount of residual lignin in OPLP substrate could be the main reason for its lower xylose yield. The initial hydrolysis rate of xylan was also lower in OPLP than that in OPSG. In the experiment that follows, we further explored the roles of residual xylan and lignin on the enzymatic hydrolysis of OPLP and OPSG substrates with the supplementation of pectinase and xylanase.

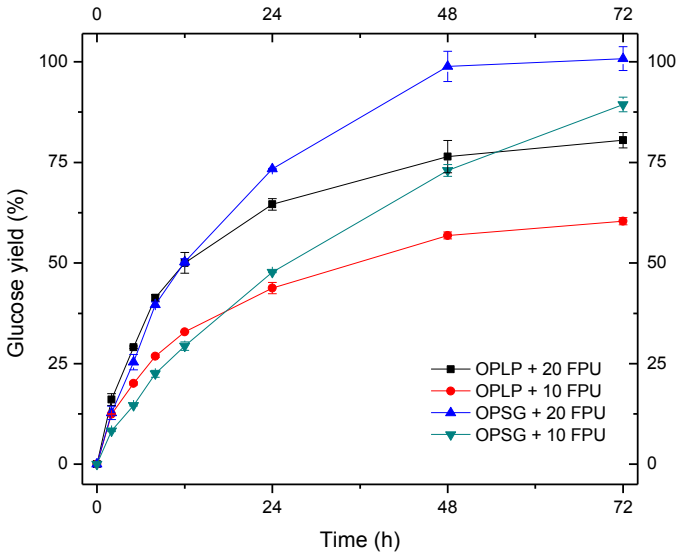

(A)

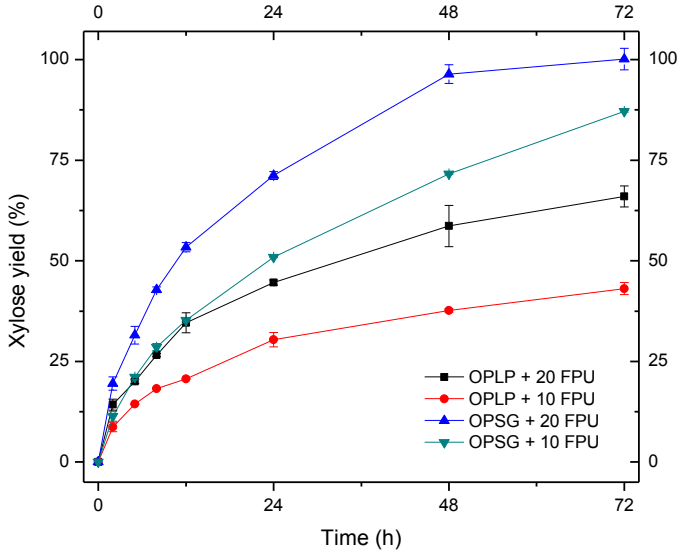

(B)

Figure 2-2. Effect of enzyme loading on the enzymatic hydrolysis of glucan (A) and xylan (B) in OPLP and OPSG substrates.

2.3.4 Effects of supplementing enzymes on enzymatic hydrolysis of pretreated biomass

The effects of supplementing pectinase and xylanase respectively on enzymatic hydrolysis of OPLP and OPSG substrates were evaluated with the enzyme loading of 10 FPU (**Figure 2-3**). Pectinase supplementation has been found to increase the glucan hydrolysis yields considerably for various pretreated substrates (Berlin et al. 2007; Lau et al. 2010). Supplementing pectinase at 3.65 mg/g glucan, the glucose yield increased from 60% to 68% for OPLP substrate after 72 h, and from 89% to 100% for OPSG substrate (**Figure 2-3A**). The xylose yield increased from 43% to 48% for OPLP substrate, and from 87% to 100% for OPSG substrate (**Figure 2-3B**). The pattern for initial hydrolysis rate did not change. The initial glucan hydrolysis rate was still higher in OPLP substrate.

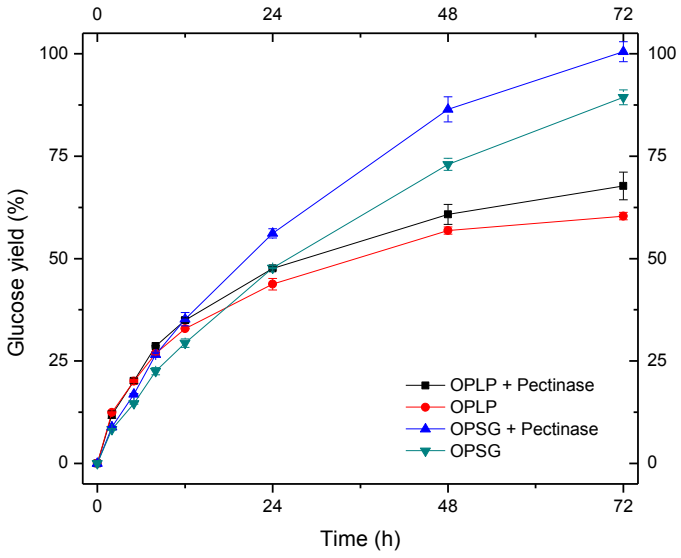

(A)

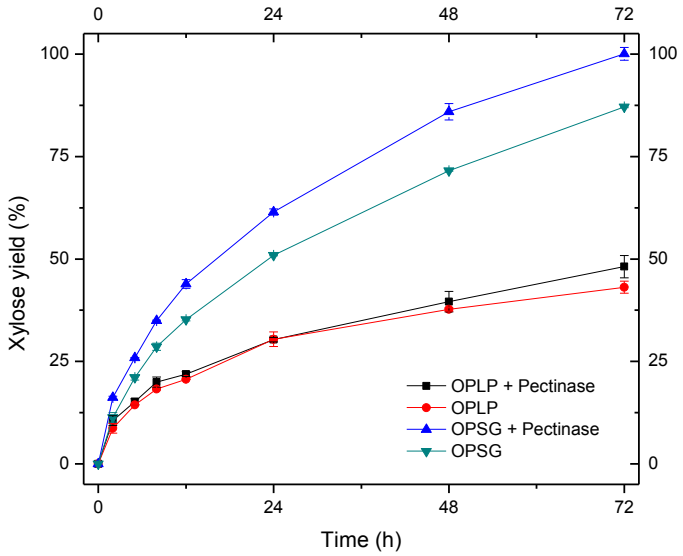

(B)

Figure 2-3. Effect of pectinase on the enzymatic hydrolysis of glucan (A) and xylan (B) in OPLP and OPSG substrates.

Supplementing xylanase at 2.7 mg/g glucan, the glucose yield increased from 60% to 67% for OPLP substrate after 72 h, and from 89% to ~100% for OPSG substrate (**Figure 2-4**). Moreover, the initial hydrolysis rates of glucan were improved differently on the OPLP and OPSG substrates. The initial hydrolysis rate of glucan in OPSG substrate was increased from 0.68 g/L/h to 1.02 g/L/h, and the initial hydrolysis rate of glucan in OPLP substrate remained almost the same at ~1.04 g/L/h. It indicated that xylanase affected the initial hydrolysis rate in hardwood by hydrolyzing the xylan or the xylooligomers present in the solution. The hardwood substrate (OPSG) could be hydrolyzed much quicker than softwood substrate (OPLP) after removing xylan, and the enzymatic hydrolysis of both substrates were still limited due to the existence of lignin.

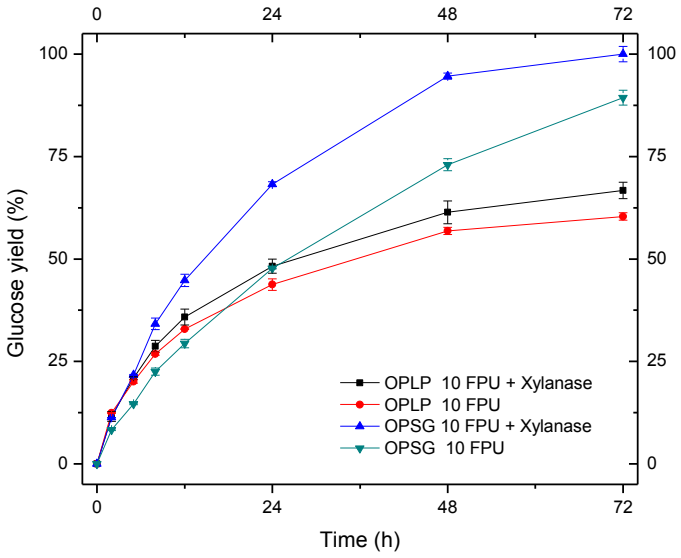

(A)

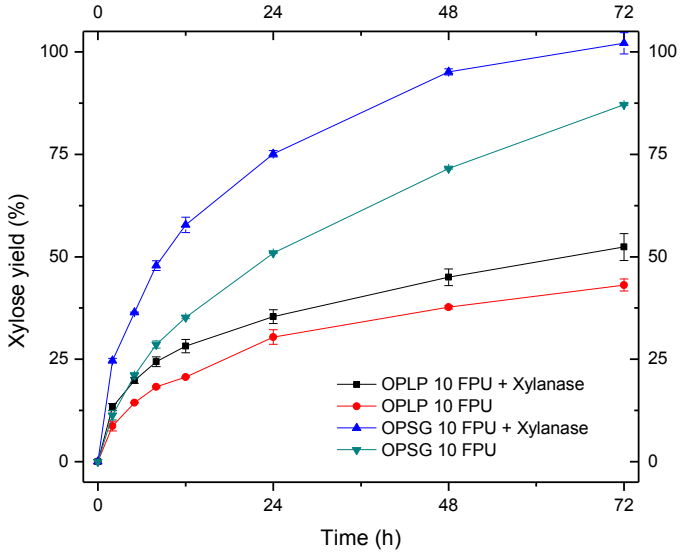

(B)

Figure 2-4. Effect of xylanase on the enzymatic hydrolysis of glucan (A) and xylan (B) in OPLP and OPSG substrates.

2.3.5 Effects of residual xylan on ethanol yields and ethyl xyloside formation in the SSF process

The ethanol yields of OPLP and OPSG substrates in the SSF process have also been compared under enzyme loadings of 10 FPU and 20 FPU (**Figure 2-5A**). The same pattern was observed in terms of the initial ethanol production rates and the final ethanol yields. OPSG substrates showed higher ethanol yields (8.8 g/L and 10.3 g/L) than OPLP substrates (7.8 g/L and 9.8 g/L) respectively after 96 h for both enzyme loadings. However, the initial ethanol production rates with OPLP substrate were 0.47 g/L/h and 0.81 g/L/h at 10 FPU and 20 FPU respectively. The initial ethanol production rates with OPSG substrate were 0.31 g/L/h and 0.62 g/L/h at 10 FPU and 20 FPU respectively. It suggested that higher residual xylan content in OPSG substrate resulted in lower initial ethanol production rates, and higher residual lignin content in OPLP substrate resulted in lower final ethanol yields. Meanwhile, we observed that it took about 58 h for the ethanol yield from OPSG in SSF to catch up with that from OPLP substrate (10 FPU). In the enzymatic hydrolysis with the same enzyme loading, it took about 17 h for the glucose yield of OPSG substrate to catch up with that in OPLP substrate. This probably was caused by the different glucan hydrolysis rate under different temperatures (37 ℃ vs 45 ℃). When enzyme loading was increased to 20 FPU, it took ~ 20 h for OPSG to reach the same ethanol yield as OPLP, and then exceeded the ethanol yield in OPLP until the end of the SSF process. Interestingly, we also found that xylose concentration increased steadily in the first 48 h and then decreased until 96 h in the SSF process under 20 FPU (**Figure 2-5B**). However, the xylose concentration kept stable after 48 h under 10 FPU. This indicated that released xylose under high enzyme loading could be converted to other products in the SSF process.

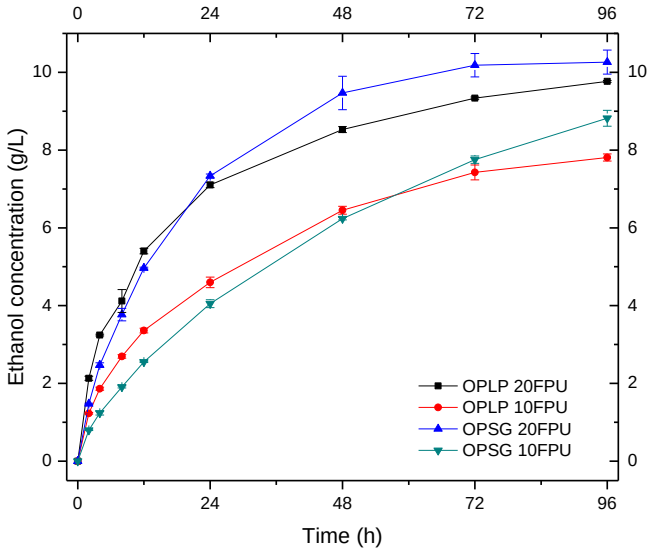

(A)

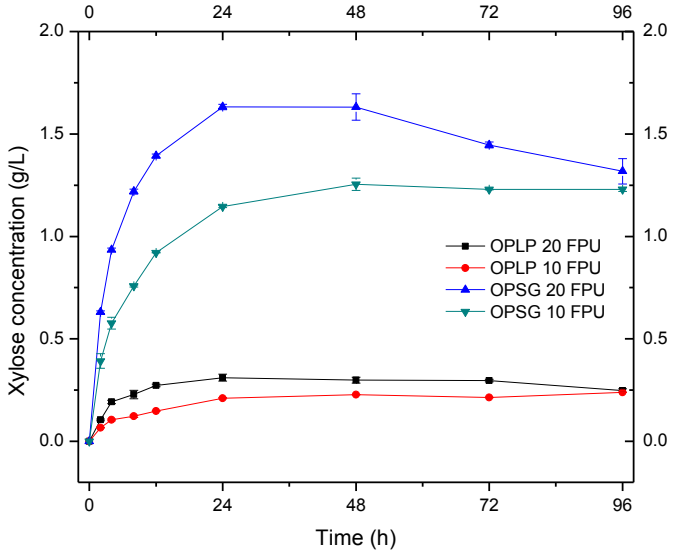

(B)

Figure 2-5. Effects of enzyme loading on ethanol yield (A) and xylose yield (B) in the SSF process.

HPLC and LC/MS were used to analyze potential product between xylose and ethanol in the SSF process. HPLC chromatograms (**Figure 2-6**) indicated the xylose concentration decreased after 48 h and another compound (ethyl xyloside) increased correspondingly. This

agreed well with the previous report in SSCF of paper sludge (Zhang et al. 2009). The mass spectra results showed that a new compound with *m/z* 179.09 ($[M+H]^+$) was produced after 48 h. A composition analysis of this compound by the Masslynx software gave a formula of $C_7H_{14}O_5$ (with 3.9 ppm mass error), which match to the chemical formula of ethyl xyloside (**Figure 2-7**). The ethyl xyloside concentration of OPSG in SSF with 20 FPU/g glucan at 96 h was 2.25 ± 0.21 g/L.

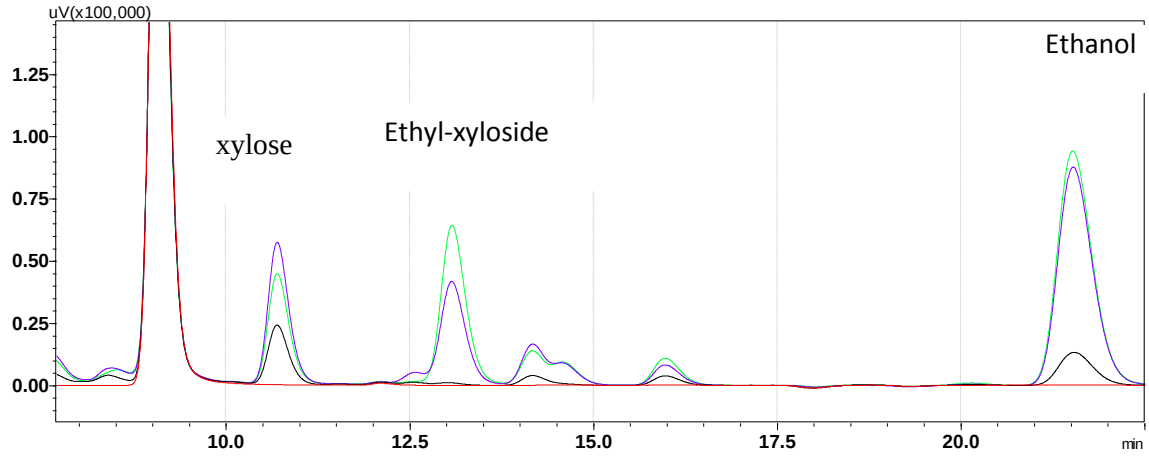

Figure 2-6. Ethyl xyloside formation in the SSF process at 0 (red), 2 (black), 48 (purple), and 96 h (green).

In the SSF process, residual xylan was also found to affect the fermentation step. The xylose concentration unexpectedly decreased after 48 h. One possible reason was that xylose or xylan reacted with ethanol to produce ethyl xyloside. A similar observation has been reported in a simultaneous saccharification and co-fermentation of paper sludge (Zhang et al. 2009). This is a reversible reaction; significant amount of xylose or xylan is converted into ethyl xyloside in the high consistency hydrolysis (**Figure 2-5B**). Due to the consumption of ethanol in this potential enzymatic catalyzed reaction, the formation of ethyl xyloside will considerably reduce the final ethanol yield if released xylose is not consumed by the microorganism. Therefore, xylose

fermenting microorganism development is critical to improve the total ethanol or other alcohols yield from glucan and xylan.

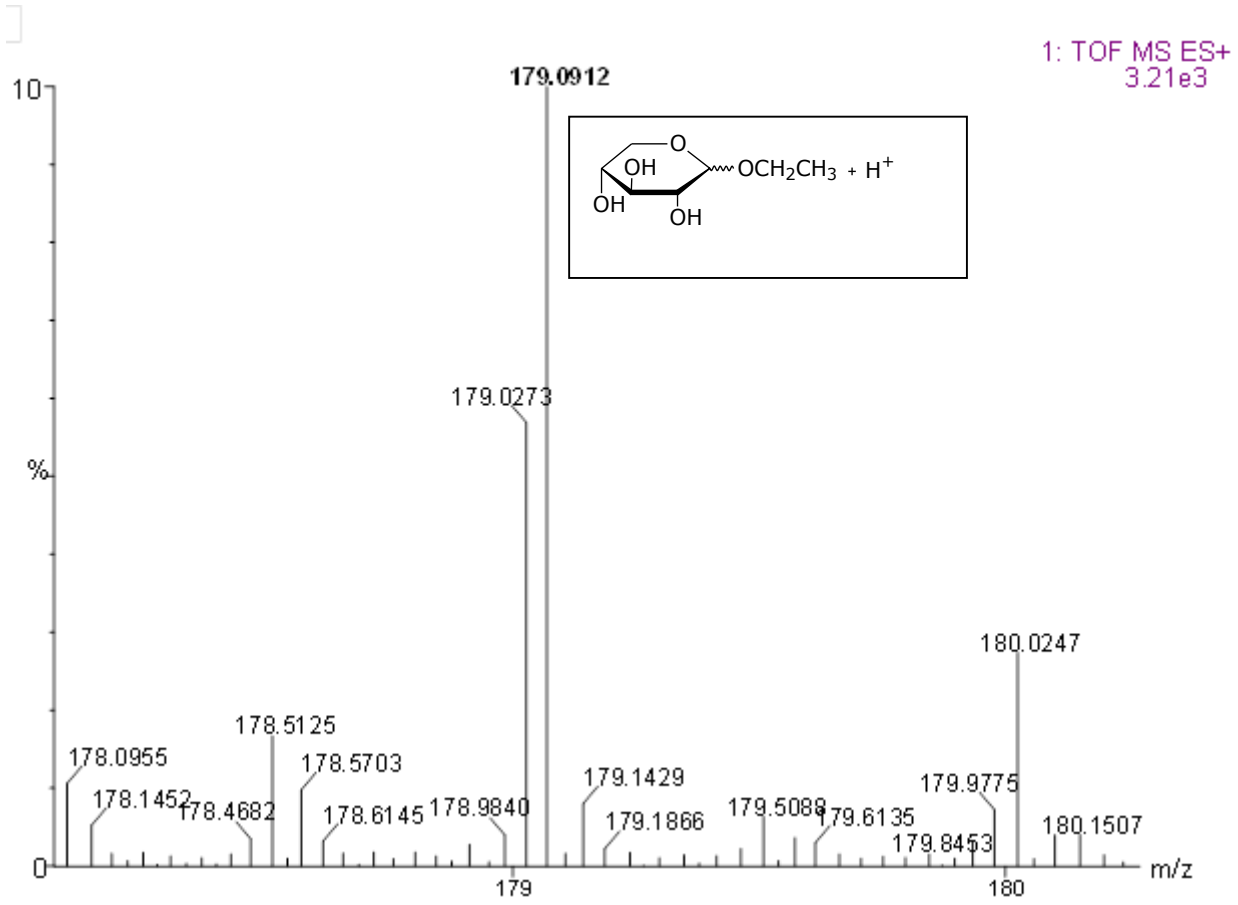

Figure 2-7. Mass spectrum of ethyl xyloside produced in the SSF process.

2.3.6 Cellulase adsorption isotherms on OPLP and OPSG substrates

Cellulase adsorption isotherms have been used to characterize the cellulase enzyme affinity to the substrates and the enzymatic hydrolysis of substrates (Tu et al. 2007a; Tu et al. 2007b). The adsorption of cellulase on OPLP and OPSG substrates was fitted using nonlinear regression by software Origin 8.0 (**Figure 2-8**). From the adsorption isotherm, it was apparent that the cellulase showed higher affinity to OPLP than OPSG based on the slope of adsorption

curve (distribution coefficient). In the case of cellulase adsorption to OPLP substrate, the Langmuir constant (K) was 3.11 mL/mg, and the maximum amount of adsorbed cellulase (Γ_{max}) was 35.09 mg/g. In the case of cellulase adsorption to OPSG substrate, the Langmuir constant was 1.31 mL/mg, and the maximum amount of adsorbed cellulase was 60.19 mg/g. It was very interesting to find that the Langmuir constant of cellulase on OPLP substrate was three fold higher than that on OPSG substrate (**Table 7**), which was anticipated to affect the initial hydrolysis rates significantly in the OPLP and OPSG substrates. The distribution coefficient (R) is another useful constant from Langmuir adsorption isotherm that can be used to estimate the relative affinity of cellulase on substrates (Kumar and Wyman 2009a; Medve et al. 1994; Tu et al. 2007a). The distribution coefficient can be expressed as

$$R = \Gamma_{max} \times K$$

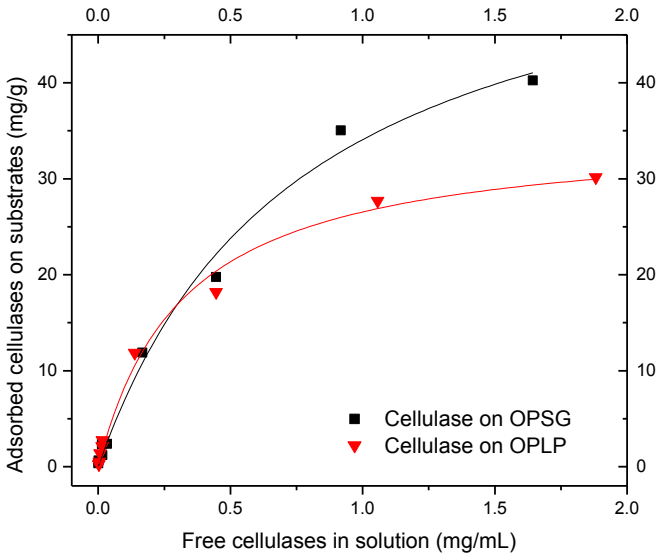

Figure 2-8. Cellulase adsorption isotherms on OPLP and OPSG substrates at 4 ℃.

Table 7. Langmuir constant from cellulase adsorption on pretreated biomass.

Cellulase	Γ_{max} (mg/g)	*K*(mL/mg)	*R*(L/g)
Cellulase on OPLP	35.09	3.11	0.11
Cellulase on OPSG	60.19	1.31	0.08
Celluclast on EPLP*	87.69	3.48	0.31
Celluclast on SELP*	101.05	1.45	0.15

***** from our previous data(Tu et al. 2007b): EPLP-ethanol pretreated lodgepole pine and SELP-steam exploded lodgepole pine.

Our results indicated that the distribution coefficient was higher for the adsorption of cellulase on softwood OPLP substrate (0.11 L/g) than on hardwood OPSG substrate (0.08 L/g). These coefficients were in the similar range as those reported in the previous work. (Kumar and Wyman 2009a) It was interesting that the lignin content (19%) in OPLP substrate was much higher than that in OPSG substrate (9.0%), but relative affinity (based on distribution coefficient) were found to be higher on OPLP substrate. It indicated that lignin probably did not play a significant role in initial adsorption of cellulase on substrates.

Langmuir adsorption isotherm has been often used to characterize affinity of cellulase on substrates and enzyme accessibility to cellulose (Hong et al. 2007; Tu et al. 2007b). Here, we found a good linear correlation between Langmuir adsorption isotherm (distribution coefficient) and the initial hydrolysis rate of glucan ($R^2 = 0.98$ **Figure 2-9**). Previously, others have tried to build a correlation between the amount of adsorbed enzyme and the initial hydrolysis rate, or pore size and the initial hydrolysate rate (Grethlein 1985; Lee et al. 1994). Factors such as surface area, crystallinity and lignin content have also been investigated for their potential correlation with the initial hydrolysis rate (Gharpuray et al. 1983). However, few studies have been focused on the relationship between distribution coefficient and the initial hydrolysis rate of

glucan. The distribution coefficient, R, represents a combination of maximum adsorbed enzyme (Γ_{max}) and Langmuir constant (K). This indicates the initial hydrolysis rate is related to adsorbed enzymes and their affinity to the substrates.

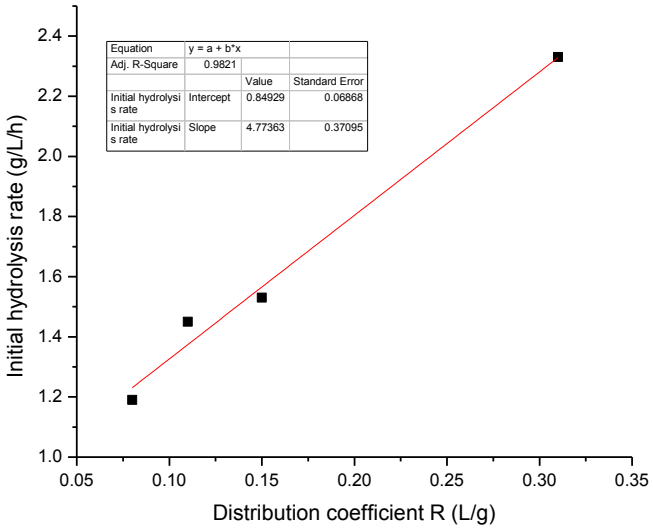

Figure 2-9. Correlation between the distribution coefficient (R) and the initial hydrolysis rate of glucan.

2.3.7 Correlation of residual xylan and lignin and enzymatic hydrolysis

We also observed that the amount of residual xylan in substrates affected the initial hydrolysis rate, and the amount of lignin affected the final hydrolysis yield because the xylan effects could be removed gradually by hydrolysis of the xylan. Effects of xylan and lignin removal on enzymatic hydrolysis of lignocellulose have been explored on different substrates in the past decades (Qing and Wyman 2011; Selig et al. 2009; Yang and Wyman 2004; Zhang et al. 2011). Xylan and lignin have been suggested as two important physical barriers to enzymatic hydrolysis of cellulose, and even inhibit cellulase activity (Qing and Wyman 2011). Accessory

enzymes (xylanolytic activities) are often required in cellulase mixture to improve the cellulose hydrolysis when xylan content is high (Selig et al. 2009). Little research has distinguished the potential different roles of xylan and lignin in limiting enzymatic hydrolysis (Lee et al. 2010). Based on the cross point of glucose yield (**Figure 2-2A**) on softwood and hardwood substrates, we could distinguish two phases in hydrolysis: the initial hydrolysis phase is controlled by residual xylan, and second hydrolysis phase is governed by the residual lignin. The Lignin droplets on the plant cell wall do not seem to affect the initial hydrolysis rate of cellulose (glucan), probably the bulk lignin plays a greater role in limiting enzymatic hydrolysis in the second stage. We calculated approximately 4-5% of residual xylan is the critical point for the phase change. In order to quantitate the correlation between the initial hydrolysis rate and xylan content, in the preliminary result we compared the results from organosolv pretreated lodgepole pine (EPLP), Loblolly Pine (OPLP), Sweetgum (OPSG) and hybrid polar (EPHP) under 20 FPU enzymatic hydrolysis. We found the linear correlation (Pearson' r = -0.80) between the amount of residual xylan and the initial hydrolysis rate was there (**Figure 2-10A**). The linear correlation between the amount of residual lignin and the final hydrolysis yield was also fair (Pearson' r = -0.78, **Figure 2-10B**). These correlations indicated the distinct roles of residual xylan on the initial hydrolysis rate and residual lignin on the final hydrolysis yield. However, the residual lignin and xylan in OPSG and OPLP are probably structurally and compositionally different. The residual lignin in OPSG is syringyl-guaiacyl lignin, and one in OPLP is guaiacyl lignin. In addition, the phenolic hydroxyl groups, carbonyl groups and methoxyl groups in two types of residual lignin could be different as well. As for residual xylan, hardwood does not contain arabinose side chain, while softwood does contain small amount of arabinose as indicated in **Table 1**. To address this issue, we will further investigate the effect of residual lignin and xylan

on hydrolysis in the future work by designing new experiments to pretreat hardwood at various conditions and prepare a number of substrates with different lignin and xylan contents.

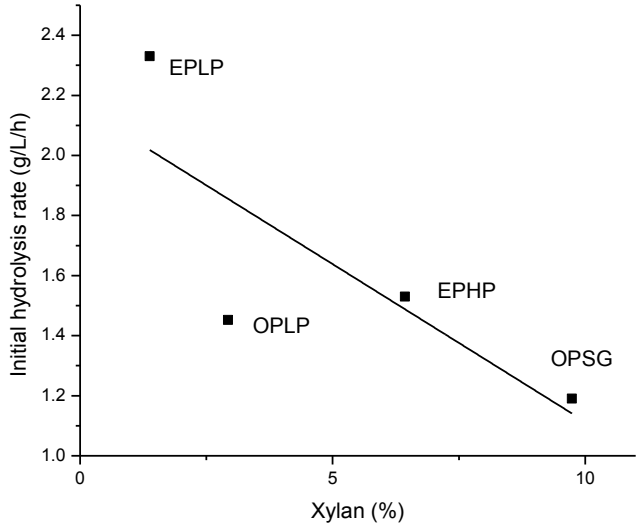

(A)

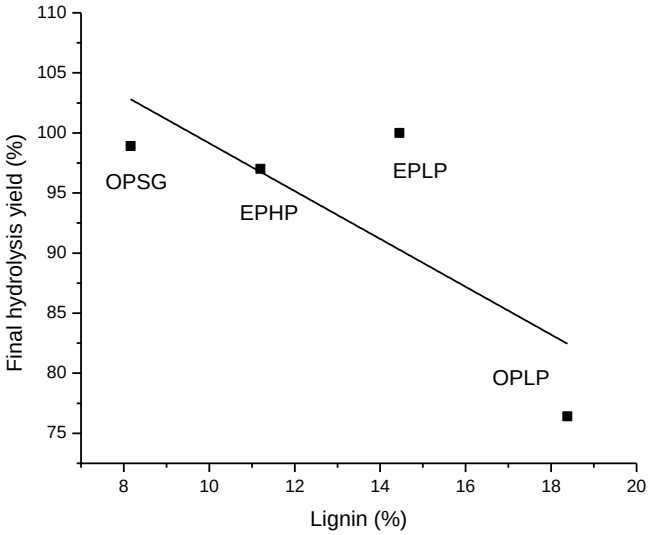

(B)

Figure 2-10. Negative correlation between the amount of residual xylan and the initial hydrolysis rate (A) and between the amount of residual lignin and the final hydrolysis yield of glucan (B).

2.4 Conclusion

In summary, enzymatic hydrolysis of organosolv pretreated softwood and hardwood showed totally different hydrolysis curve pattern under the same enzyme loading. The initial hydrolysis rate from OPLP substrate was much faster than that from OPSG substrate, probably due to the high xylan content 9.7% in OPSG substrate. However, the final hydrolysis yield of glucan from OPSG was 29% higher than that from OPLP substrate probably due to the higher lignin content and lower enzyme accessibility (related to pore size, crystallinity and degree of polymerization) in OPLP substrate. Consequently, the enzymatic hydrolysis of organosolv pretreated substrates could be divided into two phases: the first phase is mainly controlled by residual xylan, and the second phase is dominated by residual lignin. The phase changing point is located in the range of 4-5% xylan. We also found that the initial hydrolysis rate of glucan was correlated very well with distribution coefficient from Langmuir adsorption isotherm. In addition, we observed released xylose in the SSF process can be converted into xyloside by potential enzymatic catalysis of xylose and ethanol. This indicates that xylose must be used in the SSF process or removed before fermentation. Otherwise, it will negatively affect the final ethanol yield. Future work is needed on the correlation of residual xylan and initial hydrolysis rate with various woody biomass and visualization of residual xylan on enzymatic hydrolysis.

Chapter 3 Kinetic study of catalytic conversion of hemicelluloses sugars into lactic acid under alkaline condition

3.1 Background

Lignocellulosic biomass, primarily composed of carbohydrates, offers great potential for bio-fuels and value-added chemicals in the biorefinery industry (Bull 1999; Ragauskas et al. 2006). Within the production of useful chemicals from carbohydrates, lactic acid (2-hydroxypropanoic acid) is particularly useful due to its molecular versatility. As an important industrial product, lactic acid (LA) is used as a precursor for other chemicals such as food preservatives, oxygenates, green solvents and biodegradable polymers (poly-lactic acid) (Datta and Henry 2006).

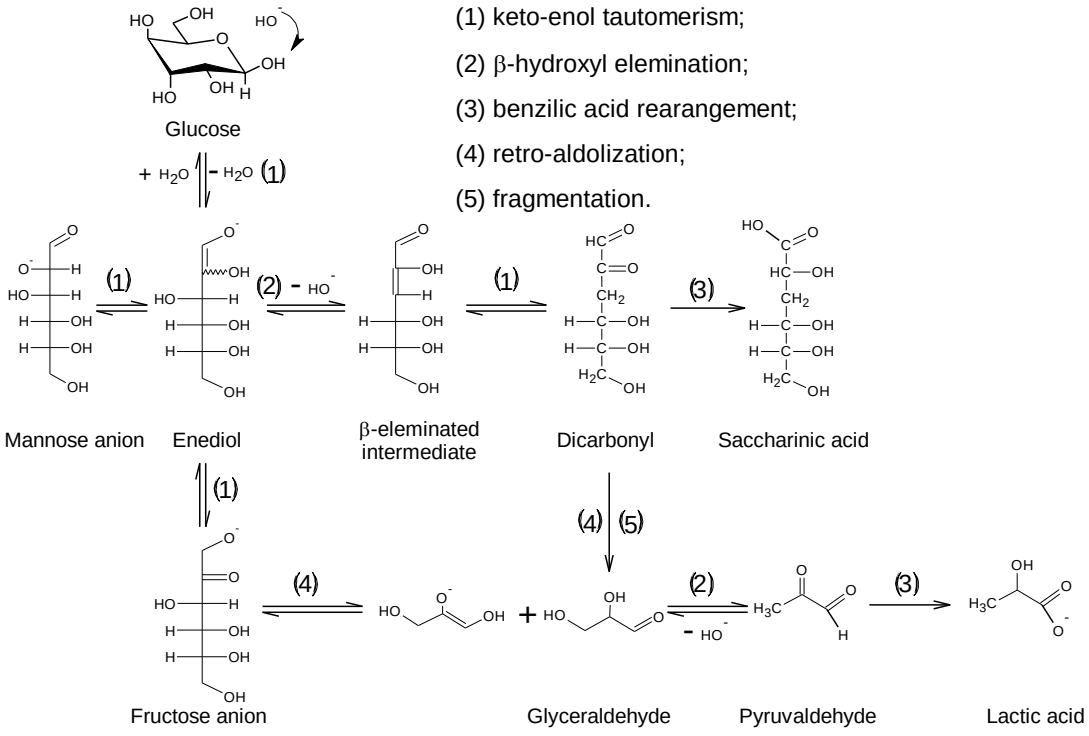

Figure 3-1. Proposed reaction mechanism for the production of lactic acid from glucose.

The reaction of sugar (the basic unit of carbohydrates) under aqueous alkaline condition has been known and studied for over one hundred years (Evans 1942; Isbell et al. 1969; Speck 1958). It involves the reaction of mutarotation, ionization, enolization, isomerization, and degradation (**Figure 3-1**). The reaction mechanism can be generally summarized as follows: the sugars first isomerized through enediol intermediate in a process known as Lobry de Bruyn-Alberda van Ekenstein rearrangement. Next, the unstable α-dicarbonyl compounds were formed by the elimination of a hydroxyl group from the β-C of the intermediates. Under alkaline conditions the α-dicarbonyl compounds were subjected to degradation through fragmentation and benzilic acid rearrangement into smaller compounds and saccharinic acids, respectively. Aldolization and retro-aldolization were also involved in the reactions. The initial reactions, most notably mutarotation, ionization, isomerization, and enolization of sugar, have been extensively investigated and their mechanisms are well understood (Bamford et al. 1950; Kooyman et al. 1977; MacLaurin and Green 1969). Specifically, the sugar alkaline degradation was systematically studied by De Bruijn (De Bruijn 1986) and the chemical production of LA under alkaline condition was reviewed by Montgomery (Montgomery 1949). LA is the principal degradation product from sugar when strong alkalis are used. Recently, raw biomass and biomass model compounds thereof were used to produce LA at very high temperatures (around 300 ℃) under alkaline degradation conditions (Kong et al. 2008; Yan et al. 2010; Yan et al. 2007). It has been reported (Yan et al. 2010) that 27% and 20% LA were produced from glucose at 300 ℃ for 60 s with 2.5 M NaOH and 0.32 M $Ca(OH)_2$, respectively. Improvement of yields of LA and its derivatives were obtained from glucose at high temperature with Zn-catalysts (42%) (Bicker et al. 2005) and zeotype catalysts (45%) (Holm et al. 2010).

However, the catalytic conversion of sugars to LA with aqueous alkali was not clearly elucidated. In this chapter we studied the catalytic conversion kinetics of sugars under different alkaline solutions. Three common hemicelluloses monomeric sugars (glucose, xylose, and mannose) as well as fructose were compared to understand the mechanism of LA production by alkaline catalyst. The effects of reaction temperature, alkaline concentration, nature of the alkali, and initial sugar concentration on the LA production were investigated. We have demonstrated the conversion of biomass model sugars into LA in a simple alkaline catalyzed reaction. The LA development method could be of great potential for industrial biorefinery of lignocellulosic biomass.

3.2 Materials and methods

Chemicals and materials

Glucose (assay 98%) and xylose (99%) were purchased from Fluka (Buchs, Switzerland). mannose (99%) and lyxose (99%) were purchased from Sigma-Aldrich (St. Louis, MO). Fructose was purchased from Spectrum Chemical MFG (New Brunswick, NJ). Lactic acid (1 N), sodium glycolate (97%), $Ca(OH)_2$ (95%), tetraethylamoniumhydroxide (35% w/w), and benzyltrimethylamoniumhydorxide (20% w/w) were purchased from Alfa Aesar (Ward Hill, MA). NaOH (50%) and $Ba(OH)_2$ $8H_2O$ were purchased from J. T. Baker (Phillipsburg, NJ). NH_4OH (ACS grade) and KOH (ACS grade) were purchased from Fisher Scientific (Fair Lawn, NJ). H_2SO_4 (95-98%) was purchased from EMD Millipore (Billerica, MA). All the chemicals or reagents were used as received. Deionized water was used throughout this work (Barnstead Nanopure UV Ultrapure Water System).

Reaction kinetic study

All reactions were carried out in 16 ml glass tube with screw caps in water bath at constant temperature (±0.5 ℃). Specifically, sugar solutions of 16 g/L and NaOH with according concentrations were pre-arranged respectively. The sugar solution (5 mL) and the aqueous NaOH (5 mL), both previously thermo-stated, were added into glass tube with rapid shaking. The mixture contained 8 g/L sugar and desired concentration of NaOH. The tube was quickly inserted into the water bath and zero time was recorded immediately. Portions (0.5 mL) of the reaction mixture were withdrawn at known intervals (1, 5, 10, 15, 20, and 30 min) and added rapidly to 0.5 mL water containing H_2SO_4 in ice-bath to quench the reaction and neutralize the sample. The neutralized samples were subjected to centrifugation and filtration before HPLC or LC/MS analysis.

The thermodynamic parameters (pre-exponential factor A, activation energy E_a, and enthalpy of activation $\Delta H^{\ddagger}$) were calculated according Arrhenius and Eyring equation at reaction temperatures ranging from 40-70 ℃.

HPLC and GC/MS analysis

The sugars and carboxylic acid were quantitated by the previously described Shimadzu HPLC system (Li et al. 2013). In detail, the concentrations of sugars, lactic acid, formic acid, and glycolic acid were determined by a Shimadzu (LC-20A) HPLC system consisting of an autosampler, LC-20AD pump, and RID-10A detector, with a 300 mm × 7.8 mm i.d., 9 μm, Aminex HPX-87H column, and a 30 mm × 4.6 mm i.d. guard column of the same material (Bio-Rad, Hercules, CA). The mobile phase was composed of 5 mM sulfuric acid running isocratic at

0.6 mL/min. The temperature of the column was maintained at 45 ℃ throughout the run. The organic acids were analyzed using an Ultra Performance LC Systems (ACQUITY, Waters Corp., Milford, MA) coupled with a quadrupole time-of-flight mass spectrometer (Q-Tof Premier, Waters) with electrospray ionization (ESI) in ESI^--MS mode operated by the Masslynx software (V4.1). Each sample, in H_2O, was injected onto a C18 column (ACQUITY UPLC® BEH C18, 1.7 μm, 2.1 x 50 mm, Waters) with a 150 μL/min flow rate of mobile phase of solution A (95% H_2O, 5% acetonitrile, 0.1% formic acid) and solution B (95% acetonitrile, 5% H_2O, 0.1% formic acid) in a 10 min gradient starting at 95% A to 5% A in 4 min and back to 95% in 6 min.

The production yield of lactic acid is defined as the ratio of mols of C in lactic acid over that in the starting sugar (see below).

$$Y_{\mathrm{LA}} = \frac{mol\text{-}C\ of\ lactic\ acid}{mol\text{-}C\ of\ the\ starting\ sugar} \times 100\%$$

3.3 Results and discussion

3.3.1 Alkaline-catalyzed sugar conversion kinetics

The alkaline catalyzed reaction kinetics of sugars – glucose, fructose, mannose, and xylose– were investigated at different temperatures varying from 40 to 70 ℃ (**Figure 3-2**). As expected, both the conversion rate and maximum conversion of sugars increased with increasing temperature. Fructose showed the fastest conversion rate followed by xylose, glucose, and mannose. The catalytic reaction included two parts: initially the sugars interconverted into their isomers, known as the Lobry de Bruyn-Alberda van Ekenstein transformation (Speck 1958), which were detected by HPLC with refractive index (**Figure 3-3**); and the enediol intermediates

degraded into LA, saccharinic acids, and other carboxylic acids detected by LC/MS in the negative ESI.

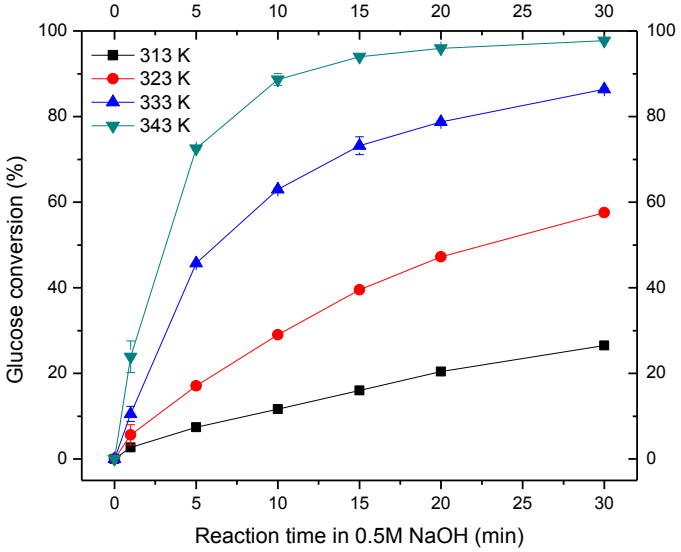

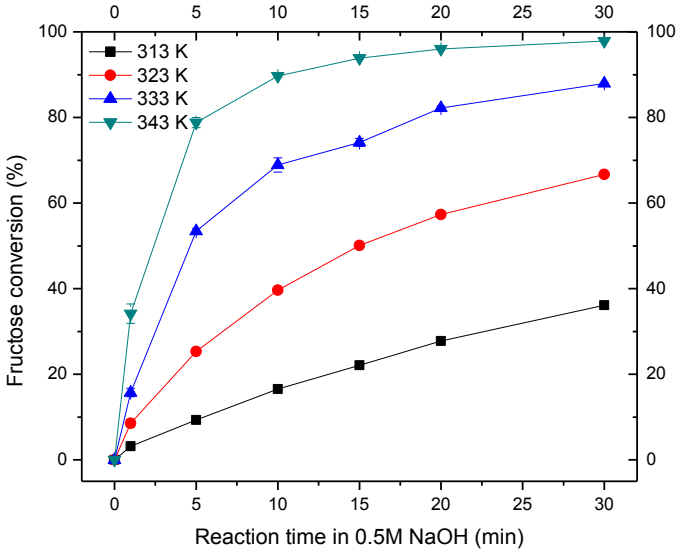

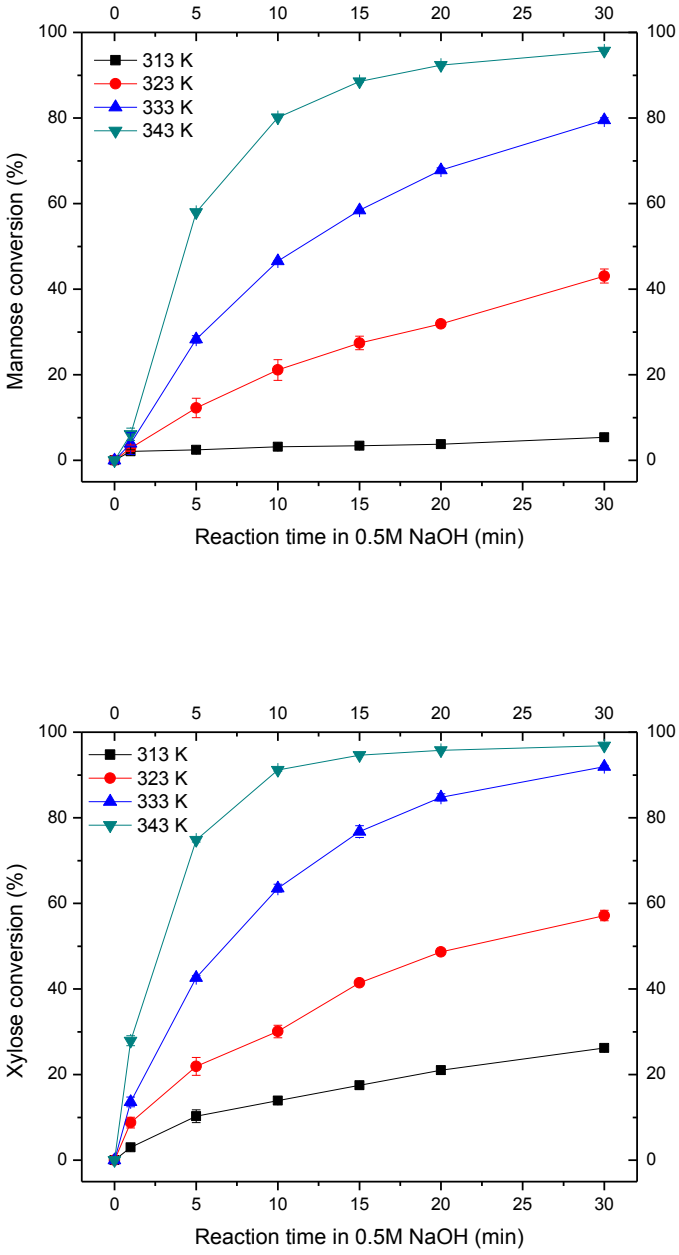

Figure 3-2. Conversion yields of glucose, fructose, mannose, and xylose in 0.5 M NaOH at 40 to 70 ℃.

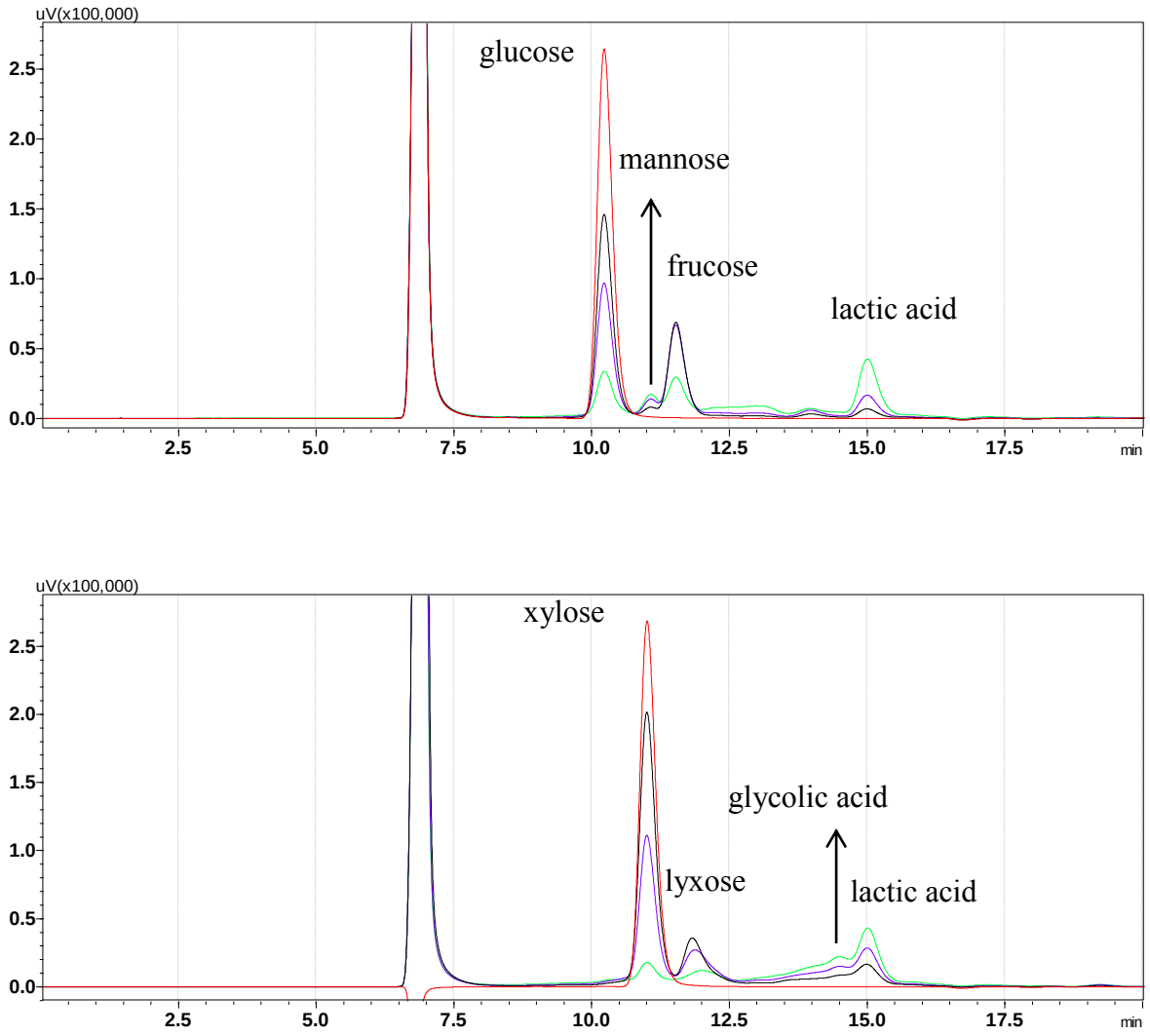

Figure 3-3. HPLC chromatograms of monosaccharides interconversion to their isomers.

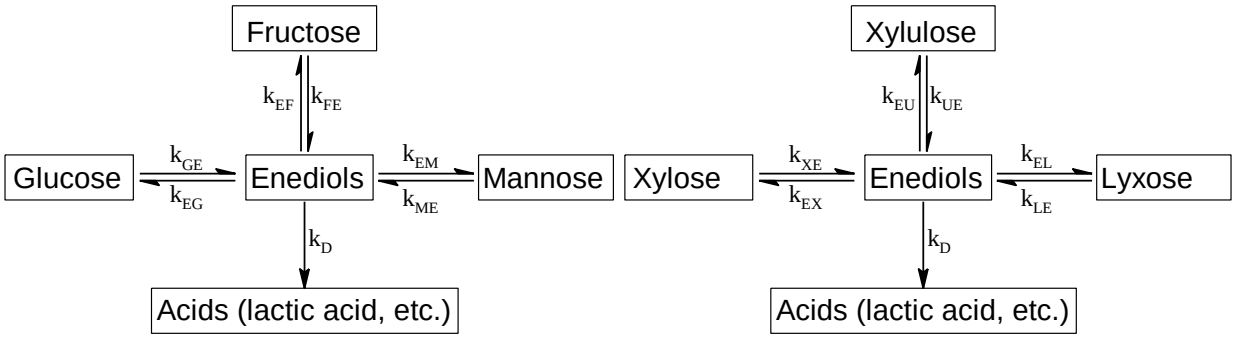

Figure 3-4. Kinetic models for catalytic conversion of sugars.

We developed kinetic models for the alkaline catalytic conversion of sugars including isomerization and degradation (**Figure 3-4**). No other isomers such as altrose (Adorjan et al. 2004) or piscose (Debruijn et al. 1987) were included in the model because only trace amounts of them were detected in the investigated experimental conditions. The starting sugar conversion profiles failed to show a pseudo first-order exponential decay when the logarithm value of sugar concentration versus reaction time was plotted. This deviation agreed with previous results (Bamford et al. 1950; Debruijn et al. 1987) due to the reversible isomerization reactions in sugars. To find the overall reaction rate, we pooled all the detected isomers together (e.g. glucose, fructose, and mannose in C6 sugar; xylose, xylulose, and lyxose in C5 sugar) and simplified sugar conversion reactions as expressed below.

$$\text{Pooled sugars} \xrightarrow{k_D} \text{Degradation products}$$

It was found that sugar conversion followed a pseudo-first-order reaction in terms of the summed concentrations of isomers. However, a deviation from the pseudo-first-order reaction was previously reported (Debruijn et al. 1987). In this study, no deviation was observed probably because higher alkali concentration (0.5 M NaOH) advanced the equilibrium of the transformation (Bamford et al. 1950). According to equation 1 and 2, we calculated apparent conversion rate constant k_D at different temperature in **Table 8**.

$$\frac{d[T]}{dt} = -k_D * [T] \qquad 1.$$

In which [T] represents the concentration of the sum of sugar isomers. Equation 1 can be integrated to equation 2. The degradation rate constants were calculated by plotting logarithmic value of $[T]/[T_0]$ against reaction time t (min).

$$ln\frac{[T]}{[T_0]} = -k_D * t \quad 2.$$

Table 8. Apparent rate constants of sugar alkaline conversion.

T (K)	Glucose (min^{-1})		Fructose (min^{-1})		Mannose (min^{-1})		Xylose (min^{-1})	
313	0.003	R^2= 0.996	0.003	R^2= 0.982	0.002	R^2= 0.921	0.006	R^2= 0.946
323	0.010	R^2= 0.998	0.010	R^2= 0.984	0.008	R^2= 0.982	0.020	R^2= 0.992
333	0.037	R^2= 0.997	0.034	R^2= 0.996	0.029	R^2= 0.999	0.058	R^2= 0.992
343	0.107	R^2= 0.985	0.094	R^2= 0.980	0.077	R^2= 0.993	0.154	R^2= 0.988

It was found that as C6 sugar, glucose and fructose with similar k_D showed much higher value than mannose; while xylose showed the fastest degradation rate which suggested less steric hindrance on C5 sugar. The difference in rate constants from C6 sugars disagreed with the results that fructose and glucose had the same intermediate for degradation (Bamford et al. 1950). Bamford also concluded that an interconversion equilibrium with constant concentration ratio of glucose, fructose, and mannose were ultimately reached (Bamford and Collins 1955); presumably, these C6 sugars should have the same degradation rate constants. The deviation from expected apparent degradation constants values of the three sugars probably was due to two factors: (1) other intermediates formation limited the reaction rate; and (2) the common intermediate degradation rate was limited by the steric structure to various degrees.

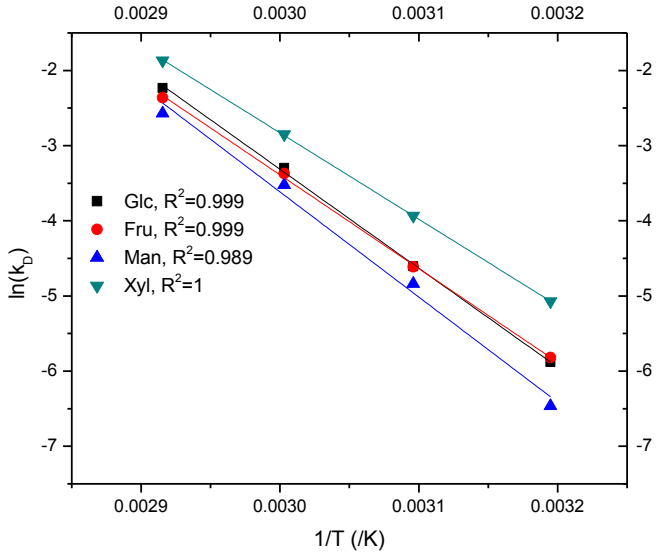

Figure 3-5. Arrhenius plot based on apparent sugars conversion rate constants (k_D) at temperatures from 40 to 70 ℃.

The kinetics at four different temperatures were investigated to determine the activation parameters of the sugar catalytic reaction. The Arrhenius plots (**Figure 3-5**) and activation parameters (**Table 9**) indicated the C6 sugars showed similar reaction dynamics (*Ea* was of similar value for glucose, mannose, and fructose). However, xylose required less activation energy than the C6 sugars which was probably related to a less steric hindrance to the transitional states.

Table 9. The activation parameters of sugars alkaline conversion.

Sugar	A (min^{-1})	Ea (kJ/mol)	$\Delta H^{\ddagger}$ (kJ/mol)
Glucose	5.1512E+15	109.4	106.7
Fructose	5.911E+14	103.7	100.9
Mannose	4.5387E+16	116.3	113.6
Xylose	5.5867E+13	95.6	92.8

3.3.2 Mathematic model for the catalytic conversion of hemicellulose sugars

The experimental kinetic data of C6 sugars at 60 ℃ were fitted to a mathematical model. For that purpose, two more assumptions were made based on the model in **Figure 3-4**: all reactions were of first order and at steady state.

$$\frac{dE}{dt} = k_{GE} * [Glc] + k_{FE} * [Fru] + k_{ME} * [Man] - (k_{EG} + k_{EF} + k_{EM} + k_{D}) * [E] = 0 \quad (3.)$$

Defining k_E as:

$$k_{EG} + k_{EF} + k_{EM} + k_{D} = k_{E} \quad (4.)$$

Then

$$[E] = \frac{k_{GE}}{k_{E}} * [Glc] + \frac{k_{FE}}{k_{E}} * [Fru] + \frac{k_{ME}}{k_{E}} * [Man] \quad (5.)$$

Therefore, the concentration of enediols (E) was proportional to the sugar's concentrations and the unidentified enediols could be skipped in the consecutive reaction. The kinetic model of C6 sugars in **Figure 3-4** was modified into a calculable model (**Figure 3-6**). The three C6 sugars conversion data were simulated by software Tenua to calculate all the rate constants. The resulting sets of differential equations were solved and the kinetic rate constants were determined by iterative fit optimization (**Table 10**). The computer-simulated results with the optimized rate constants were compared with the real data in **Figure 3-7**.

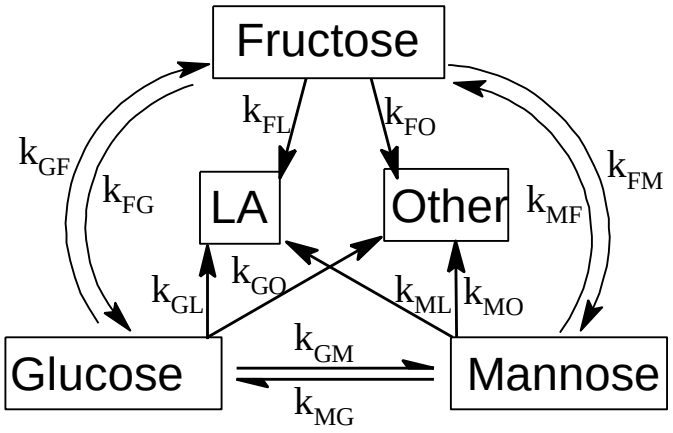

Figure 3-6. Modified kinetic model for C6 sugar alkaline conversion (other: other carboxylic acids).

Table 10. The rate constants for C6 sugar conversion in alkaline medium (0.045 M sugar, 0.5 M NaOH, 60 ℃).

Rate constant	k_{GF}	k_{FG}	k_{GL}	k_{GO}	k_{FM}	k_{MF}	k_{FL}	k_{FO}	k_{MG}	k_{GM}	k_{ML}	k_{MO}
(min^{-1})	0.109	0.090	0.012	0.012	0.037	0.050	0.026	0.050	0.027	0.010	0.008	0.014

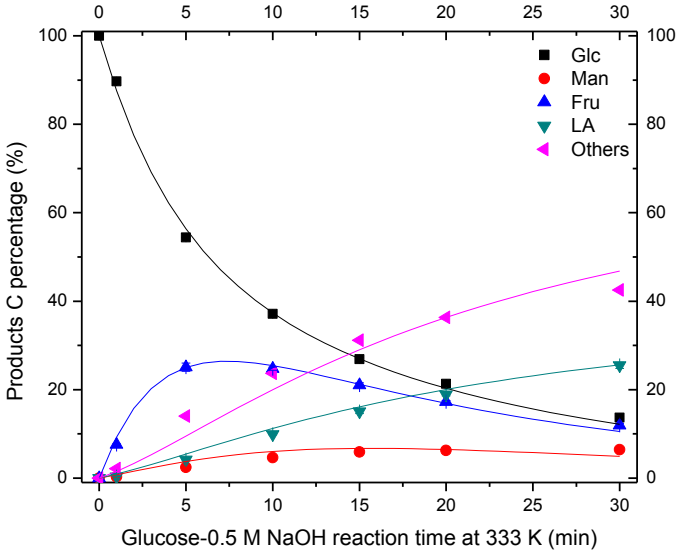

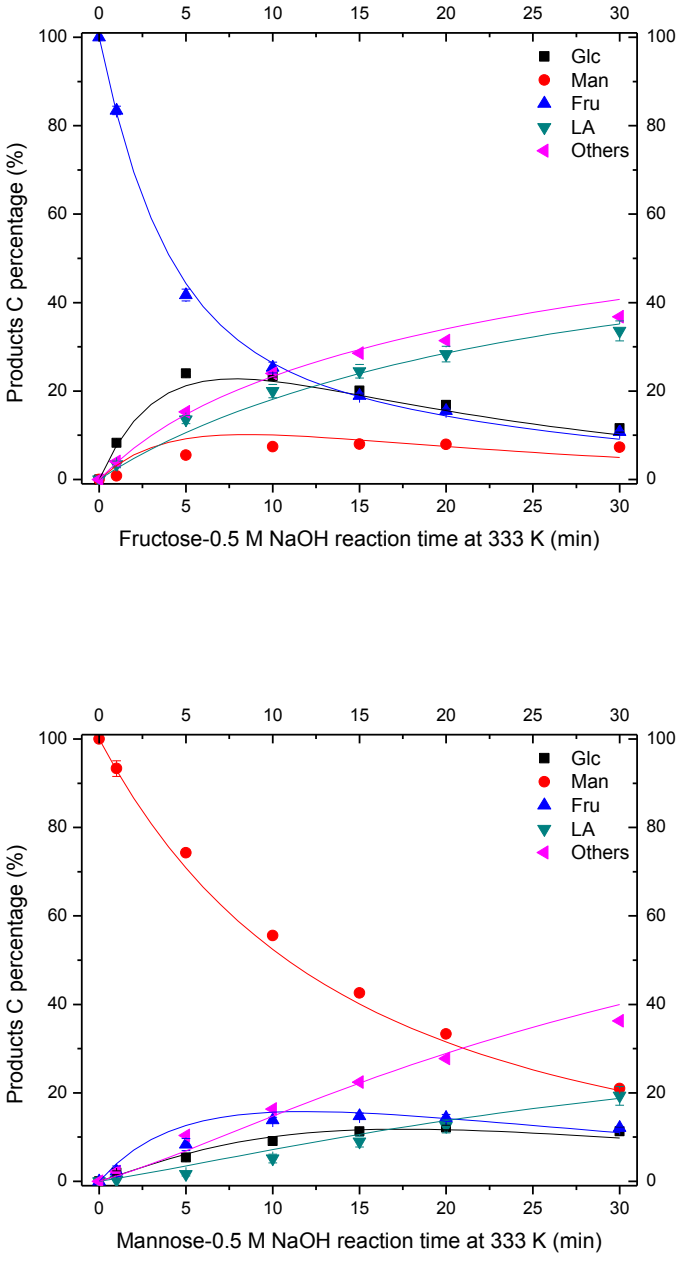

Figure 3-7. Simulation curves of C6 sugars conversion under alkaline condition at 60 ℃ (experimental data are shown in symbols).

Considering the experimental data shown by symbols corresponding three different starting sugars and the differential reaction equations shown by solid lines (**Figure 3-7**), the match between experimental and calculated values was satisfactory. This outcome strongly

supported the two assumptions used in the model and confirmed the pseudo first order kinetic for all individual reactions in the conversion schematic model in **Figure 3-6**.

3.3.3 Effects of alkali type on the yield of lactic acid from glucose

A few monobasic and dibasic alkalis with the same concentration of [OH^-] were screened in catalyzing glucose conversion to LA, because divalent cations (Yang and Montgomery 1996a; Yang and Montgomery 1996b) and quaternary ammonium hydroxide (Torstensen 1939) were previously documented to enhance LA formation. The LA production rate (**Figure 3-8**) and yield of 56% (**Table 11**) were remarkably improved by $Ba(OH)_2$, which agreed with previous result of 57% (Esposito and Antonietti 2013). NH_4OH did not yield any LA even within 48 h despite of observed Lobry de Bruyn-Alberda van Ekenstein transformation. Contrary to the previous result (Esposito and Antonietti 2013), $Ca(OH)_2$ exhibited a slower rate and less yield of LA than NaOH. This decrease in LA production was likely caused by the low solubility of $Ca(OH)_2$ in the system (0.25 M, 60 ℃). KOH and NaOH showed similar catalytic effects on LA production (46% vs 49%); while tetraethylamoniumhydroxide (TEAOH) and benzyltrimethylamoniumhydorxide (BTAOH) slightly improved the yield and rate of LA compared with the monobasic catalysts (NaOH and KOH). The LA yield (51%) catalyzed by BTAOH was consistent with the previous result (Torstensen 1939). These results suggested that the LA production was associated with OH^- concentration and the nature of alkali.

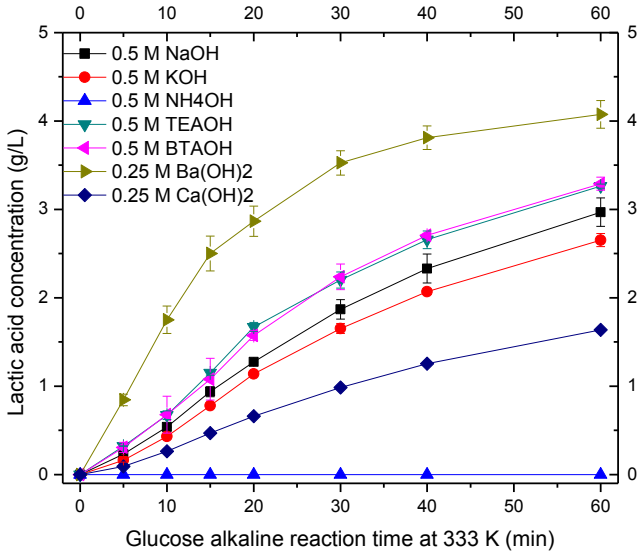

Figure 3-8. Lactic acid production profile from glucose with different alkaline catalyst.

Table 11. Lactic acid yield from glucose by different alkaline catalyst (0.045 M glucose, 60 ℃, 48 h).

	NH_4OH	$Ca(OH)_2$	KOH	NaOH	BTAOH	TEAOH	$Ba(OH)_2$
Initial pH	11.89	12.72	13.77	13.42	13.82	13.91	13.55
LA (g/L)	0.00	2.47	3.68	3.89	4.02	4.15	4.46
LA yield (%)	0.00	30.87	46.03	48.66	50.28	51.85	55.79

To confirm the positive effect of $Ba(OH)_2$ on LA production, mannose, fructose, and xylose were tested in comparison with catalyst NaOH. As expected, $Ba(OH)_2$ also improved the LA production rate for mannose, fructose, and xylose (**Figure 3-9**). The yields of LA were appreciably improved from 38 to 44% and 33 to 46% for mannose and xylose respectively (**Table 12**). Interestingly, the yield of LA from xylose was comparable with that from C6 sugars. The enhanced catalytic effect on LA production by $Ba(OH)_2$ was probably due to the function of

divalent cation Ba^{2+} favoring retro-aldolization reaction as a result leading to LA formation (Bicker et al. 2005).

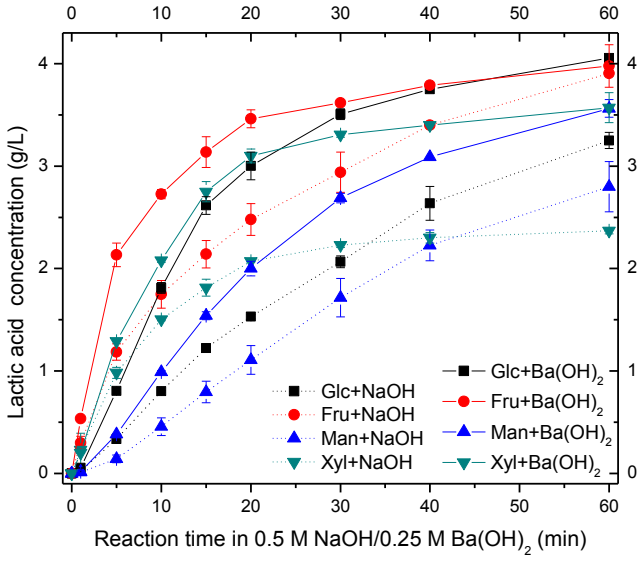

Figure 3-9. Lactic acid production from glucose, fructose, mannose, and xylose in 0.5 M NaOH and 0.25 M $Ba(OH)_2$ at 60 ℃.

Table 12. Lactic acid yield from glucose, fructose, mannose, and xylose at 60 ℃.

	Glucose	Fructose	Mannose	Xylose
0.5 M NaOH 3 h	44.76%	56.79%	37.98%	32.69%
0.25 M $Ba(OH)_2$ 4 h	51.75%	56.10%	43.74%	46.27%

3.3.4 Effects of reaction temperature on lactic acid production from sugars

The effects of reaction temperatures ranging from 40 to 90 ℃ on the yield of LA were investigated (**Figure 3-10**). In agreement with previous research (Shaffer and Friedemann 1930), the yield of LA slightly decreased with increasing reaction temperature. Among the investigated

sugars, fructose exhibited the highest yield of LA at 40 ℃ (55%), followed by glucose (46%), mannose (38%), and xylose (35%). The higher yield from fructose perhaps resulted from the direct retro-aldolization into C3 compounds (**Figure 3-1**). Xylose produced the least LA probably because only one mole of C3 compounds were produced per mole xylose.

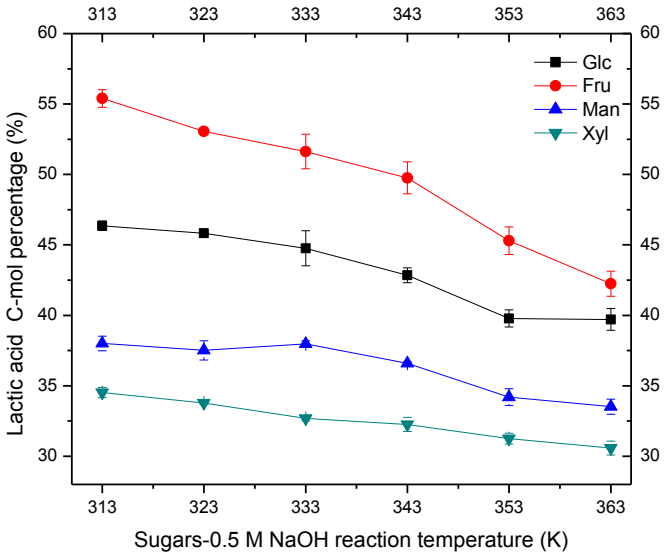

Figure 3-10. Temperature effects on the yield of lactic acid from sugars.

3.3.5 Effects of initial NaOH concentration on the yield of lactic acid from sugars

The influence of the initial alkali concentration on the yield of LA was examined at 60 ℃ with NaOH concentration varying from 0.01 to 1 M. In agreement with previous research (Evans 1942), the yield of LA from sugars was strongly dependent on the initial concentration of NaOH (**Figure 3-11**) – higher initial concentration of NaOH resulted more LA production. Interestingly, no LA formed at 0.01 M NaOH even after 4 days reaction suggested that low concentration of OH^- was not sufficient to convert sugars into LA. It was noted that after 4 days only 60% sugars were converted in 0.01 M NaOH. As the reaction proceeded, the generation of acids resulted in a

progressive decrease in the pH of the reaction mixture. The excess of base at high concentrations (> 0.05 M) overcame the pH drop in the reaction and favored the LA formation.

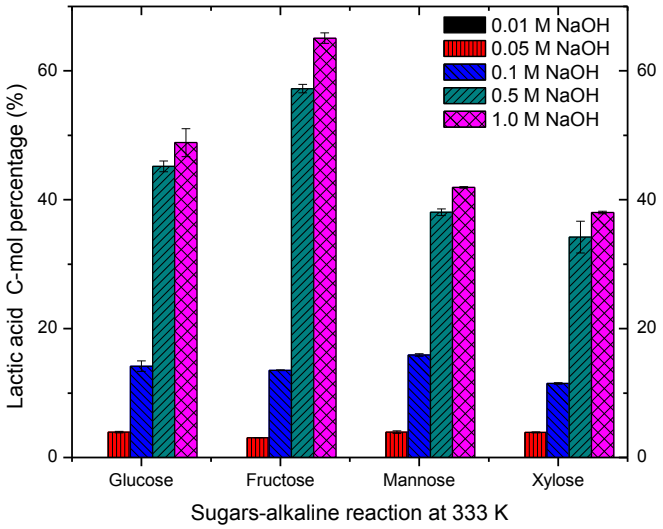

Figure 3-11. Lactic acid production at different initial NaOH concentrations.

3.3.6 Effects of initial sugars concentration on the yield of lactic acid

The initial concentration of glucose ranging from 1, 4, 8, 16, and 40 g/L were investigated to determine the sugar reactant effects on LA formation. We found an increased initial sugar concentration resulted in a decrease of LA yield (**Figure 3-12**). This result was consistent with previous results using 3-6 M NaOH (Shaffer and Friedemann 1930) and $Ca(OH)_2$ (Yang and Montgomery 1996a). A higher concentration of sugars probably resulted in more degradation byproducts with carbonyl groups. These carbonyl groups could polymerize to substances observed in dark brown color. The higher sugar concentration also increased the side reaction such as cross-aldol condensation yielding glucometasaccharinic acids (Yang and Montgomery 1996a).

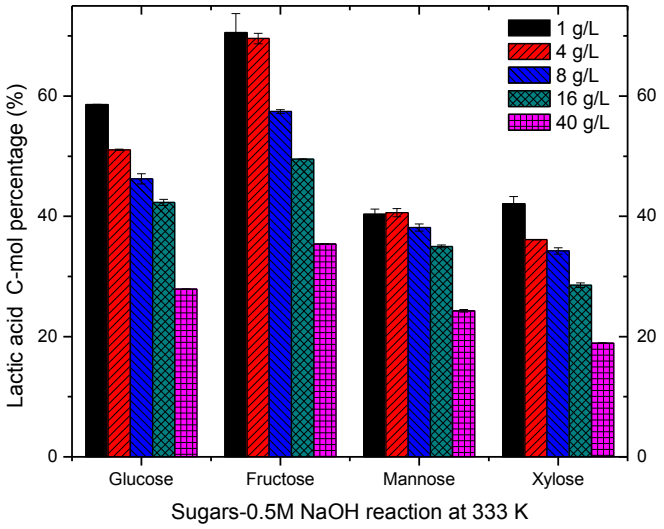

Figure 3-12. Lactic acid production at different initial sugar concentrations.

3.4 Conclusion

In summary, hemicelluloses sugars (glucose, xylose, and mannose) and fructose showed different conversion reaction rate to LA. The conversion of fructose showed the fastest reaction rate into LA and the highest yield (55%), followed by glucose (46%) and mannose (38%). Xylose was cleaved into 3-carbon compounds and glycolate and the conversion to LA was more rapidly than C6 sugars. In 0.5 M NaOH, the sugars (8 g/L) conversion followed a pseudo-first-order rate laws with respect to the overall concentrations of isomers. $Ba(OH)_2$ significantly increased the yield of LA and the LA production rate of all tested sugars. Interestingly, the yield of LA from xylose, C5 sugar, was appreciably increased by $Ba(OH)_2$ and was comparable to that of C6 sugars (mannose). In terms of the LA yield, lower initial concentration of sugar, lower reaction temperature, and higher alkaline concentration favored the LA formation.

Chapter 4 Effect of end products inhibition on gluconic acid and xylonic acid fermentation by *Gluconobacter oxydans*

4.1 Background

The major hemicelluloses in softwoods and hardwoods are glucomannan and glucuronxylan, respectively. About 25-30% of the dry mass, hemicelluloses are readily extracted and hydrolyzed in the pretreatment process in biochemical conversion. The resulting monomeric sugars– glucose, mannose, and xylose– can be converted into valuable chemicals through microbial fermentation. Gluconic acid (GA) and xylonic acid (XA) possess a variety of applications in many fields such as food, pharmaceutical, hygienic, concrete additive, and textile bleaching (Chun et al. ; Ernest 1940; Ramachandran et al. 2006). The conversion of hemicellulose sugars to gluconic acid and xylonic acid certainly add values to the biochemical conversion of lignocellulosic biomass.

G. oxydans assimilates glucose and xylose and produces gluconic acid and xylonic acid in a quantitative amount, respectively (Buchert et al. 1988; Buchert and Viikari 1988a). The metabolism of glucose and xylose involves different pathways (Buchert and Viikari 1988a). The complete oxidation of xylose locating in the periplasmic space contains two steps: the xylose is first oxidized to xylono-γ-lactone via a membrane-bound xylose dehydrogenase; and the lactone is then subsequently hydrolyzed into xylonic acid by γ-lactonase. On contrary, the mechanism for glucose oxidation involves another cytoplasm oxidation beside the similar periplasmic space metabolism to xylose. The transported glucose is oxidized by NADP-specific glucose dehydrogenase in the cytoplasm. Buchet et al. found that the intermediate compound xylono-γ-lactone was inhibitory to the xylose fermentation by *P. fragi* (Buchert and Viikari 1988b). Olijve

et al. found the pH of the medium played an important role in glucose fermentation by *G. oxydans*. However, the inhibition mechanism of xylose and glucose fermentation is still not very well understood.

In this chapter, production of gluconic acid and xylonic acid from glucose and xylose by *G. oxydans* were studied. The inhibition of end product xylonic acid on glucose and xylose fermentation was compared. The effect of pH on the production of gluconic acid and xylonic acid were also evaluated.

4.2 Materials and methods

Microorganism and cultivation medium

Gluconobacter oxydans ATCC621 was used in this study. *G. oxydans* was maintained on mannitol agar plates (5.0 g/L yeast extract, 3.0 g/L peptone, 25 g/L mannitol, and 15 g/L agar) stored at 4 ℃. Colony of *G. oxydans* was cultivated in a liquid medium containing 70.0 g/L sorbitol, 18.4 g/L yeast extract, 1.50 g/L $(NH_4)_2SO_4$, 1.52 g/L KH_2PO_4, and 0.47 g/L $MgSO_4 \cdot 7H_2O$. All media were sterilized by autoclaving at 121°C for 15 min. The bacteria were incubated at 30 ℃ in an orbital shaker with 200 rpm for around 48 h until the exponential growth phase. The bacteria were then harvested by centrifugation and repeatedly washed with sterilized water (3 times). The optical density (OD) of the *G. oxydans* was measured at 600 nm with UV-Vis spectrometer (Genesys10, Thermo Fisher). The biomass dry weight was determined by heating bacteria in aluminum pan in convection oven (105 ℃) for more than 4 h until the weight become constant.

Growth curve determination

The growth curve of *G. oxydans* was determined by measuring the culture turbidity at 600 nm in UV-Vis spectrometer. A standard inoculum of striking a colony into 100 mL media was used for growth experiments. The correlation between absorbance and cell dry weight was determined at 60-80 h when the growth reached stationary phase.

Microbial fermentation

The 48 h growth *G. oxydans* was added into each conical flask with fermentation medium of 2 g/L initial inoculation. Each flask was then covered with a sponge and incubated at 30 ℃ in an orbital shaker at 220 rpm. Samples of fermentation liquid were taken periodically in a Biological Safety Cabinet under aseptic conditions. 0.3 mL of the aliquot mixed with *G. oxydans* were transferred into a 1.5 mL centrifuge tube and centrifuged at 12,000 rpm for 5 min. After centrifugation, supernatant was withdrawn and mixed with DI water to dilute properly for the chemical analysis. Glucose and xylose consumption rate (g/L-h) was estimated from the change of sugar concentration over the first 3 h during the fermentation. It was assumed that the biomass concentration was negligibly changed in the first 3 h of fermentation. The gluconic acid and xylonic acid yield were calculated as % of the theoretical yield by using the following formulas:

$$\%\, Yield = \frac{0.92 \times [gluconic\ acid]}{[glucose]} \times 100\%$$

$$\%\, Yield = \frac{0.90 \times [xylonic\ acid]}{[xylose]} \times 100\%$$

HPLC and LC/MS analysis

The glucose, xylose, gluconic acid (GA), xylonic acid (XA), 2-keto-gluconic acid (2KGA), and 5-keto-gluconic acid (5KGA) were quantitatively analyzed by HPLC system

(Shimadzu, Aminex HPX-87H column) using method described in Chapter 3. Aliquots (20 μL) were injected after passing through a 0.45 mm nylon syringe filter. Monosaccharides were quantified with reference to standard compounds.

GA, XA, 2KGA, 5KGA, and other products were qualitatively determined with LC/MS Systems (ACQUITY, Waters Corp.) in negative ESI-MS described in previous chapters.

Microscopy analysis of bacteria

The morphology of the bacteria cultivated for 24 h was observed using a field emission scanning electron microscopy (SEM, JEOL 7000F) described in chapter 2. About 0.1 mL of the culture was withdrawn at 24 h and diluted 10 times with DI-water. The bacteria cells were directly casted on a silicon wafer slide and air-dried under fume hood. The dried slides were immediately coated with gold for a thickness of 30 nm and observed under SEM.

4.3 Results and discussion

4.3.1 SEM analysis and growth curve of *G. oxydans*

The *G. oxydans* cells were observed with SEM in high resolution (**Figure 4-1**). Belonging to the family *Acetobacteraceae*, *G. oxydans* was typically ellipsoidal to rod shape as previously described (Holt et al. 1994). The *G. oxydans* showed shapes of ovoid with 2 μm × 1 μm size (Batzing and Claus 1973). No flagella were observed. The shape of organism differed from other subspecies described as spherical and rod shape (Ameyama 1975). Some cells were still undergoing fission which could be thought as rod like under small magnification (**Figure 4-1**). In the samples directly prepared from medium culture, the bacteria tended to aggregate in the

air drying process instead of evenly distributed on the silica wafer slide. This aggregation of cells was probably caused by the dehydration force by surface tension.

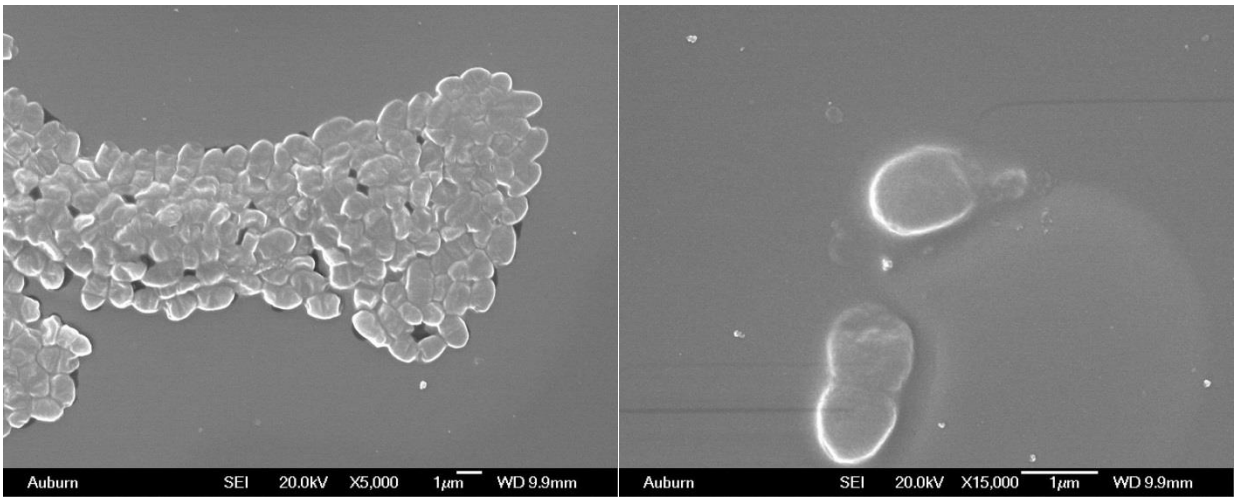

Figure 4-1. SEM images of *G. oxydans* drop-casted from a 24 h growth culture.

The batch growth of *G. oxydans* was studied in the glucose-containing media without pH control with one colony inoculum. The growth curves showed a biphasic form including two exponential phases from 12 to 40 h and 80 to 100 h (**Figure 4-2**). A similar biphasic growth was observed in a complex medium containing glycerol (Batzing and Claus 1971). In the first phase, glucose was converted into gluconate quantitatively (see details on the following sections). When the glucose was completely consumed, the *G. oxydans* continues to grow on gluconate as carbon source but at a very slow rate (Batzing and Claus 1971). That is why the generation time of the secondary exponential phase was longer than the primary exponential phase (30 vs 10 h).

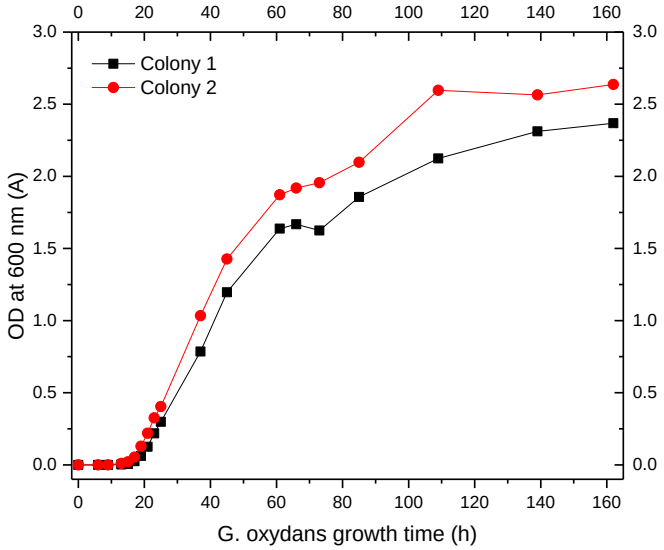

Figure 4-2. Growth curve of *G. oxydans* ATCC621 in the glucose medium.

A linear relationship was obtained between the cell dry weight concentration (X, g/L) at stationary phase and OD absorbance. The linear regression resulted in the following equation.

$$X\ (\text{g/L}) = 0.546 \times A$$

G. oxydans converts glucose into gluconic acid and ketogluconic acid. The oxidation was confirmed in Petri dish containing $CaCO_3$ by the clear zone method (**Figure 4-3**). By incubating the Petri dish for 7 days, it produced acids that dissolved the $CaCO_3$ component and formed a clear region surrounding the colonies. The clear zone was observed on the second day of incubation. After one week, colonies by the streaked line produced sufficient amount of acids to dissolve the embedded $CaCO_3$. This experiment verified the presence of gluconic acid oxidized by *G. oxydans*.

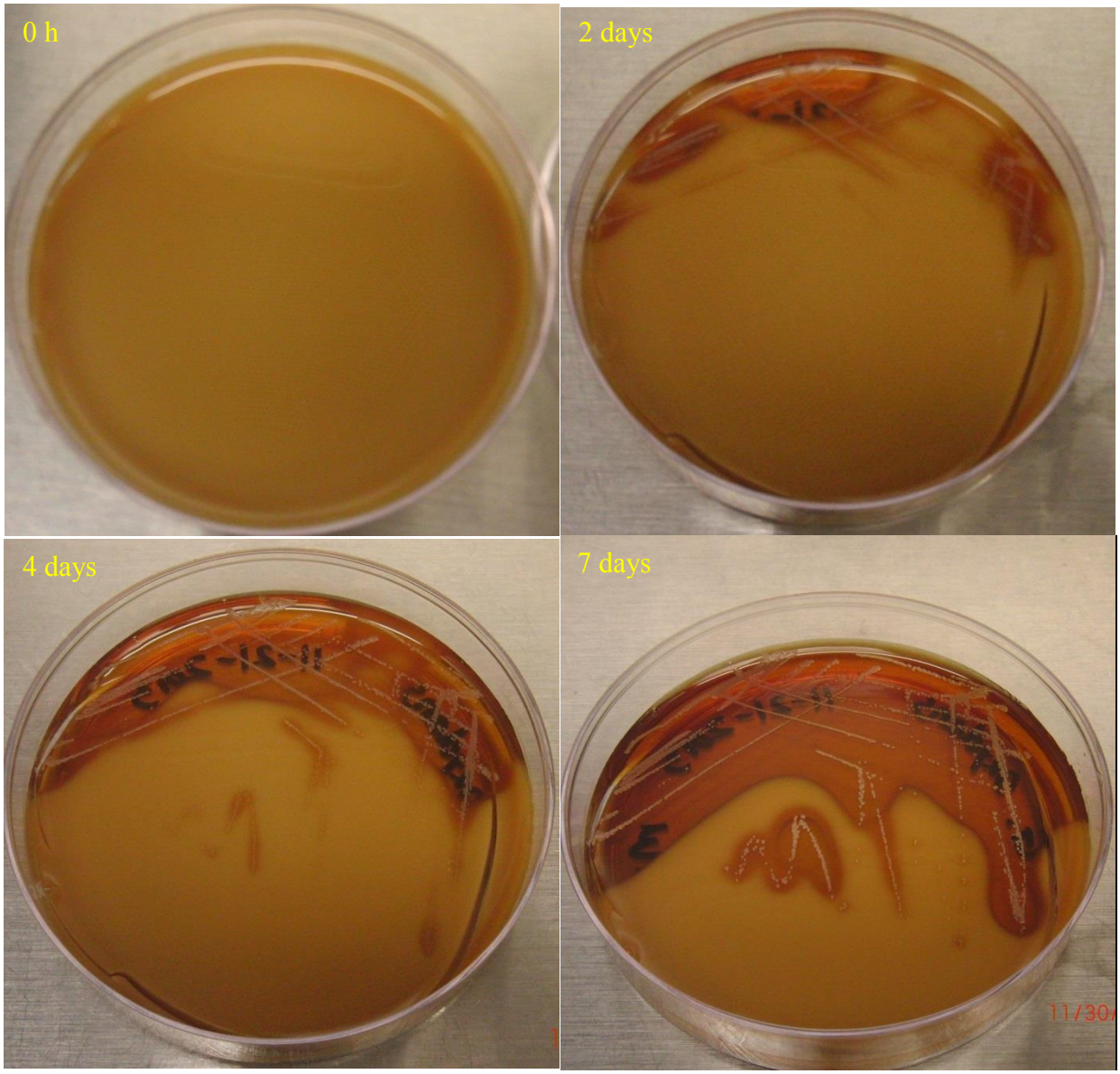

Figure 4-3. Presence of gluconic acid in $CaCO_3$-containing Petri dish incubated for 7 days.

4.3.2 Effects of medium pH on glucose and xylose fermentation

The production of gluconic acid and xylonic acid by *G. oxydans* was investigated on 20 g/L glucose or xylose, respectively, without pH control (**Figure 4-4**) and with pH control by adding 6 g/L $CaCO_3$ (**Figure 4-6**). Without pH control, the glucose and xylose showed a distinct fermentation profile corresponding to 86.8% and 60.8% of gluconic acid and xylonic yield,

respectively. The consumption rates of glucose and xylose (the first 3 h fermentation) were 2.3 and 1.5 g/L-h respectively. The glucose consumption rate remained constant at the first 9 h and decreased slightly from 9 to 12 h until the complete consumption before 24 h fermentation. However, the xylose consumption rate decreased abruptly down to 0.7 g/L-h in the second 3 h of fermentation. The xylose consumption and the xylonic acid production stopped at about 24 h and plateaued thereafter.

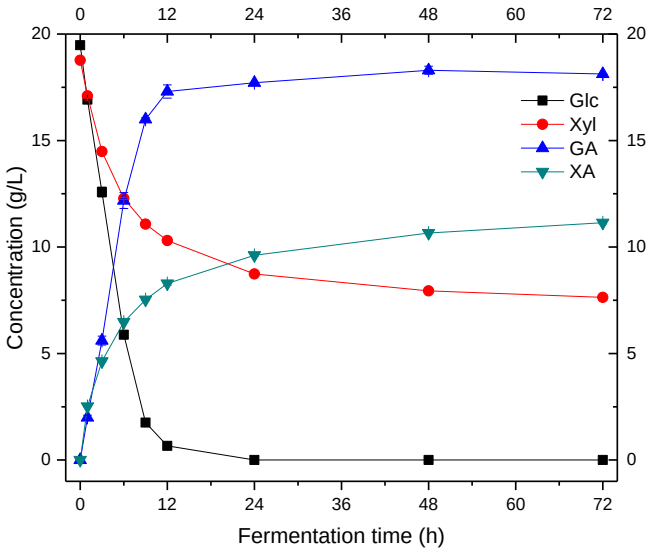

Figure 4-4. Fermentation of glucose and xylose by *G. oxydans* without pH control (GA: gluconic acid; XA: xylonic acid).

Considering the pKa values for gluconic acid and xylonic acid (3.7 and 3.6, respectively), the lower pH of medium was expected from xylose fermentation. However, the accumulation of gluconic acid gave rise to a similar medium pH drop as xylose fermentation from 5.7 to 2.0 within 12 h (**Figure 4-5**). The pH drop appeared to have more effect on decreasing the xylose consumption whereas the glucose consumption was negligibly affected. Beside the pH effect, the cease of xylose assumption could also be related to inhibitory end-products, more in the xylose

fermentation than glucose fermentation. It was reported that the accumulated glucono-δ-lactone and xylono-γ-lactone in the glucose and xylose fermentation, respectively, were inhibitory to sugar uptake by *G. oxydans*. (Milsom and Meers 1985). However, the spontaneous hydrolysis rate of glucono-δ-lactone was more rapid than xylono-γ-lactone at neutral pH (Buchert and Viikari 1988b). Hence, the repressive role of glucono-δ-lactone was not as significant as xylono-γ-lactone in the overall fermentation.

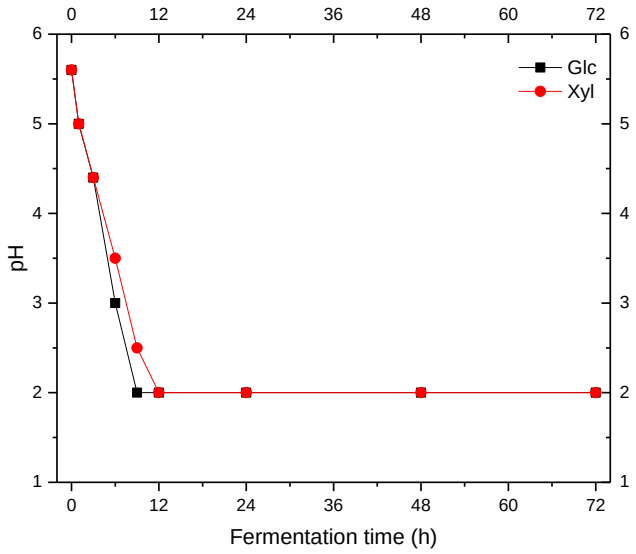

Figure 4-5. pH profile of the medium in glucose and xylose fermentation by *G. oxydans.*

The optimum pH for glucose dehydrogenase and xylose dehydrogenase was 6.0 (Buchert and Viikari 1988a). To study the effect of pH on glucose and xylose consumption, fermentation with pH control was carried out by adding 6 g/L $CaCO_3$ (amount needed for neutralizing gluconic or xylonic acid production in a theoretical yield). With a constant pH at 6.5, both glucose and xylose were consumed within 24 h and the gluconic acid yield (73.2%) peaked at 12 h fermentation whereas xylonic acid reached 91.5% at 48 h (**Figure 4-6**). A similar result was

previously found with xylose fermentation (98% at 42 h) (Buchert et al. 1988). The initial consumption rates (first 3 h) for glucose and xylose were similar, 1.8 and 1.5 g/L-h, respectively.

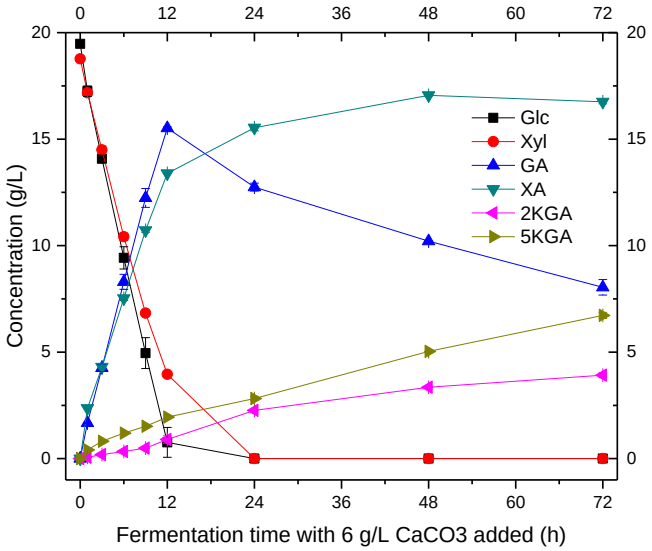

Figure 4-6. Fermentation of glucose and xylose by *G. oxydans* with pH controlled by 6 g/L $CaCO_3$ (2KGA: 2-ketogluconic acid; 5KGA: 5-ketogluconic acid).

We also observed 2-ketogluconic acid (2KGA) and 5-ketogluconic acid (5KGA) were produced with the production of gluconic acid, which agreed well with previous study (Olijve and Kok 1979). In the first 12 h, glucose was oxidized almost quantitatively to gluconic acid and a small amount of 2KGA and 5KGA were produced (**Figure 4-6**). After 12 h, the gluconic acid in the culture medium continued being oxidized into 2KGA and 5KGA suggesting the strain could utilize gluconate as alternative carbon source.

4.3.3 Inhibition of xylonic acid on xylose fermentation

The xylonic acid inhibition was carried out by with addition of 8.0 g/L xylonic acid at the beginning of initial inoculum (dark blue line) compared with xylose fermentation control (black

line) (**Figure 4-7**). It was observed that 8.0 g/L xylonic acid completely inhibited xylose fermentation without addition of $CaCO_3$ (no xylose consumption within 96 h), whereas the xylose fermentation control generated 66.7% xylonic acid. At 48 h, 10 g/L $CaCO_3$ was added into the xylose fermentation with xylonic acid (dark blue line) to change the xylonic acid to corresponding salt. It was found that nearly no xylose was consumed (pink line after 48 h). This indicated that the bacteria cell had lost the viability after incubation with xylonic acid for 48 h.

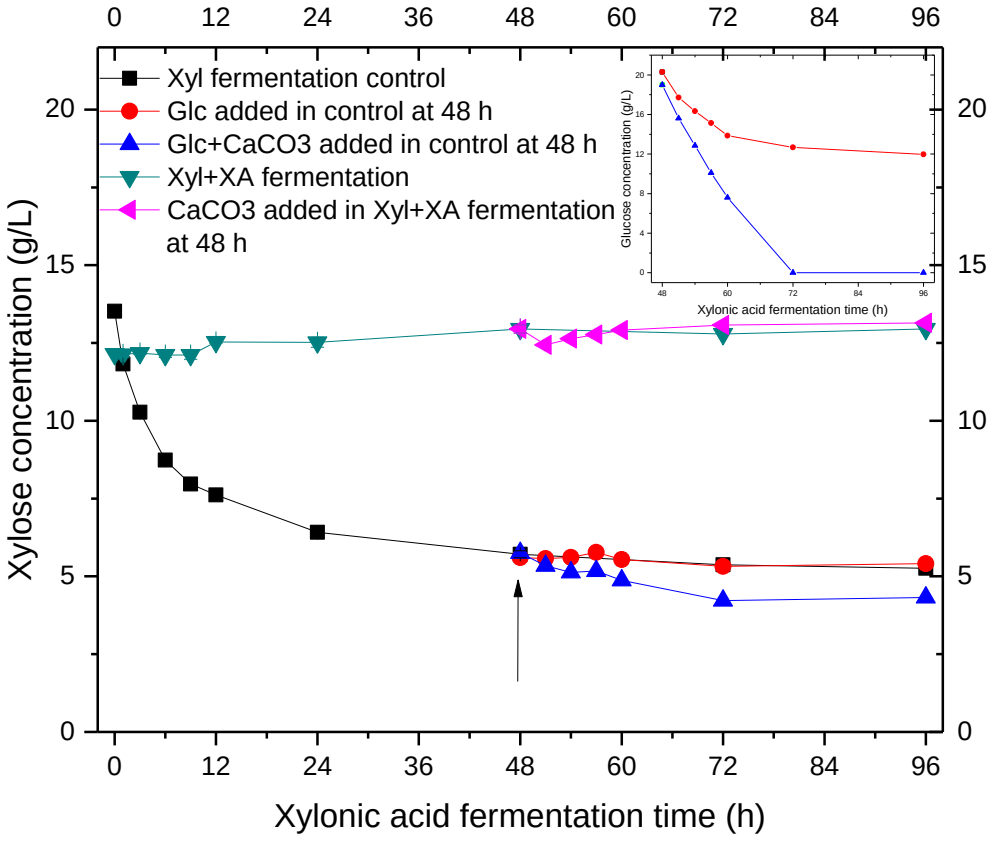

Figure 4-7. Effect of xylonic acid on xylose consumption in batch fermentation (inset: glucose consumption).

For the control, the fermentation was resumed partially after adding only 20 g/L glucose at 48 h, which was indicated by a glucose consumption of 41% (red line in inset figure of **Figure 4-7**). When glucose (20 g/L) and $CaCO_3$ (7 g/L) were added together into control, the fermentation was resumed quickly and it resulted in a complete consumption of glucose (blue line in inset figure of **Figure 4-7**). This result strongly indicated that the xylonic acid was inhibitory to glucose fermentation. The $CaCO_3$ neutralized xylonic acid and formed xylonate instead of xylono-γ-lactone which could remove the inhibitory effect. The corresponding production of xylonic acid and gluconic acid were shown in **Figure 4-8**. The xylonic acid concentration increased after 48 h when adding $CaCO_3$ was probably due to the hydrolysis of xylonolactone (Buchert and Viikari 1988b).

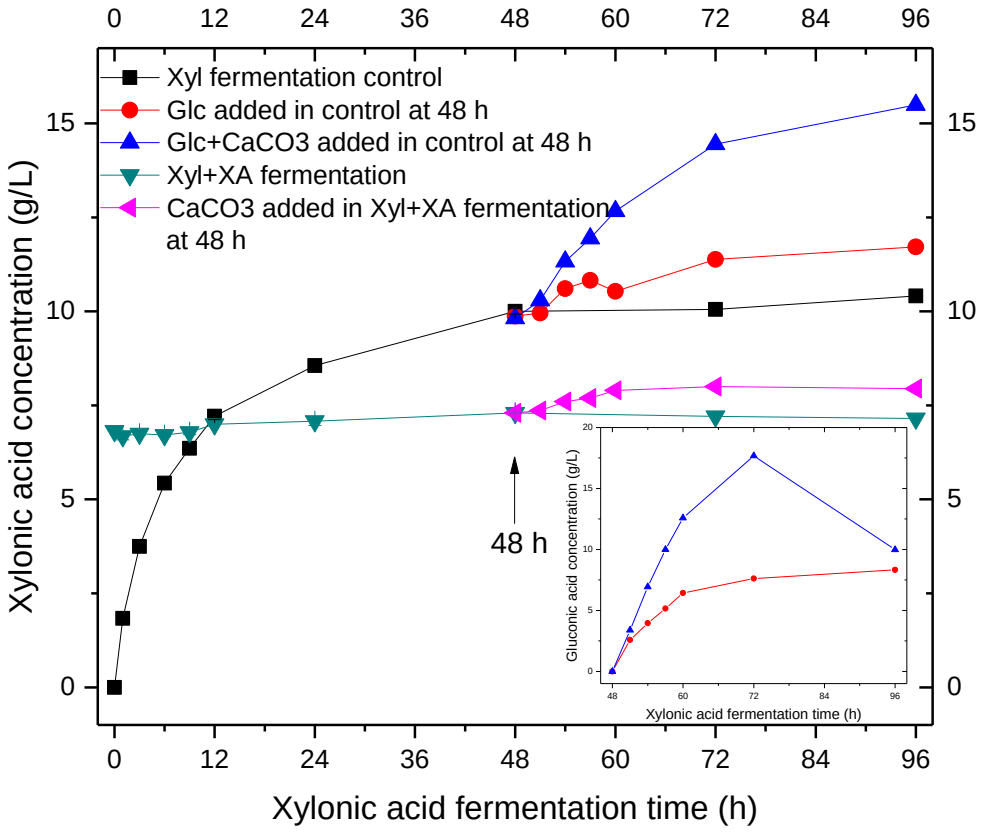

Figure 4-8. Effect of xylonic acid on xylose fermentation (inset: gluconic acid production).

4.3.4 Inhibition of xylonic acid on glucose fermentation

The inhibition of xylonic acid on glucose fermentation was performed by adding 8.0 g/L xylonic acid with the initial inoculum (dark green line) compared with glucose fermentation control (black line) (**Figure 4-9**).We found that the gluconic acid yield from glucose fermentation with xylonic acid added was only 29.5% in contrast with 97.6% in the glucose control. This result indicated that the xylonic acid strongly inhibited the glucose fermentation as well. Therefore, the xylonic acid was inhibitory to both glucose and xylose fermentation by *G. oxydans*.

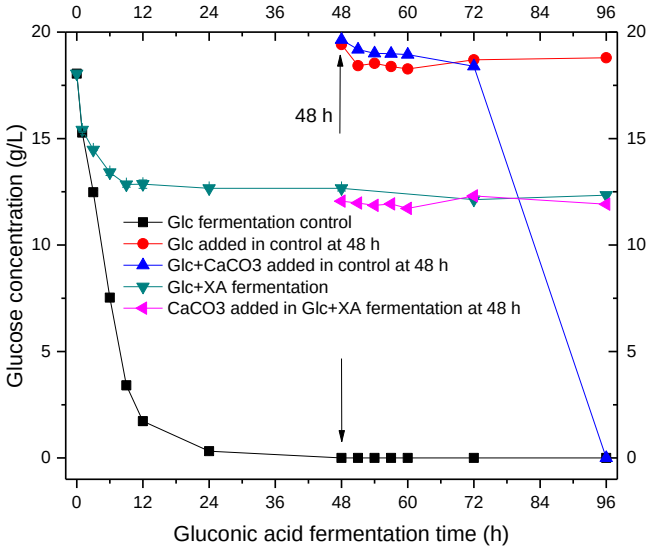

Figure 4-9. Effect of xylonic acid on glucose consumption in batch fermentation.

The glucose consumption in glucose fermentation with xylonic acid added was not resumed at 48 h with addition of $CaCO_3$ (pink line in **Figure 4-9**) probably due to the loss of bacterial viability by incubation with the added xylonic acid. In addition, the glucose fermentation was not resumed at 48 h with fresh glucose (20 g/L) added in control (red line). However, when the glucose was added with 7 g/L $CaCO_3$ together in control, glucose consumption in the fermentation was resumed after further 24 h incubation (blue line). These results indicated that xylonic acid was inhibitory to glucose fermentation. The effect of xylonic acid on the production of gluconic acid was compared in **Figure 4-10**.

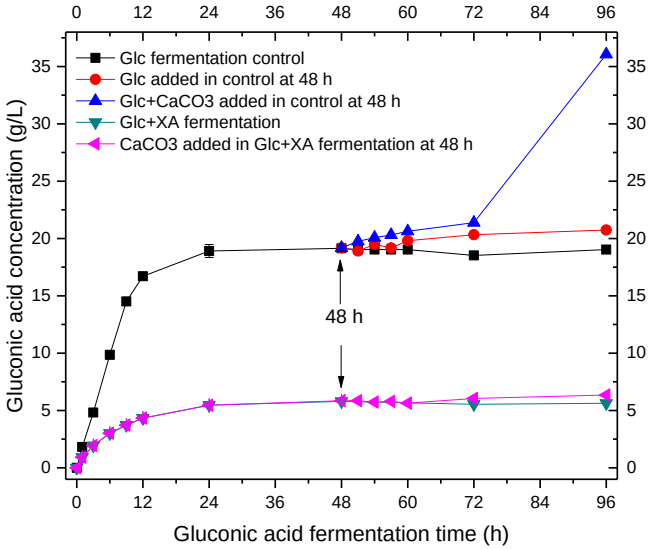

Figure 4-10. Effect of xylonic acid on gluconic acid production in batch fermentation.

4.4 Conclusion

The oxidation of glucose by *G. oxydans* without pH control showed much higher rate and yield than those of xylose. This indicated that probably the undissociated acids from xylose fermentation strongly inhibited the oxidation process. Our further study showed xylonic acid was a strong inhibitor to glucose and xylose fermentation. The addition of $CaCO_3$ was an effective way to change the undissociated acids to dissociated salts, which could reduce the inhibition significantly.

Chapter 5 Preparation and characterization of cellulose nanocrystals (CNCs)

5.1 Background

Cellulose, renewable material on earth, is a linear polymer consisting of repeated cellobiose unit linked by β-1,4-glucosidic bonds. The native cellulose is characterized by its hydrophilicity, chirality, biodegradability, modifying capacity, and versatile semicrystalline and fibrillar morphologies (Klemm et al. 2005). The natural and sustainable materials have been expanded with the emergence of cellulose nanocrystals (CNCs) (Klemm et al. 2011) which are the remained crystalline regions after cellulose hydrolysis. Cellulose nanoparticles inherit the important properties from cellulose such as morphologies, mechanical properties, hydrophilicity, and modification capacity. The potential applications for CNCs-based products are broad such as film with specific property, flexible displays, reinforcing fillers, textiles, medical and electronic devices, biomedical implants, and electro-active polymers etc. (Moon et al. 2011).

CNCs are typically isolated from cellulose by acidic hydrolysis (Habibi et al. 2010). The amorphous regions are preferentially cleaved off transversely, whereas the crystalline regions are remained as intact nanoparticles with a width of 5-50 nm. The induced geometrical dimensions (length, width, and surface area) of CNCs depend strongly on the cellulose sources, the nature of acid, and the conditions of isolation (Dong et al. 1998; Habibi et al. 2010). The CNCs from HCl hydrolyzed cellulose (HCl-CNCs) tend to flocculate at an increased concentration due to the inter-particle aggregation (Araki et al. 1998). However, the dispersion of H_2SO_4 hydrolyzed CNCs (H_2SO_4-CNCs) in water is significantly improved due to the introduction of negatively charged sulfate groups (Marchessault et al. 1961; Marchessault et al. 1959). The H_2SO_4-CNCs form a stable liquid crystalline phase with birefringence (Revol et al. 1992). Spherical CNCs

were prepared when cellulose was treated with a mixture of HCl and H_2SO_4 (Wang et al. 2008), which exhibited less sulfate groups and stable colloidal suspension. Besides the type of acids used, the source of cellulose also affects the CNCs properties remarkably in terms of geometrical dimensions, rheological properties, and thermo-stabilities. Few studies have been focused on addressing the influence of acids and cellulose sources on the properties of CNCs.

This chapter was to prepare CNCs from Avicel and filter paper with HCl or H_2SO_4 and to characterize their physical and chemical properties. The enzymatic hydrolysis of HCl-CNCs and H_2SO_4-CNCs was compared as well. Time Domain NMR was used to characterize the hydrophilicity of CNCs. In addition, the rheological phase behavior was compared by polarized microscope between H_2SO_4-CNCs isolated from Avicel and filter paper.

5.2 Material and methods

Chemicals and materials

The microcrystalline cellulose (MCC/Avicel PH101), 2-methylpyridine borane complex ($C_6H_7N\ BH_3$ 95%) were purchased from Sigma Aldrich (Milwaukee, WI). Toluene (extra dry) was purchased from ACROS Organics. Pyridine (99%) and acetic anhydride (99%) were from Alfa Aesar. Hexane (ACS), HCl (5.0 N), H_2SO_4 (ACS, 96%) were purchased from BDH. Methanol (99.8%, HPLC grade) was from EMD. DI-water was produced by the Barnstead Nanopure UV Ultrapure Water System (Thermo Fisher Scientific, Marietta, OH).

Cellulose nanocrystals preparation

CNCs were prepared and isolated from Avicel and filter paper (Grade 454, VWR) by acid hydrolysis according to the methods with modification (Araki et al. 1998; Bondeson et al. 2006). In the preparation of H_2SO_4 treated CNCs, 40 g Avicel or filter paper was hydrolyzed by 700 g (~455 mL) 64% H_2SO_4 at 45 ℃ water bath for 50 min with continuous magnetic stirring. The reaction was quenched by adding 600 mL ice-cold water. The suspension was then centrifuged (3000 rpm) at 4 ℃ for 15 min. The supernatant was decanted and fresh DI-water was refilled to wash the precipitate. This washing cycle was repeated until the fine particles did not sediment. The turbid supernatant was collected and dialyzed in Spectra/Por 2 membrane tube with MWCO 12-14 kD (Rancho Dominguez, CA) thoroughly against DI-water for 3 days with change of water at every 12 h. The suspension was finally sonicated with a tip sonifier (Branson 450, Danbury, CT) for 5 min at 60% output and 70% duty cycle. The suspension was further concentrated at 40 ℃ in rotary evaporator and freeze dried. The resulting CNCs from Avicel and filter paper were designated by H_2SO_4-CNCs and H_2SO_4-CNCs-FP respectively. For the HCl-CNCs, 10 g Avicel was hydrolyzed in 500 mL 4 M HCl at 80 ℃ for 5 h. The isolation process was the same as that for H_2SO_4-CNCs.

SEM and AFM analysis

The dried samples were coated with 20 nm thickness layer of gold by PELCO SC-6 Sputter Coater. Samples for SEM were observed using a field emission scanning electron microscopy (SEM, JEOL 7000F), with accelerating voltage at 20 KV. The atomic force microscopy (AFM) measurements were performed with a Nano-R atomic force microscope from Pacific Nanotechnology. Calibration was performed by scanning a calibration grid with a known dimension. All scans were performed in air with aluminum coated cantilever SPM tips

(MikroMasch). When the tip was brought into the proximity of a sample surface, the cantilever is deflected by the repulsive forces between the tip and the sample. The deflection is measured by a laser reflected from the cantilever tip to a photodiode detector.

Elemental analysis

All the nanoparticle powders were dried in oven equipped with vacuum (200 mbar) at 45 ℃ overnight before elemental analysis (Series II CHNS/O analyzer, PerkinElmer). Carbon, hydrogen, nitrogen, and sulfur contents were achieved through their quantitative conversion to CO_2, H_2O, NO_2, and SO_2, respectively, by combustion.

Zeta potential determination

The zeta potential (ζ, mV) of CNCs aqueous suspensions (0.05 wt%) was measured by Zetasizer Nano ZS (ZEN3500, Malvern) without adjusting the ionic strength. Size and zeta potential scanning was conducted after 1 min equilibrium at 25 ℃. All suspensions were scanned in triplicates and the average ζ values were calculated by the software (zetasizer 7.02) based on the electrophoretic mobility.

Time domain NMR analysis

The time-domain NMR experiments was conducted using previous described method (Elder and Houtman 2013). In detail, the freeze dried CNCs were saturated with deionized water in desiccator for 20 days. The samples were periodically analyzed by a Bruker mq20-Minispec analyzer with an initial experiment in the freeze dried condition. Samples were placed in 18-mm NMR tubes with a depth of 20 mm. The experiments were performed at 40 ℃ with a 0.7-T

permanent magnet for a 20-MHz proton resonance frequency. The T_2 (spin-spin) relaxation times were determined with the Carr-Purcell-Meiboom-Gill pulse sequence, with pulse separation of 0.08 ms, 128 echoes collected, and 32 scans with a 5s recycle delay. The relaxation time distributions were calculated from the decay curves with CONTIN.

X-ray diffraction (XRD) analysis

The XRD pattern was obtained with the Ni-filtered CuKα radiation generated by a Bruker D8 Discover X-ray diffractometer. The CuKα radiation at 30 kV and 36 mA is filtered out from the data using a single-channel analyzer on the output from Lynxeye detector. The source slits were Cu Sollers with 1.00 mm goniometer radius, and the detector slits were 2.5 °. Dried cellulose samples (approximately 0.1 g) were directly mounted onto a quartz substrate. Scans were obtained from 5 to 50 degrees 2θ in 0.01 degree steps for 0.5 seconds per step.

Fourier transform infrared spectroscopy (FTIR) analysis

FTIR spectra of Avicel, H_2SO_4-CNCs, HCl-CNCs, and modified CNCs were measured using a FTIR-ATR Spectrometer (Spectrum 400, PerkinElmer). All spectra in the range of 600-4000 cm^{-1} were obtained in a transmittance mode on a diamond crystal top-plate at room temperature with a background against air. For each measurement, approximately 5 mg of the dry powder samples were pressed onto the crystal. The spectrum was recorded by the accumulation of 64 scans with a resolution of 4 cm^{-1}. The baselines were corrected and the spectra were deconvoluted accordingly.

Nitrogen adsorption analysis

The nitrogen adsorption/desorption isotherms of the CNCs samples were obtained at liquid nitrogen temperature using Tristar 3020 (Mciromeritics). All samples were outgassed at 80 ℃ for 12 h under vacuum to remove the moisture and other contaminants prior to the measurement. The surface areas of the samples were obtained by means of the standard method of Brunauer, Emmett, and Teller (BET) applied in a relative pressure range from 0.05 to 1 (Brunauer et al. 1938).

Polarized optical microscopy analysis

All the liquid colloidal samples were sonicated using a Branson 350 bath sonicator for 3 minutes in order to disperse agglomerates which may have formed during the preparation process. The color micrographs were taken with a Nikon (Melville, NY) Eclipse 80i optical microscope using an LU Plan Fluor 20x/0.45NA Nikon objective lens at room temperature (Ureña-Benavides et al. 2011). The samples (10 μL) were dropped on a microscope slide and sandwiched between a glass slide and a glass coverslip to against the evaporation.

Thermal gravity analysis (TGA)

The thermal properties of all samples were measured by TG-IR Interface Pyris 1 TGA analyzer (PerkinElmer). The samples (6 mg) were heated at a rate of 10 K/min in flowing N_2 at 20 mL/min.

5.3 Results and discussion

5.3.1 SEM analysis of CNCs

The cellulose sources usually have influence on the dimension, morphology, and surface area of CNCs even with the same isolation procedure (Habibi et al. 2010). SEM analysis of the Avicel, H_2SO_4-CNCs, and HCl-CNCs revealed that CNCs had a needlelike structure with size about 300 nm × 10-20 nm (**Figure 5-1**). The dimensions of H_2SO_4-CNCs and HCl-CNCs were similar in length but the HCl-CNCs and H_2SO_4-CNCs-FP were twice as wide as that of H_2SO_4-CNCs, which resulted in a different aspect ratio (30 vs 15). Our result showed that H_2SO_4-CNCs dimension from Avicel, 10 nm × 200 nm, was in agreement with previous study (Cho and Park 2011). The length of H_2SO_4-CNCs was larger than those prepared by Bai (Bai et al. 2009) because they used longer hydrolysis time (5 h vs 1 h). Our H_2SO_4-CNCs with lower yield (34.53%) was probably caused by large liquid to solid ratio (12 vs 9 mL/g). The stronger hydrolysis condition leaded to more fine fractions with lower yield. The tendency for agglomeration of HCl-CNCs was probably due to the hydrogen bonds neutral surface whereas in H_2SO_4-CNCs a repulsive force derived from the charged sulfate groups evenly scattered the CNCs. The H_2SO_4-CNCs-FP were shorter (mostly 100 nm) probably due to less crystallinity of filter paper (61%) than Avicel (65%) (Park et al. 2009). Prolonged reaction time or increased acid to cellulose ratio reduced the dimensions of CNCs (Beck-Candanedo et al. 2005; Dong et al. 1998). Therefore, the crystalline regions of filter paper actually were exposed to acids for longer time resulting in a shorter CNCs length.

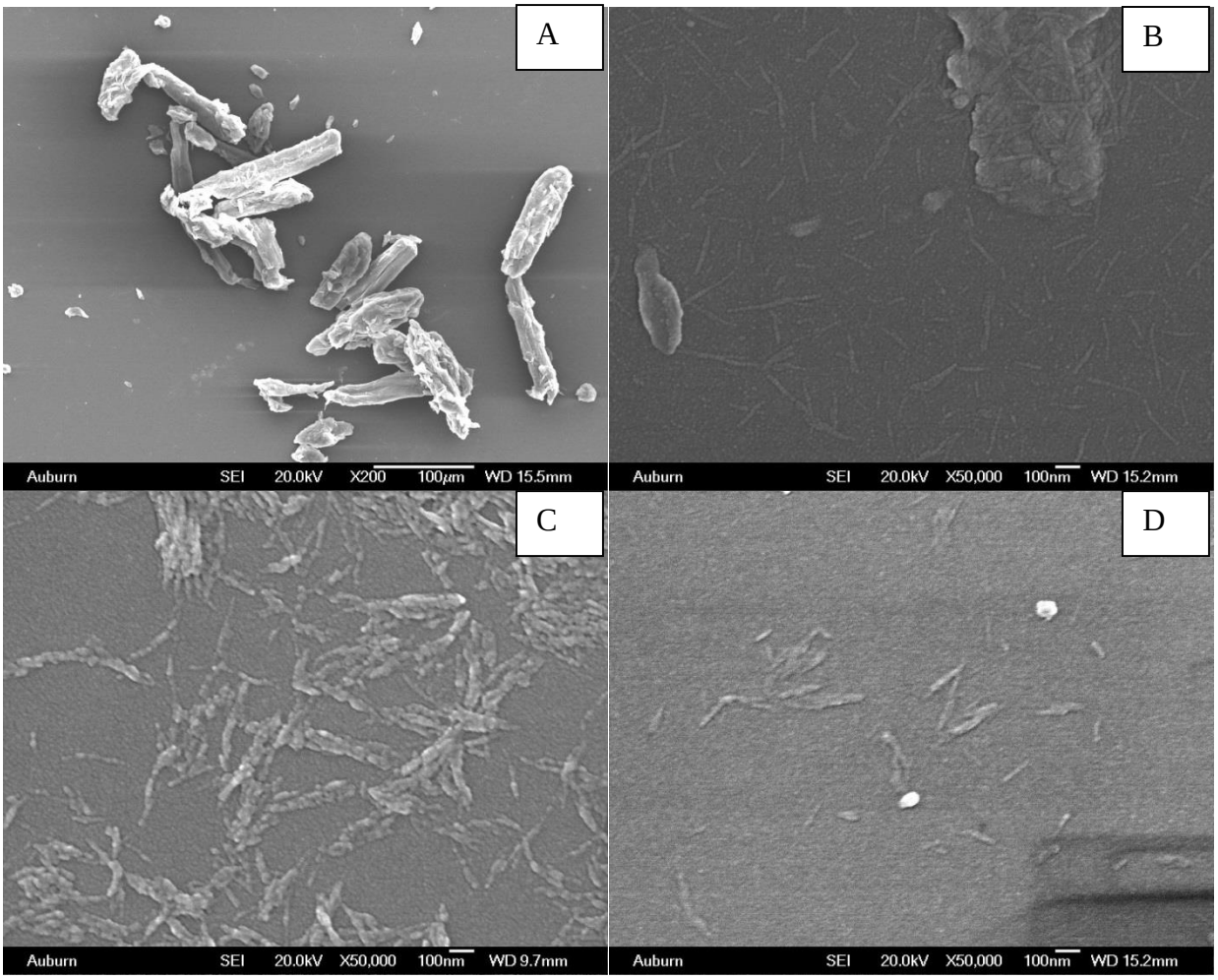

Figure 5-1. SEM images of (A) Avicel, (B) H_2SO_4-CNCs; (C) HCl-CNCs; and (D) H_2SO_4-CNCs-FP.

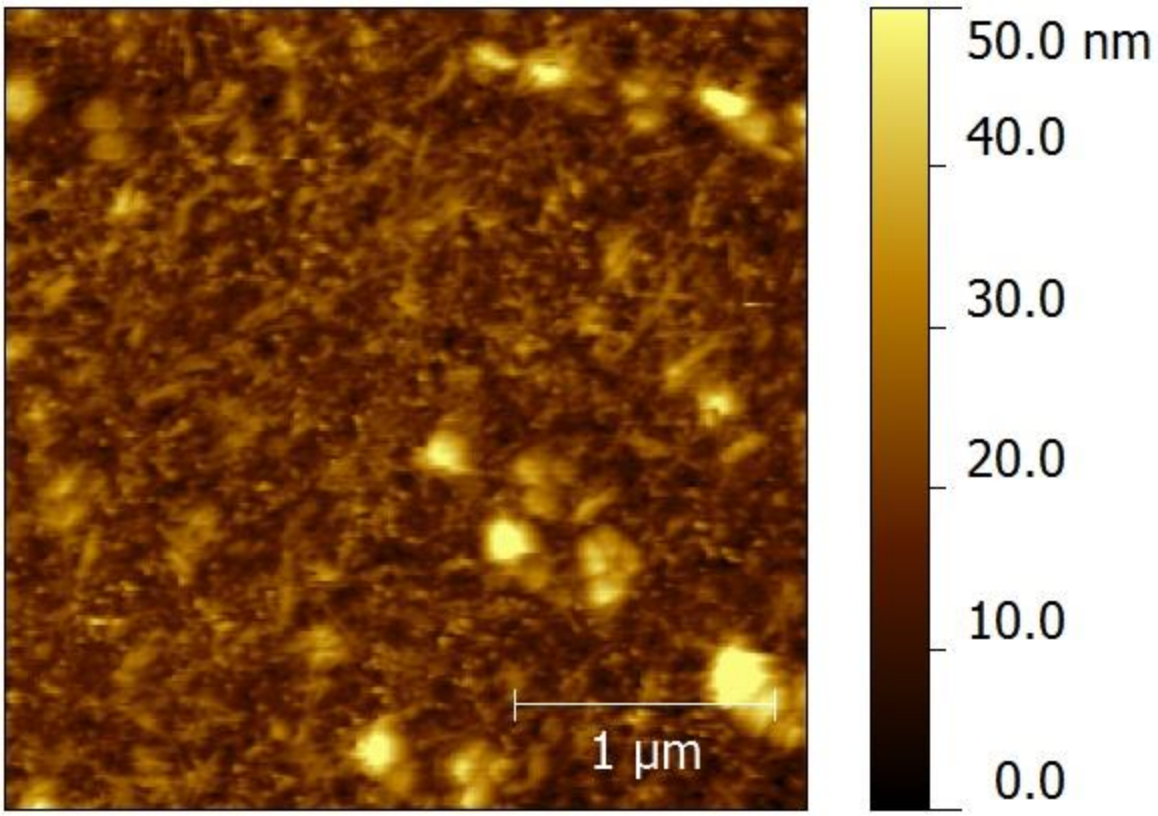

Figure 5-2. AFM image of H_2SO_4-CNCs (a film drop-casted from 0.5 wt% suspension).

Surface morphology and topology of CNCs layers were usually characterized by atomic force microscopy (AFM) (Podsiadlo et al. 2005). It was found that the H_2SO_4-CNCs were scattered on the glass substrate in fibrillar form of 300 nm × 15 nm (**Figure 5-2**). The AFM result confirmed the dimension of H_2SO_4-CNCs detected by SEM.

5.3.2 TGA analysis of CNCs

The H_2SO_4-CNCs and HCl-CNCs showed a different thermal degradation pattern in that H_2SO_4-CNCs compromised the thermal stability in contrast to HCl-CNCs (**Figure 5-3**). The Avicel and HCl-CNCs went through two decomposition stages, namely, below 180 ℃ and 180 to

500 ℃. In the stage below 180 ℃, the weight loss was primarily caused by the evaporation of water. During the stage from 180 to 500 ℃, the weight loss (70%) was attributed to the pyrolysis of cellulose through decomposition, depolymerization, and dehydration (Kim et al. 2001). The HCl-CNCs lost less weight than Avicel, which indicated a lower amorphous content after the HCl hydrolysis (Shafizadeh 1976). Compared to HCl-CNCs, the H_2SO_4-CNCs from either Avicel or filter paper presented a decomposition starting at 190 ℃. This degradation behavior was attributed to the catalytic effect of sulfate groups on the cellulose degradation reaction (Roman and Winter 2004). The two-stage degradation pattern, 190 to 350 ℃ and 350 to 500 ℃, suggested that two regions in the H_2SO_4-CNCs are involved in the decomposition: the low temperature degradation stage corresponded to the more accessible amorphous region with high sulfated groups, whereas the higher temperature one was related to the interior crystal region with little sulfonation (Kim et al. 2001; Roman and Winter 2004). The CNCs isolated from filter paper exhibited the same thermal stability as these from Avicel (**Figure 5-3**), which confirmed the sulfate groups had accelerated the decomposition of CNCs.

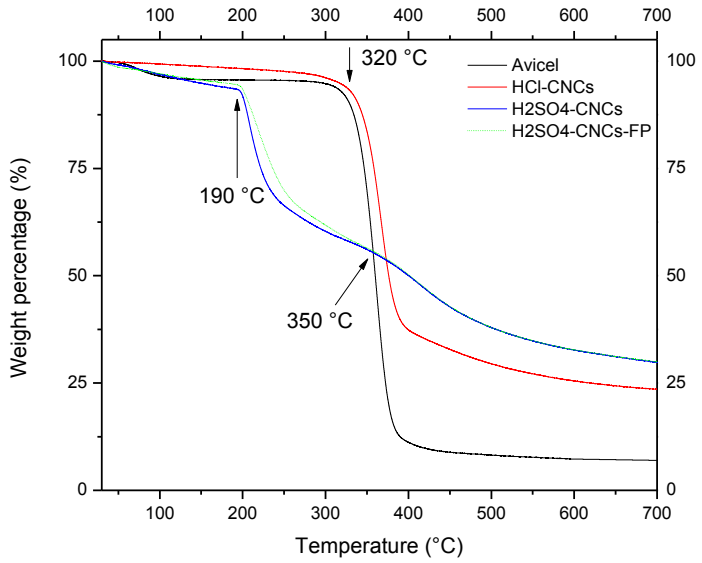

Figure 5-3. TGA curves of Avicel, HCl-CNCs, H_2SO_4-CNCs, and H_2SO_4-CNCs-FP.

5.3.3 Surface area determination and XRD analysis of freeze dried CNCs

The N_2 adsorption-desorption isotherms at 77 K of Avicel and H_2SO_4-CNCs showed type II adsorption curve with H3 hysteresis (**Figure 5-4**). The pore sizes of Avicel and H_2SO_4-CNCs after freeze dry were about 15.3 and 17.3 nm indicating the inter-crystal voids had cumulated during the frozen and sublimation process. The results were consistent with other report (Lu and Hsieh 2010). The BET surface areas were 0.8 and 4.1 m^2/g for Avicel and H_2SO_4-CNCs, respectively. These cumulative mesopores resulted in about five times more specific surface area than Avicel. Yet, our results were less than what Lu and Hsieh reported (1.5 and 13.3 m^2/g) (Lu and Hsieh 2010). The main difference could be caused by the frozen method used: their rapid freeze with liquid nitrogen prevented the aggregation of CNCs by hydrogen bonding. Our slow freezing process in a freezer provided sufficient time for the interaction of cellulose nanoparticles, thus created smaller surfaces. The aggregation of cellulose nanoparticles was

easier by the hydrogen bonding between hydroxyl groups when fewer sulfates were present on the CNCs surface (Han et al. 2013). This could also be the reason why we failed to get the adsorption-desorption curve for HCl-CNCs due to a stronger agglomeration.

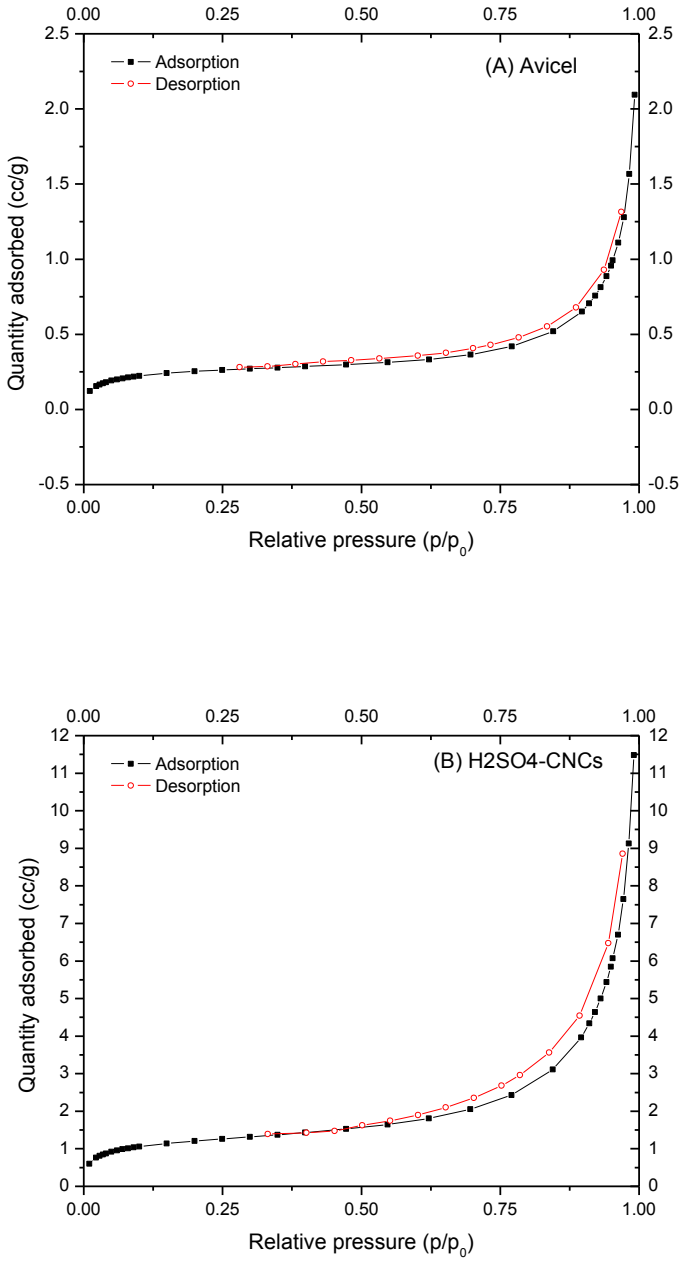

Figure 5-4. N_2 adsorption and desorption isotherms at 77K for (A) Avicel and (B) H_2SO_4-CNCs.

A nitrogen adsorption analyzer (Micromeritics ASAP 2000), was usually used to determine the specific surface area of nanoparticles based on the BET theory (Liou 2004; Luo et al. 2013; Rouquerol et al. 2013). Others calculated the specific area of several hundred m^2/g for CNCs from bacterial cellulose by summing individual nanoparticle surface area (Grunert and Winter 2002). The BET surface area is mainly used to determine particles with porous structure. So, surface area from calculation is more representative than that from BET method.

XRD spectrum has been used as a qualitative or semi-quantitative evaluation of the amounts of amorphous and crystalline domains in cellulose (Park et al. 2010b; Wada et al. 2004). Diffraction angles at $2\theta = 14.7°$, 16.4°, 22.6°, and 34.4° were used to characterize the cellulose I polymorphism of Avicel PH101 (Park et al. 2010b) (**Figure 5-5**). With the assumption that the I_β phase in the longitudinal direction along axis b, these 2θ angles correspond to the crystal lattice planes of (101), $(10\bar{1})$, (002), and (040). The cellulose I_β crystalline structure of cellulose was retained after acid treatment. The sharpened peaks and increased intensity of CNCs confirmed the higher crystallinity index than the original Avicel.

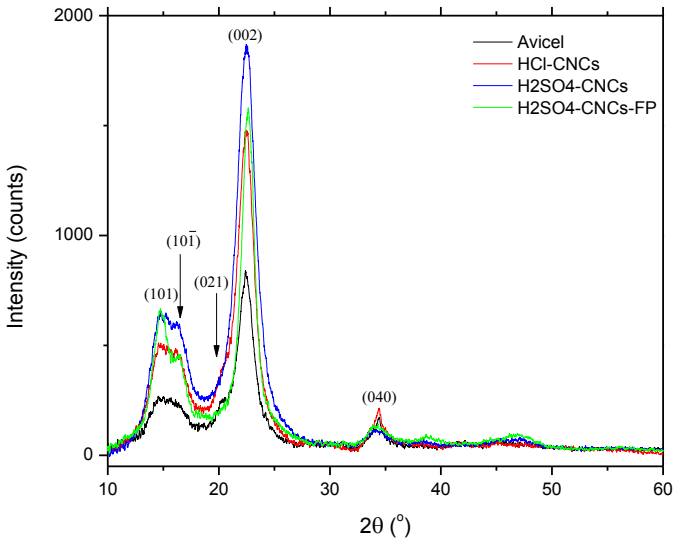

Figure 5-5. XRD spectra of Avicel, HCl-CNCs, H_2SO_4-CNCs, and H_2SO_4-CNCs-FP.

5.3.4 Zeta potential determination and elemental analysis of CNCs

The zeta potential (ζ) was measured to study the surface charges and electrostatic repulsion of cellulose materials. Both the average size and ζ were measured from 0.05 wt% aqueous suspension (**Table 13**). HCl-CNCs showed larger size than H_2SO_4-CNCs because of the mild hydrolysis intensity by 4 M HCl. The ζ values of Avicel suspension and HCl-CNCs were unmeasurable because they were not well dispersed in aqueous solution even after sonification. The H_2SO_4-CNCs from Avicel (50 and 100 min reaction time) and filter paper carried negative ζ values due to the presence of ester ($-OSO_3^-$ group on surface), -28.77 ±0.23, -62.13 ±1.10 and -30.73 ±0.78 mV, respectively. These results were consistent with previous reports (de Morais Teixeira et al. 2010; Hasani et al. 2008). The higher absolute value of ζ from 100 min hydrolysis was mainly caused by larger amount of sulphate groups on the surface. Moreover, longer hydrolysis time (100 vs 50 min) resulted in a shorter CNCs length (118 vs 335 nm).

Table 13. Elemental analysis and zeta potential of Avicel and CNCs.

Sample	Average length	Elemental analysis (%)				Zeta potential
		C	H	N	S	(mV)
Avicel	100 μm[a]	43.49	6.82	0.08	0.29	ND
Avicel sonicated	2 μm[a]	42.25	5.84	0.02	0.12	ND
HCl-CNCs	496 nm	42.60	6.64	0	0.26	ND
H_2SO_4-CNCs-50	335 nm	39.58	6.56	0	0.89	-28.77±0.23
H_2SO_4-CNCs-100	118 nm	41.28	6.72	0	1.21	-62.13±1.10
H_2SO_4-CNCs-FP	220 nm	41.73	6.51	0	0.95	-30.73±0.78

a: value from SEM; ND: not determined.

Elemental analysis results (**Table 13**) showed that Avicel had sulphur content (0.29%) before acids hydrolysis. The S% in HCl-CNCs (0.26%) further confirmed this result. However, the H_2SO_4-CNCs had about 0.6% higher S% than HCl-CNCs, that was introduced by H_2SO_4 hydrolysis in the form of sulphate half-ester (Abitbol et al. 2013a).

5.3.5 Lyotropic phase behavior of CNCs

The nanoparticle size and electrostatic surface charges were different between H_2SO_4-CNCs and HCl-CNCs, so was the lyotropic phase behavior (**Figure 5-6**). Specifically, the H_2SO_4-CNCs showed colloidal dispersion which was stabilized by the electrostatic repulsion force from the negatively charged sulfate groups on the CNCs surface, whereas HCl-CNCs agglomerated in the sediment (**Figure 5-6a'**). After standing at room temperature overnight, the colloidal suspension of H_2SO_4-CNCs (3.0 wt%) separated into isotropic phase on the top and anisotropic phase at the lower layer (**Figure 5-6d**).

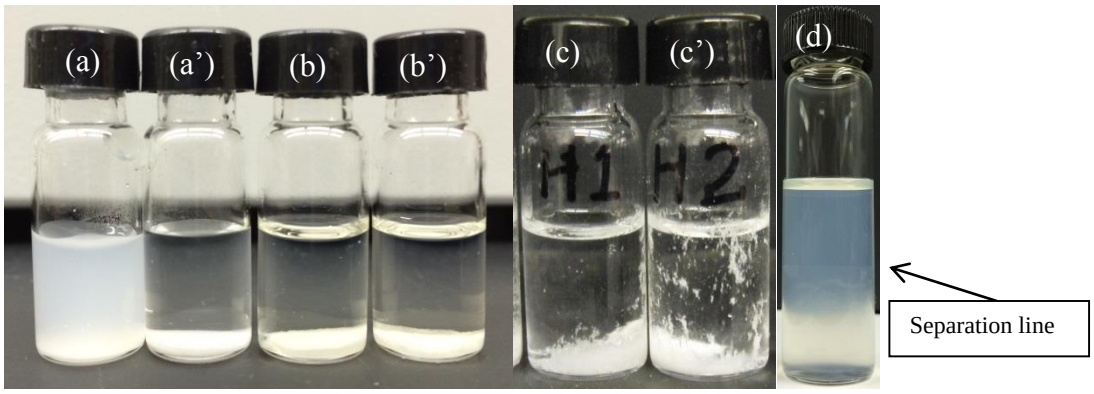

Figure 5-6. Dispersion of 1 wt% CNCs (left: H_2SO_4-CNCs; right: HCl-CNCs) in solvents after 15 min bath sonification (a: water; b: gasoline; c: hexane; d: biphasic separation) and the biphasic separation of 3.0 wt% H_2SO_4-CNCs.

When the suspension concentration of H_2SO_4-CNCs was increased to 6.7 wt%, the tactoid regions were observed under crossed light (**Figure 5-7**). The equidistant black and white fingerprint-like bands suggested a uniform birefringence and a cholesteric texture, which was depending on the size of nanoparticles and their crystalline axes orientation (Revol et al. 1992). These fingerprint-like domains could merge and form a large contour region after longer settling time. The space between the finger bands indicated a 10 μm half cholesteric pitch for chiral nematic liquid crystal.

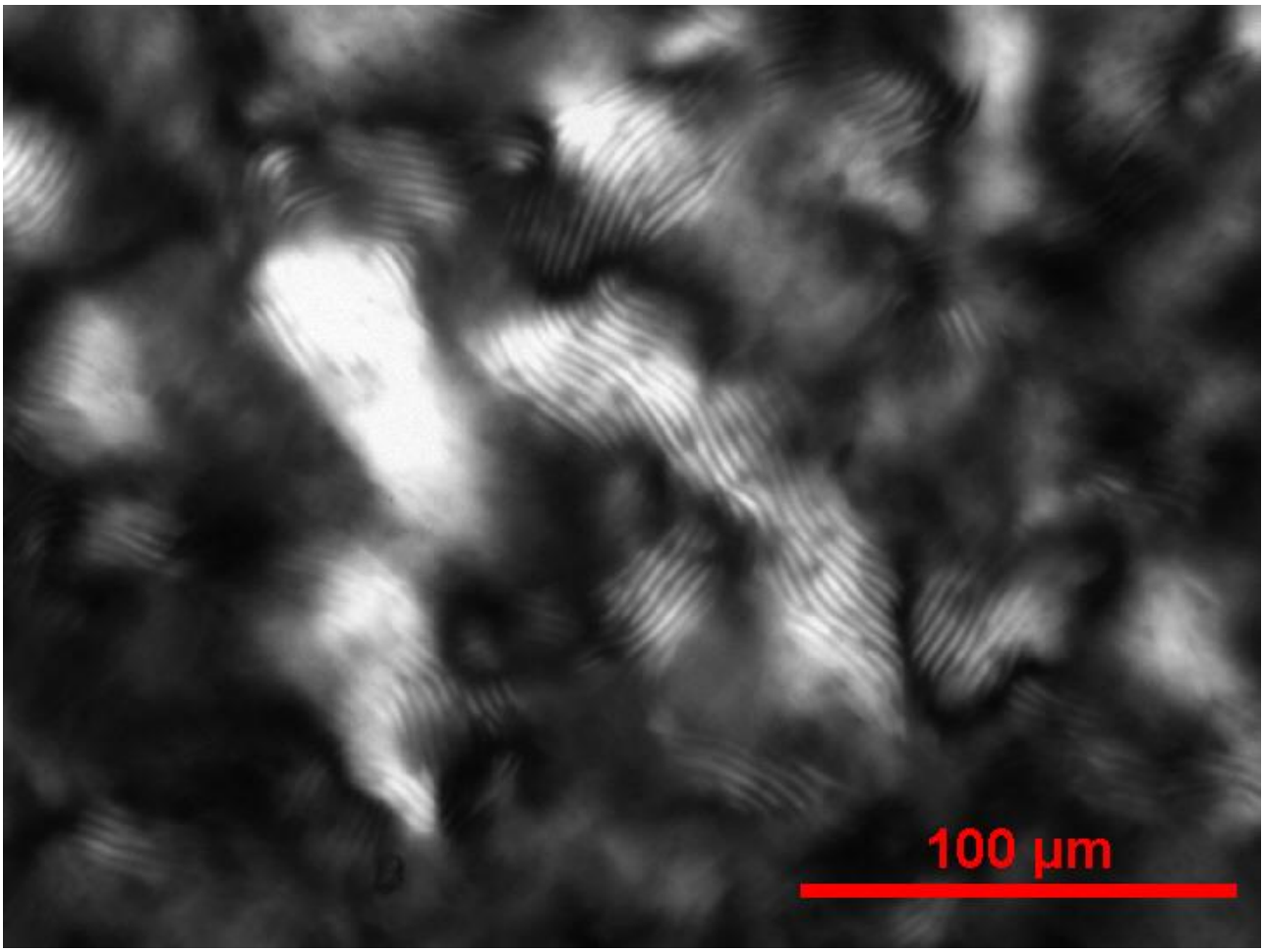

Figure 5-7. Polarized optical micrograph of 6.7 wt% H_2SO_4-CNCs-100 (the picture was taken 15 min in equilibrium after the drop casting).

The cross-polarized optical images of increased H_2SO_4-CNCs concentration were taken to study the lyotropic property of nanoparticles from Avicel (**Figure 5-8**) and filter paper (**Figure 5-9**). Both CNCs showed liquid crystals and strong birefringence with increased concentrations (Ureña-Benavides et al. 2011). For the H_2SO_4-CNCs (3 wt%), relatively small fraction of liquid crystal (white regions) was dispersed in vast region of isotropic phase. The bright liquid crystal region would turn to dark when the specimen was rotated, while the isotropic regions remained unchanged. When the concentration was increased to 6 wt%, the liquid crystal domains increased and a well scattered mixture of liquid crystal and isotropic

regions were observed (**Figure 5-8B**). At 10 wt%, smaller isotropic regions were observed under the microscope suggested by the unchanged dark domains (**Figure 5-8C**). At 15 wt%, CNCs revealed completely birefringent and discontinuous multicolor stripes suggesting a precholesteric type of ordering (**Figure 5-8D**). However, a few isotropic domains were still observed at this concentration. The observed lyotropic nano-rod dispersion under polarized microscope agreed with those from previous reports (Dong and Gray 1997; Dong et al. 1996; Ureña-Benavides et al. 2011).

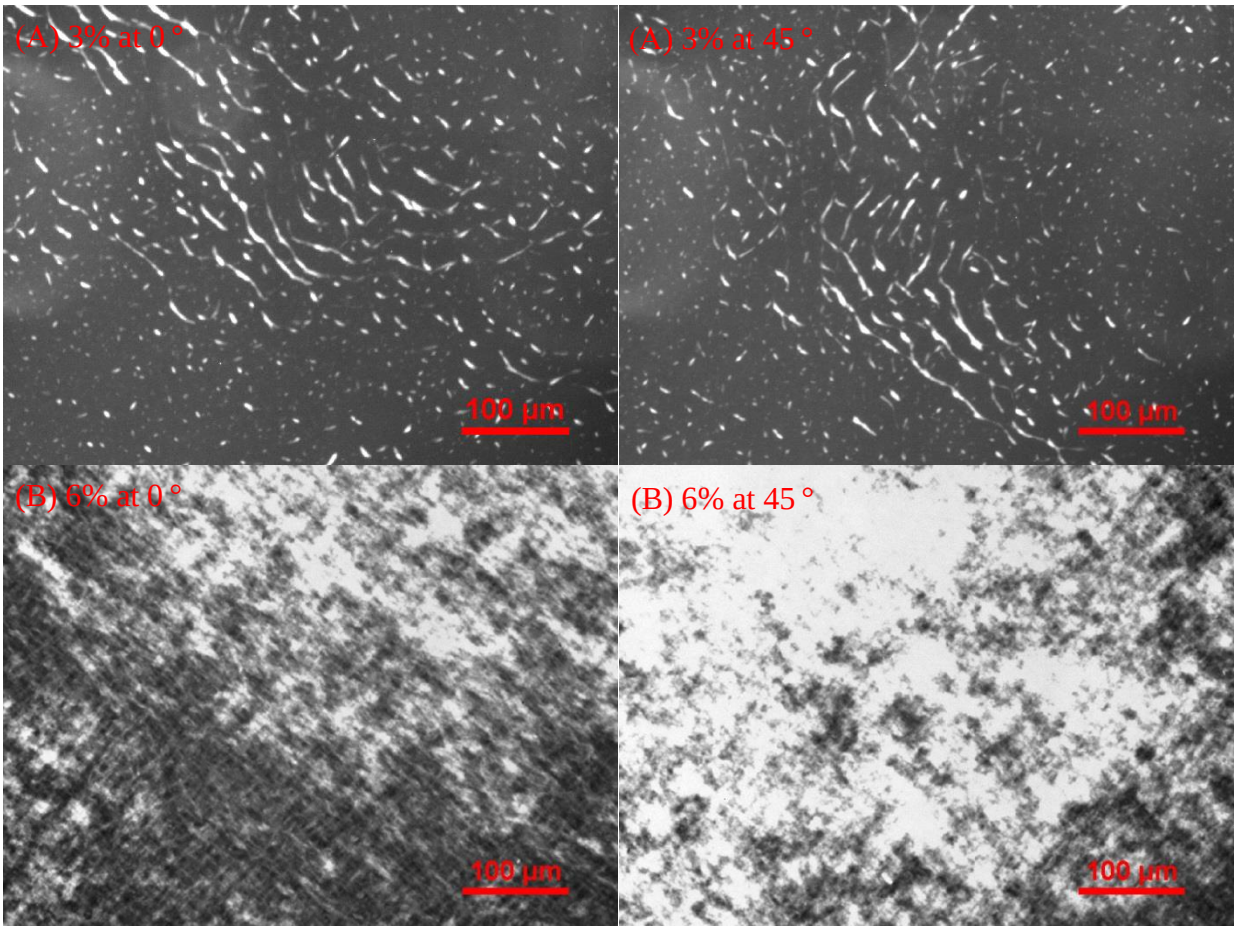

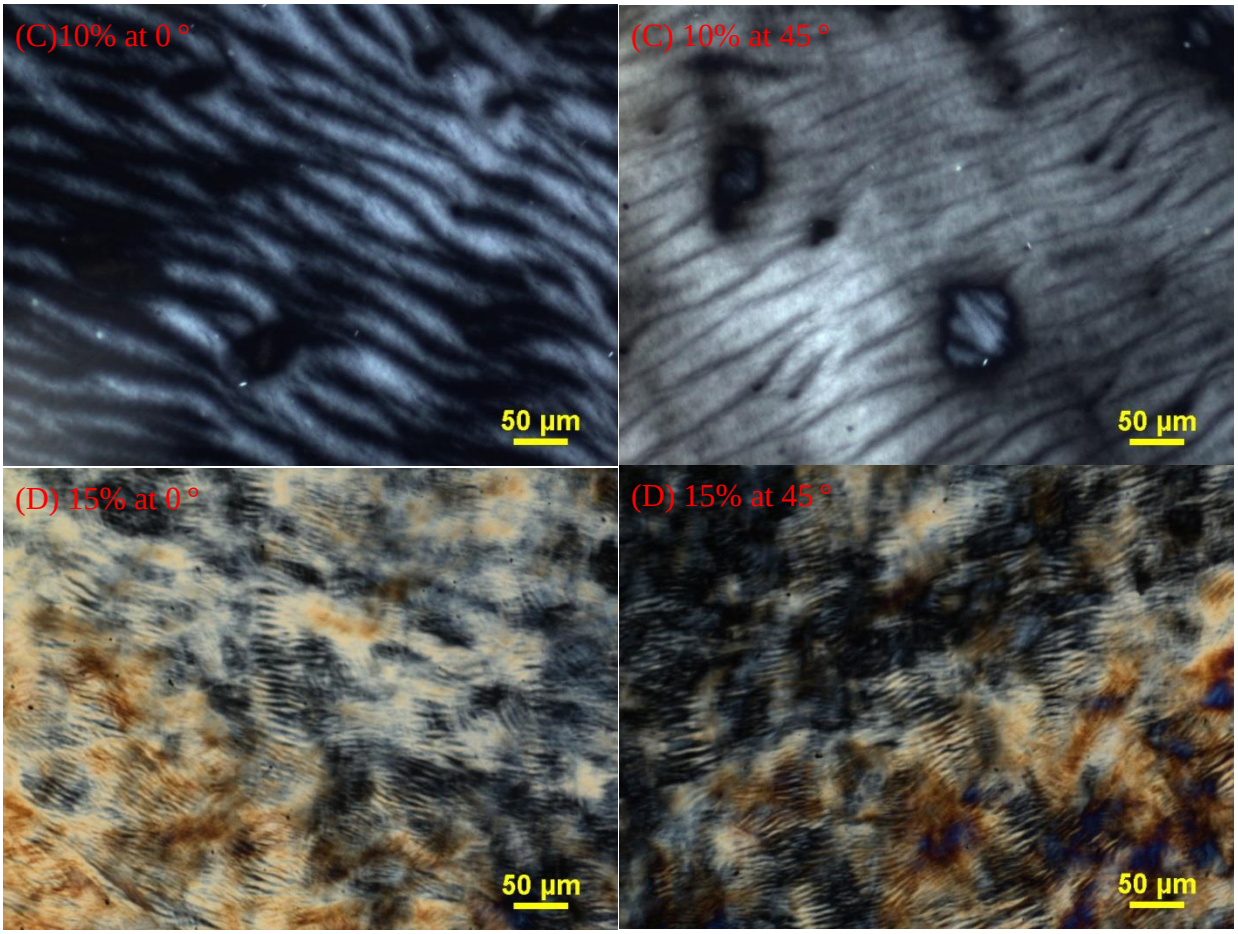

Figure 5-8. Polarized light microscopy images of H_2SO_4-CNCs-100 suspensions with different weight percentage at 25 ℃.

Although H_2SO_4-CNCs-FP showed a similar lyotropic dispersion to that from Avicel, it revealed a different dispersion uniformity and birefringence. An increased birefringence and liquid crystal domains were observed when the concentration was increased (**Figure 5-9**). However, the H_2SO_4-CNCs-FP exhibited a more uniform dispersion than H_2SO_4-CNCs with the same hydrolysis time (**Figure 5-9F** vs **H**). Poor dispersion of H_2SO_4-CNCs was attributed to its low sulfur content (0.89 vs 0.95%) determined by the elemental analysis and weaker electrostatic repulsion (ζ = 28.7 vs 30.7 mV).

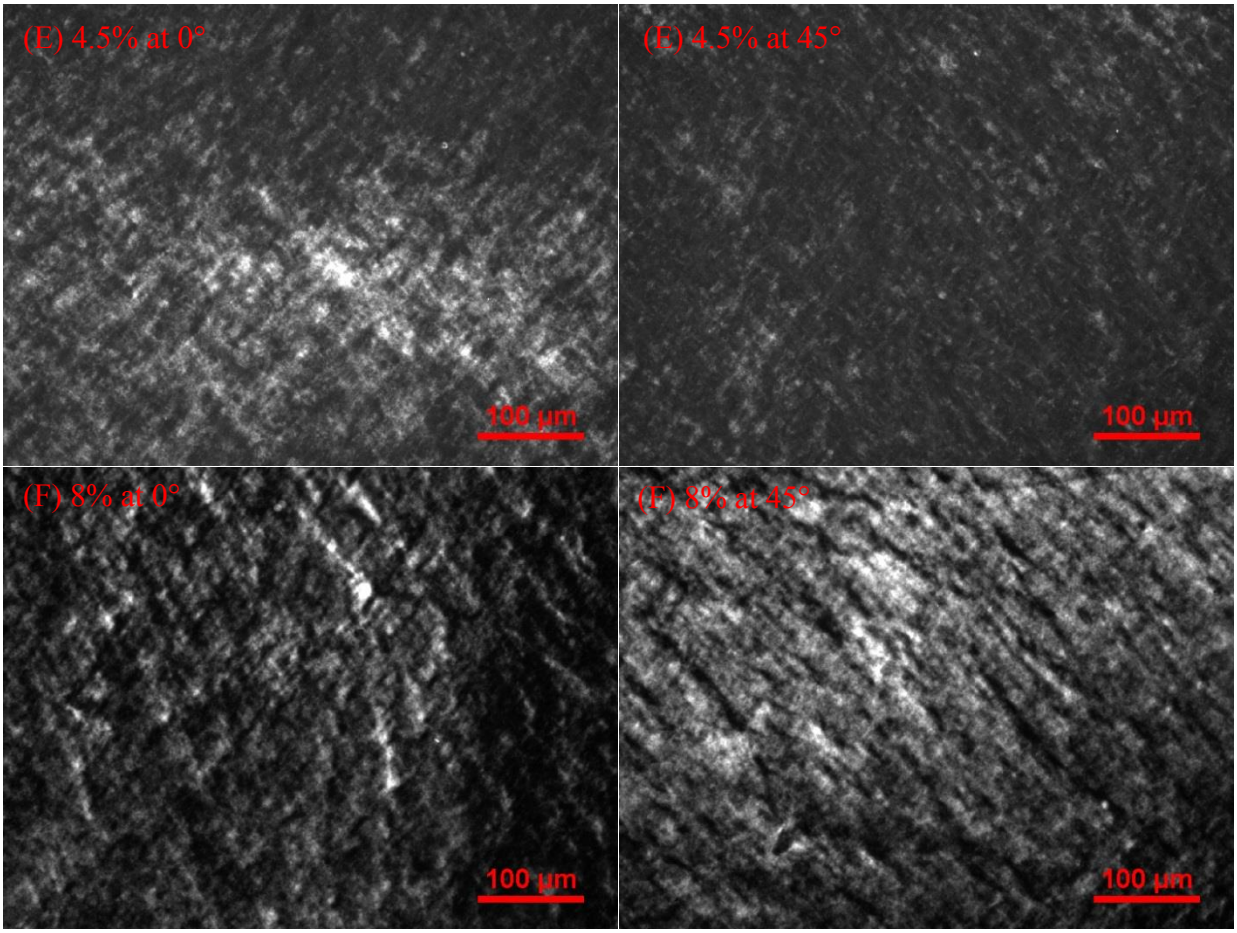
(E) 4.5% at 0°
100 µm
(E) 4.5% at 45°
100 µm
(F) 8% at 0°
100 µm
(F) 8% at 45°
100 µm

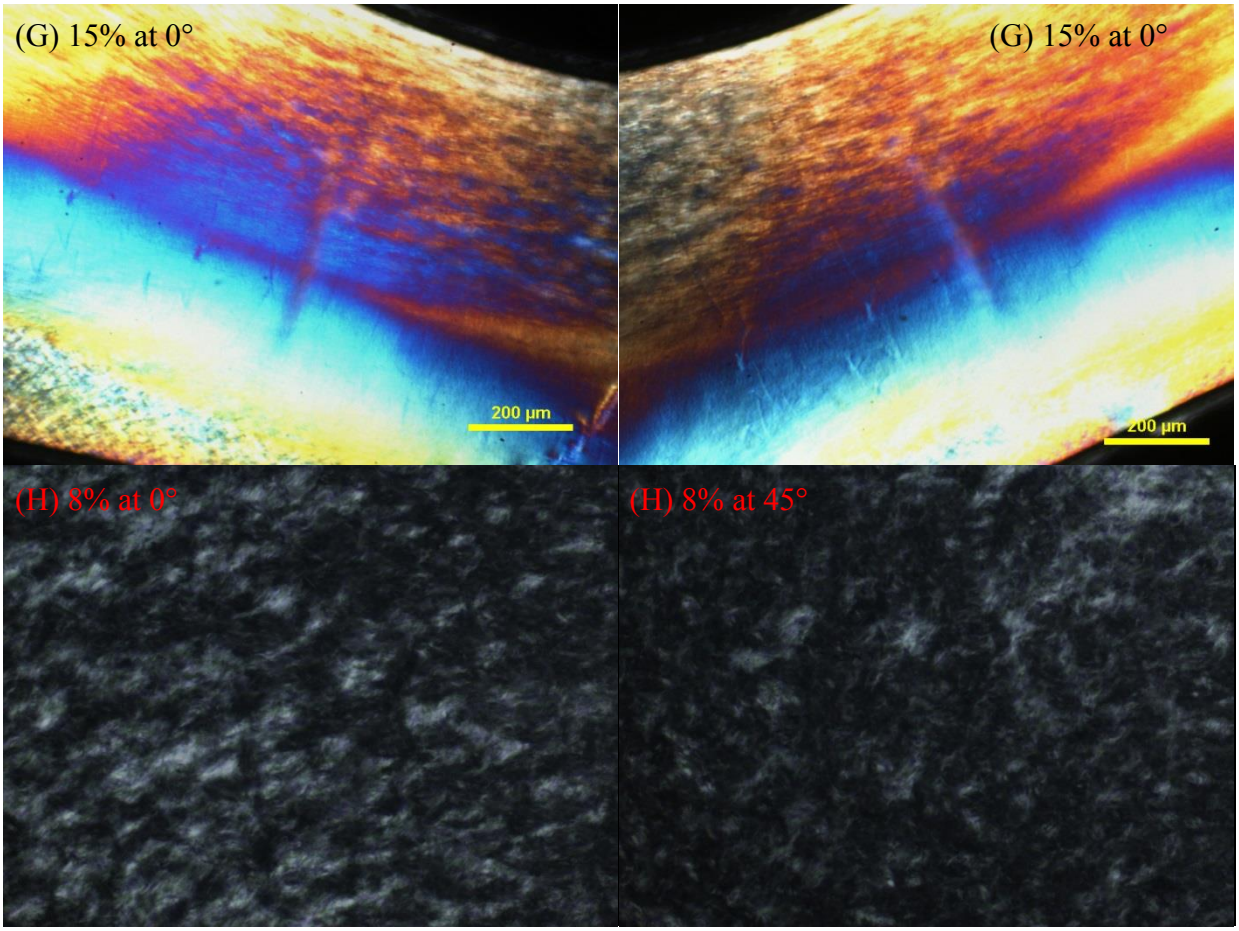

Figure 5-9. Polarized light microscopy images of H_2SO_4-CNCs-FP (E, F, and G) and H_2SO_4-CNCs-50 (H) suspensions at 25 ℃.

5.3.6 Time domain NMR study of CNCs

The T_2 relaxation time of Avicel, HCl-CNCs, H_2SO_4-CNCs, and H_2SO_4-CNCs-FP acquired at interval days were compiled. Shown in **Figure 5-10**, T_2 relaxation time got longer for all samples when the materials adsorbed moisture until saturated with water, because more spin-spin freedom were created when more water was absorbed. The first relaxation time peaked at 0.2 ms was assigned to the primary bound water in between cellulose chains (Felby et al. 2008). Peaks observed in each sample at 1-10 ms were assigned to the cellulose surface associated water when the particles adsorbed more water. When the CNCs continued adsorbing water,

another water molecules peak appeared at 25 ms (H_2SO_4-CNCs-100). The third water peak was assigned to capillary water in cavities and between CNCs nano-rods compared with T_2 of pure water at 2000 ms (Elder and Houtman 2013). Interestingly, the HCl-CNCs had a little longer T_2 than H_2SO_4-CNCs. Probably the presence of sulfate groups on the CNCs restricted the T_2 spinning of protons because of the greater solvation of water molecules with sulfate groups by hydrogen bonds (Gragson et al. 1996). However, no capillary water was detected on Avicel and HCl-CNCs probably due to their intrinsic morphology and absence of sulfate groups.

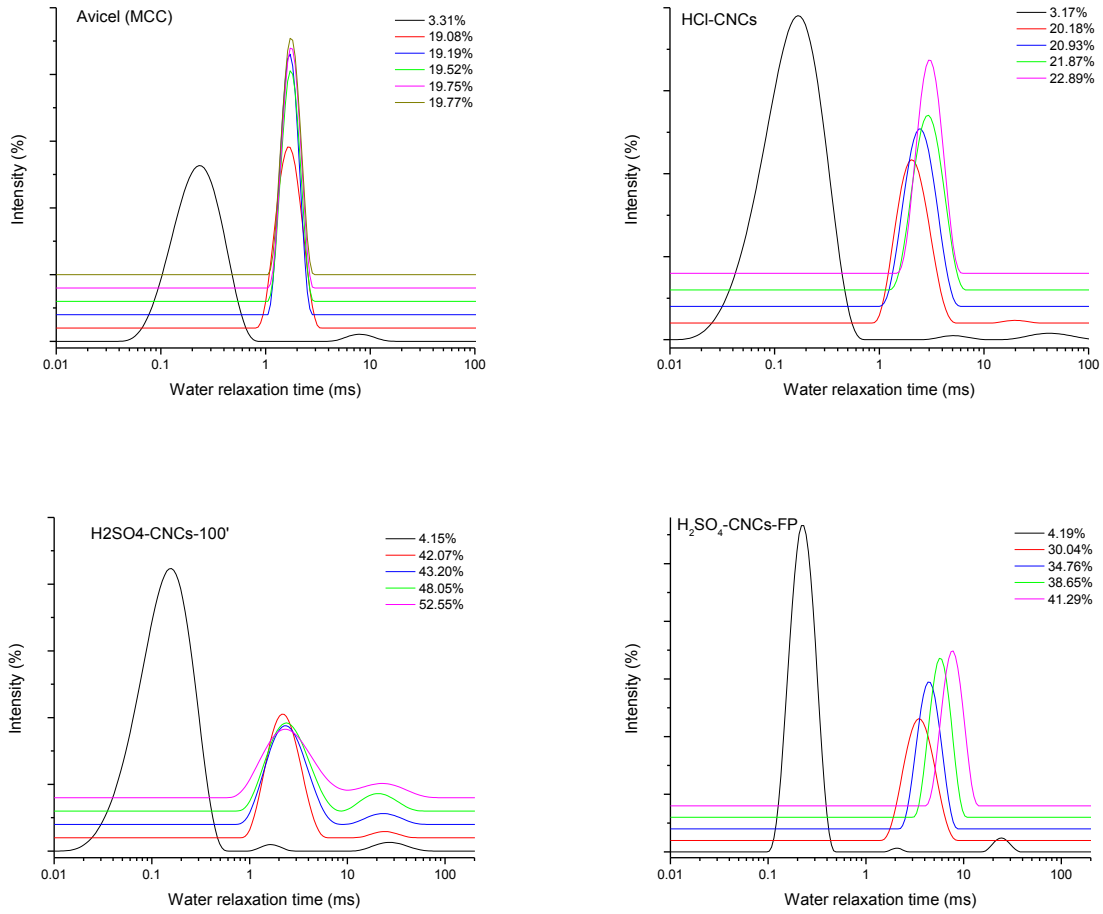

Figure 5-10. T_2 distribution of CNCs samples and Avicel with different moisture content.

5.3.7 Enzymatic hydrolysis of CNCs

The Avicel, H_2SO_4-CNCs, HCl-CNCs, and H_2SO_4-CNCs-FP were hydrolyzed with Novozyme 22C at 10 FPU/g glucan. The released glucose from each substrate was compared in **Figure 5-11A**. Neither the H_2SO_4-CNCs nor H_2SO_4-CNCs-FP was hydrolyzed by Novozyme 22 C. A remarkable hydrolysis difference between H_2SO_4-CNCs and HCl-CNCs was observed, however. With 72 h hydrolysis, the HCl-CNCs showed 80% yield, whereas the H_2SO_4-CNCs and H_2SO_4-CNCs-FP were only 28% and 8%, respectively. Very likely, the sulfate groups on the H_2SO_4-CNCs surface hindered the enzyme recognizing the degradable point on the surface (Araki et al. 1998; Zhang 2014). Less enzymatic hydrolyzabililty of H_2SO_4-CNCs-FP than H_2SO_4-CNCs was attributed to the higher sulfate groups indicated by the higher S% (0.95 vs 0.89%). Also, the two substrates possessed different crystallinity intrinsically, which might be another reason for the different hydrolysis performance. Other than monomeric glucose released from H_2SO_4-CNCs, a sulfate ester of cellobiose was identified by HPLC (**Figure 5-11B**) and confirmed by 2D NMR (Zhang 2014). This result suggested the activity of β-glucosidases was restricted by the presence of sulfate groups.

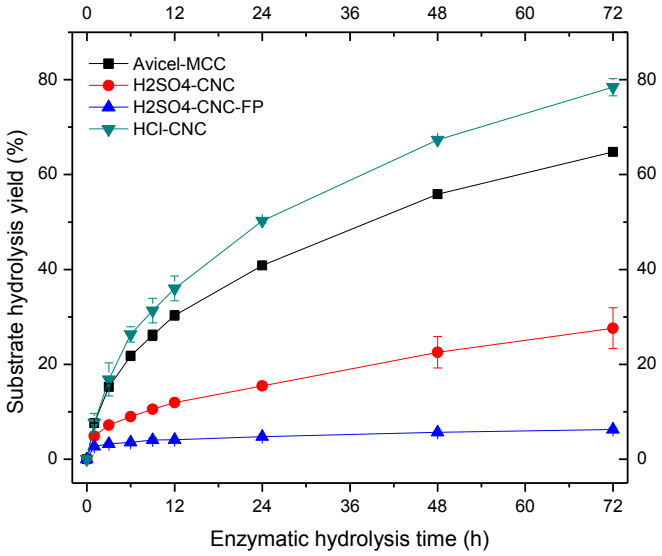

(A)

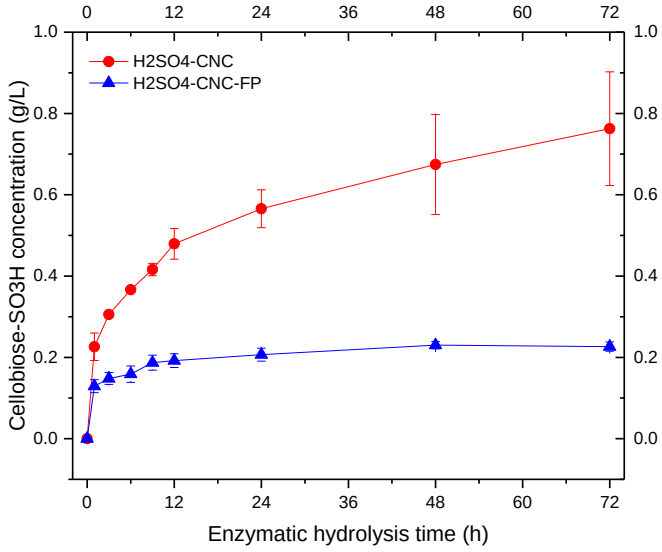

(B)

Figure 5-11. Enzymatic hydrolysis of Avicel, HCl-CNCs, H_2SO_4-CNCs, and H_2SO_4-CNCs-FP (A) and the production of cellobiose sulfate (B).

Interestingly, the HCl-CNCs had a better enzymatic hydrolysis performance than the untreated Avicel (**Figure 5-11A**). This could be due to two reasons: (1) less sulfate groups presented on the HCl-CNCs than Avicel (0.26 vs 0.29%); (2) HCl-CNCs were more accessible

by enzymes because of their larger surface area after acid hydrolysis. In order to verify the second reason, Avicel with different sonification time were used to test their enzymatic hydrolyzability (**Figure 5-12**). Longer sonification time gave rise to smaller particle size and larger surface area. As expected, the longer sonicated Avicel showed better cellulolytic result.

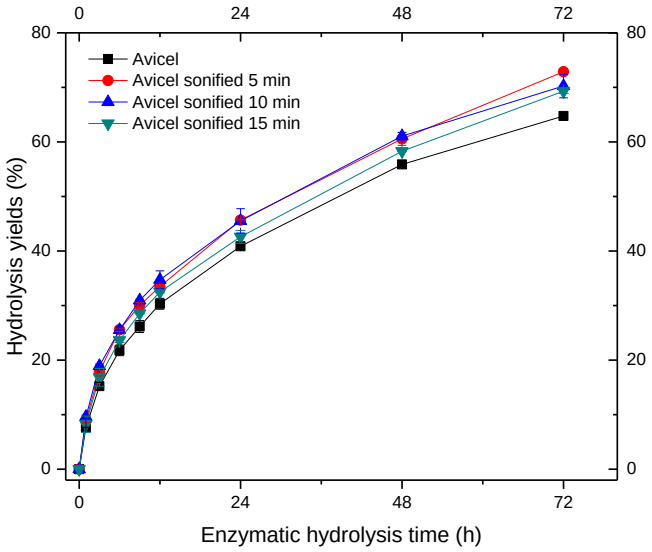

Figure 5-12. Enzymatic hydrolysis of sonicated Avicel.

5.4 Conclusion

In this chapter, the CNCs with different surface chemistry and physical properties were prepared by treating Avicel and filter paper with H_2SO_4 and HCl. The H_2SO_4-CNCs and HCl-CNCs showed similar dimension (300 nm × 10-15 nm) but the former had higher aspect ratio. An increased specific surface area from 0.83 to 4.1 m^2/g was observed in H_2SO_4-CNCs. Covalently introduced sulfate group (0.8% S) stabilized the phase behavior of H_2SO_4-CNCs in solution by the repulsive electrostatic force between negatively charged $–SO_3^-$. However, the sulfate groups comprised the thermostability of H_2SO_4-CNCs when compared with HCl-CNCs.

A chiral nematic phase was observed on the H_2SO_4-CNCs at 6.7 wt%, which confirmed the liquid crystal preordering of CNCs. Both the H_2SO_4-CNCs prepared from Avicel and filter paper showed lytropic phase behavior, but with different birefringence pattern probably due to the geometric dimensions of the nanoparticles. Time domain NMR was used to identify three types of water locations in the CNCs: (1) primary bound water in the CNCs, (2) surface associated water, and (3) capillary water in cavities. Moreover, the HCl-CNCs and H_2SO_4-CNCs had different hydrolyzability by Novozyme 22C. The HCl-CNCs had a little better hydrolysis performance opposed to Avicel probably because the increased surface area enhanced the accessibility of enzyme. Interestingly, the H_2SO_4-CNCs significantly impeded the enzymatic hydrolysis probably due to the presence of negatively charged sulfate groups.

Chapter 6 Chemical modification of cellulose nanocrystals

6.1 Background

Derived from the most abundant biopolymer, cellulose nanocrystals (CNCs) have been investigated for the development of sustainable materials and nanocomposites (Habibi et al. 2010; Klemm et al. 2011). Due to the inherent renewability, sustainability, and fascinating physicochemical properties, CNCs show great potential to be used for engineered materials (Habibi et al. 2010; Moon et al. 2011). However, the application of CNCs is strongly restricted by the presence of hydroxyl groups resulting in agglomeration by strong interfacial interaction (Missoum et al. 2013). On the other hand, the hydroxyl groups provide a feasible platform for chemical modification to improve CNCs dispersibility and compatibility.

Chemical modification is frequently used to alter the surface chemistry of CNCs. Both small molecules and polymers have been grafted to CNCs to adjust the hydrophilic-hydrophobic balance (Habibi 2014; Missoum et al. 2013). These modification reactions include sulfonation, oxidation, esterification, etherification, silylation, urethanization, and amidation. For instance, esterification of CNCs with acid anhydride has been achieved with high efficiency and yield (Bledzki et al. 2008; Freudenberg et al. 2005; Jonoobi et al. 2010; Sassi and Chanzy 1995; Tarvainen et al. 2003). Microcrystalline cellulose (MCC) modified with acetyl chloride showed homogeneous dispersion and improved matrix compatibility (Mukherjee et al. 2013). In addition, dispersion in non-polar solvent has been obtained by coating with surfactant (Heux et al. 2000). The cellulose nanoparticles with improved dispersibility were still difficult to be used in nanocomposites due to lack of the covalent bonding (Dufresne 2013). This issue can be potentially solved by coupling CNCs with reactive polymers. An improved mechanical

properties of composites was obtained by compounding cellulose fibers with polypropylene-maleic anhydride (Felix and Gatenholm 1991).

In this chapter, several surface chemical modifications of CNCs were performed to change their physical and chemical properties. We chemically modified CNCs with acetic anhydride and polyisobutylene succinic anhydride (PIBSA) to improve their dispersion in organic solvents. Also, we oxidized HCl-CNCs by NaClO/NaBr with the mediation of TEMPO to introduce negative surface charges to improve its aqueous stability. A lab-made dye was used to label CNCs as a potential for dispersion marker. Finally, the CNCs were modified with TSC at the reducing end by the reducing amidation reaction to covalently adsorb onto gold substrate. These chemical modifications will extend the application of CNCs in engineered materials.

6.2 Materials and methods

Chemicas and materials

Chemicals and materials are the same as described in the previous chapter.

Cellulose nanocrystals preparation

The HCl-CNCs and H_2SO_4-CNCs were prepared and isolated using method described in previous chapter.

Thiosemicarbazide (TSC) modification of CNCs

The functionalization of CNCs with TSC used a modified method from literature (Lokanathan et al. 2013; Yokota et al. 2008). Thiosemicarbazide, 600 mg, (CH_5N_3S, 99%, Alfa Aesar) was added to 200 mL H_2SO_4-CNCs aqueous suspension (10 mg/mL) buffered with 0.1 M

sodium acetate (NaAc, pH 5) and stirred continuously. The reaction was performed at 70 ℃ for 48 h. A total of 300 mg 2-methylpyridine borane complex (Pc, MW107, $C_6H_7N\ BH_3$ 95%, Sigma Aldrich) was added at each 12 h. At the end, the reaction mixture was cooled down to room temperature and neutralized with 1 M HCl for the excessive reducing agent. The mixture was then thoroughly dialyzed against DI-water for 3 days with water change at every 12 h. The functionalized CNCs (CNCs-TSC) suspension was used for various characterization works.

TEMPO-mediated carboxylation of CNCs

The 2,2,6,6-tetramethylpiperidine-1-oxyl (TEMPO) radical mediated oxidation of CNCs was carried out using published method with minor modifications (Habibi et al. 2006; Montanari et al. 2005; Tahiri and Vignon 2000). In a typical run, 510 mg HCl-CNCs, equivalent of 3.15 mmol anhydroglucose units (AGU) in 100 mL water were sonicated (Branson Sonifier 350) for 5 min, then 15 mg TEMPO (0.094 mmol) and 162 mg NaBr (1.57 mmol) were added with stirring. A certain amount of NaClO solution (14.5% available chlorine) was added drop-wise to reach different molar ratio of NaOCl/AGU. The suspension was stirred at room temperature for about 1 h with pH maintained at 10.5 by adding a 0.5 M NaOH solution dropwise. The NaOH was added until no pH variation indicating the completion of reaction. The reaction was terminated by adding ca. 1 mL methanol to react with the excess of NaClO and the pH was adjusted back to 7 with 0.5 M HCl. The residual insoluble fraction was recovered by centrifugation and washed thoroughly with DI-water. The free acid form of carboxylated cellulose was obtained by two more centrifugation and washing with 0.1 N HCl. Oxidized CNCs were dialyzed against DI-water for 2 days and then freeze dried and weighed to determine the mass recovery.

CNCs acetylation

The acetylation of CNCs was carried out by the methods as previously reported with slight modification (Jonoobi et al. 2010; Kim et al. 2002). The chemical reaction during the acetylation process was schemed (**Figure 6-1**). A portion of 500 mg freeze dried HCl-CNCs were suspended in 20 mL acetic anhydride (Ac_2O) and 10 mL pyridine (95%) with stirring. The reaction flask was maintained at 65 ℃ in an oil-bath incubator at atmospheric pressure under reflux overnight. The insoluble fraction was collected by centrifugation and thoroughly washed with DI-water to remove unreacted Ac_2O, pyridine, and acetic acid by-products. The acetylated CNCs (HCl-CNC-Ac) were vacuum-dried at 40 ℃ overnight, then placed in a desiccator at room temperature for various characterizations.

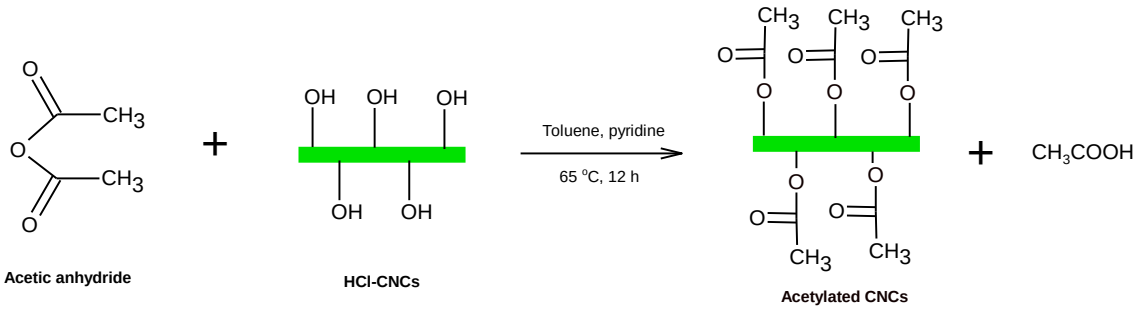

Figure 6-1. Chemical reaction of acetic anhydride with HCl-CNCs.

Graft of PIBSA onto CNCs

The PIBSA was grafted onto CNCs by the method previously reported (Coleman-Kammula 1989). A total of 1020 mg oven-dried HCl-CNCs (6.3 mmol AGU) was added into a mixture of 100 mL toluene and 5 mL pyridine, then 6.3 g PIBSA (6.3 mmol) was added with stirring. The reaction was maintained at 100 ℃ in an oil bath for 48 h. At the end of the reaction, the insoluble fraction was collected by centrifugation and then was subject to acetone extraction in a Soxhlet extractor overnight in order to remove unreacted anhydride and other by-products.

The polymer grafted CNCs (HCl-CNCs-PIBSA) was oven-dried overnight and stored in a desiccator for future use.

Synthesis of 4-ABBP and fluorescent labeling of CNCs

The 4-amino-N-Bromobutyl phthalimide (4-ABBP) was synthesized by the method in literature with modification (Ishihara et al. 1994). The CNCs was labeled with 4-ABBP by an approach as previously reported with modification (Abitbol et al. 2013b). The HCl-CNCs (100 mg, 0.63 mmol AGU) was reacted with 4-ABBP (190 mg 0.63 mmol) in 100 mL toluene with the addition of 20 μL 1 M NaOH. The reaction was maintained at 70 ℃ in the dark in an oil bath with stirring overnight. To remove the bulk of the toluene and unreacted 4-ABBP, repeated centrifugation and washing with ethanol step were employed until the supernatant was clear. The 4-ABBP labeled HCl-CNCs (HCl-CNCs-4-ABBP) suspension in ethanol was stored in refrigerator in the dark.

Fluorescence micrographs of the HCl-CNCs-4-ABBP were obtained using an Olympus BX53 upright microscope equipped with an X-Cite (series 120 Q) illuminator and an Olympus DP73 Camera. Samples were prepared by drop-casting 5 μL 0.5 wt% ethanol suspensions onto the surface of a glass slide.

SEM, TGA, and FTIR analysis of modified CNCs

The details of SEM, TGA, and FTIR analysis are in the previous chapter.

Contact angle measurement of CNCs films

Contact angles (θ) with water were measured in a static status with a standard contact angle Goniometer (Rame-Hart Model 200). The hydrophobicity of the surface was conducted by the sessile drop method at room temperature. A digital picture was taken for θ calculation right after a small water droplet was released and stayed on the surface of the CNCs film. The averaged θ value of triplicates was used for evaluating the hydrophobicity and surface energy of the modified CNCs by the Owens– Wendt approach (Owens and Wendt 1969).

6.3 Results and discussion

6.3.1 SEM analysis of modified CNCs

SEM analysis was used to examine the surface of modified HCl-CNCs (**Figure 6-2**). The non-modified HCl-CNCs displayed with rough surface, while the PIBSA grafted HCl-CNCs (**Figure 6-2B**) and acetylated HCl-CNCs (**Figure 6-2C**) were swollen with round surface. HCl-CNCs-PIBSA showed a width of about 100 nm versus 30 nm in HCl-CNCs. This morphological change was probably due to the grafting of PIBSA and an increased surface hydrophobicity (Kim et al. 2002). The fluorescence labeled HCl-CNCs did not show the swollen surface (**Figure 6-2D**).

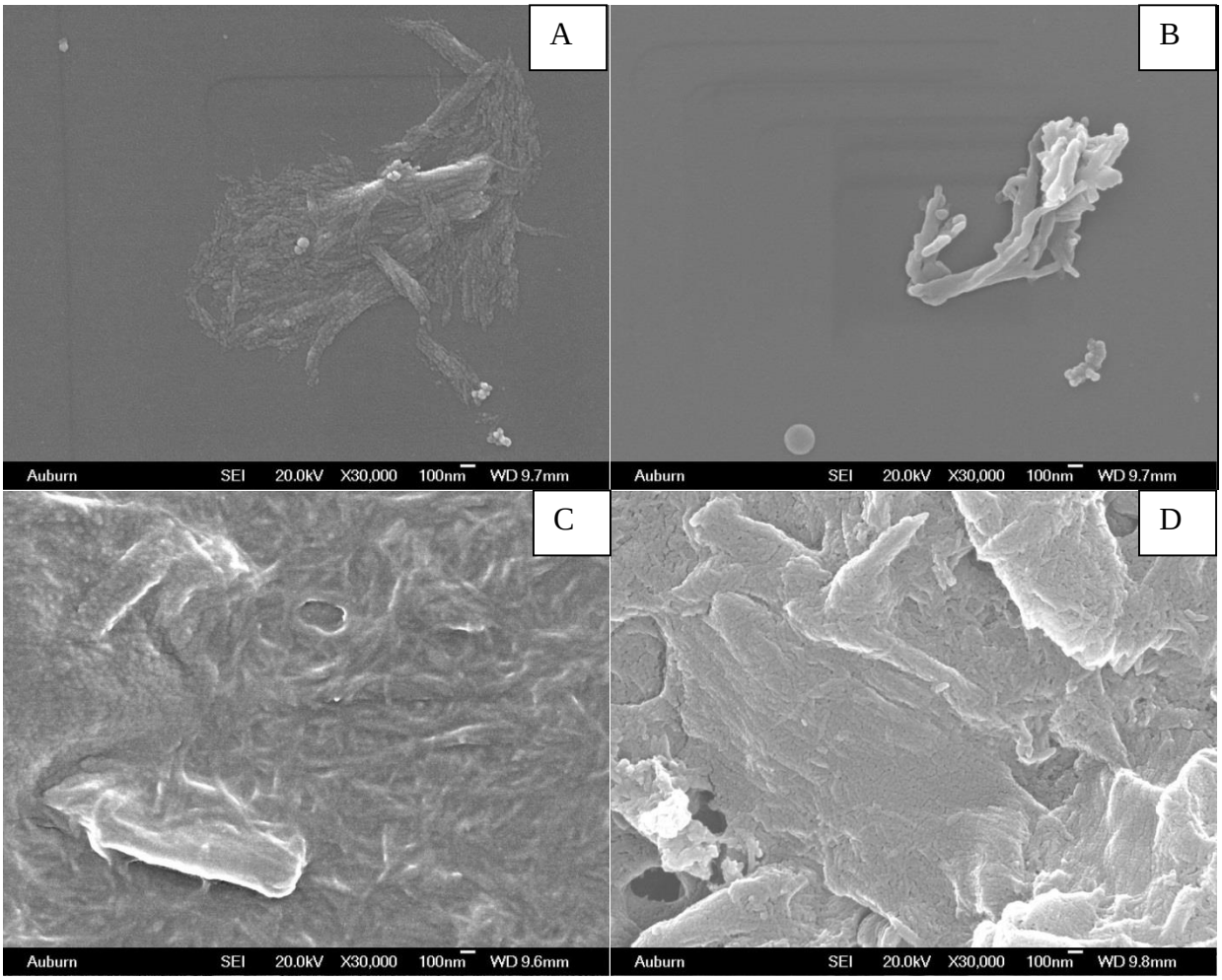

Figure 6-2. SEM images of (A) HCl-CNCs, (B) HCl-CNCs-PIBSA; (C) HCl-CNCs-Ac; and (D) HCl-CNCs-4-ABBP.

6.3.2 Thermal stability of modified CNCs

The HCl-CNCs modified with PIBSA and Ac_2O decreased their thermostability (**Figure 6-3**). The HCl-CNCs-Ac decomposed from 300 ℃ and the HCl-CNCs-PIBSA started decomposition at 200 ℃. The less thermostability of HCl-CNCs-PIBSA was attributed to the grafted PIBSA.

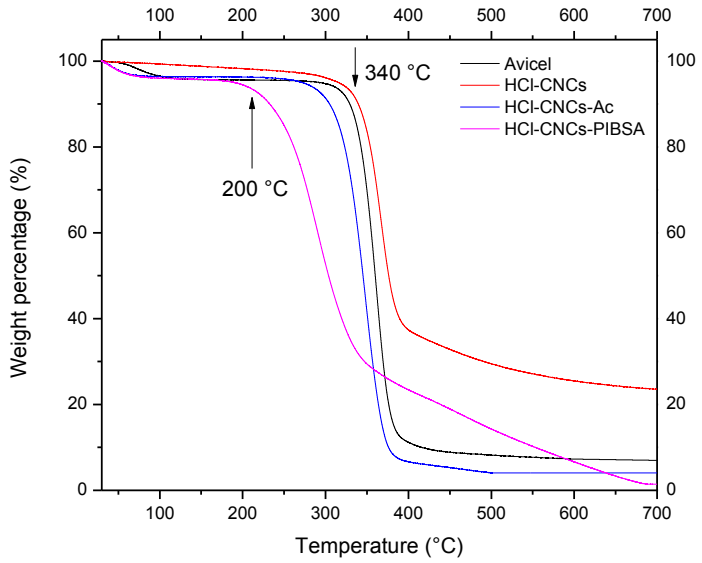

Figure 6-3. TGA curves of modified HCl-CNCs.

6.3.3 Contact angle determination of modified CNCs films

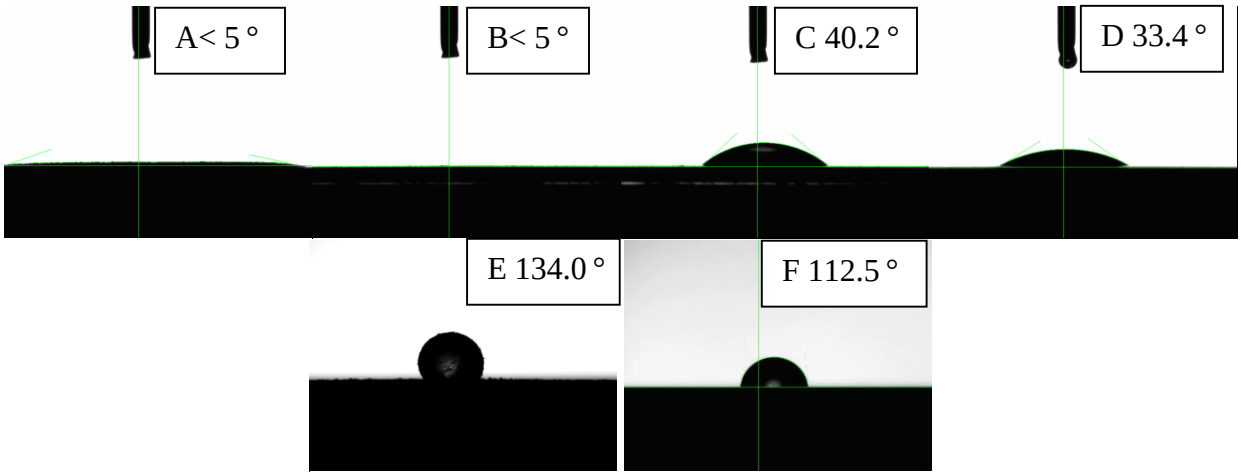

Figure 6-4. Images of water contact angle on the drop casted CNCs films. (A: sonicated Avicel; B: HCl-CNCs; C: H_2SO_4-CNCs; D: H_2SO_4-CNCs-FP; E: HCl-CNCs-PIBSA; F: HCl-CNCs-Ac)

The contact angles with water were measured for the films made from unmodified and modified HCl-CNCs (**Figure 6-4**). The results showed there were dramatic changes on CNCs surface, from hydrophilic to hydrophobic, which suggested successful chemical modification

with PIBSA (contact angle = 134.0 °) and acetic anhydride (contact angle = 112.5 °). The films of H_2SO_4-CNCs isolated from Avicel and filter paper presented contact angles of 40.2 and 33.4 °, respectively. The HCl-CNCs-PIBSA was dispersed in solvents with different polarities (**Figure 6-5**). The solvent polarities from high to low are in an order of H_2O (10.2), acetone (5.4), $CHCl_3$ (4.4), ethylacetate (4.3), toluene(2.4), and hexane (0.06). We found that PIBSA was better dispersed in acetone, $CHCl_3$, and ethyl acetate of medium polarity.

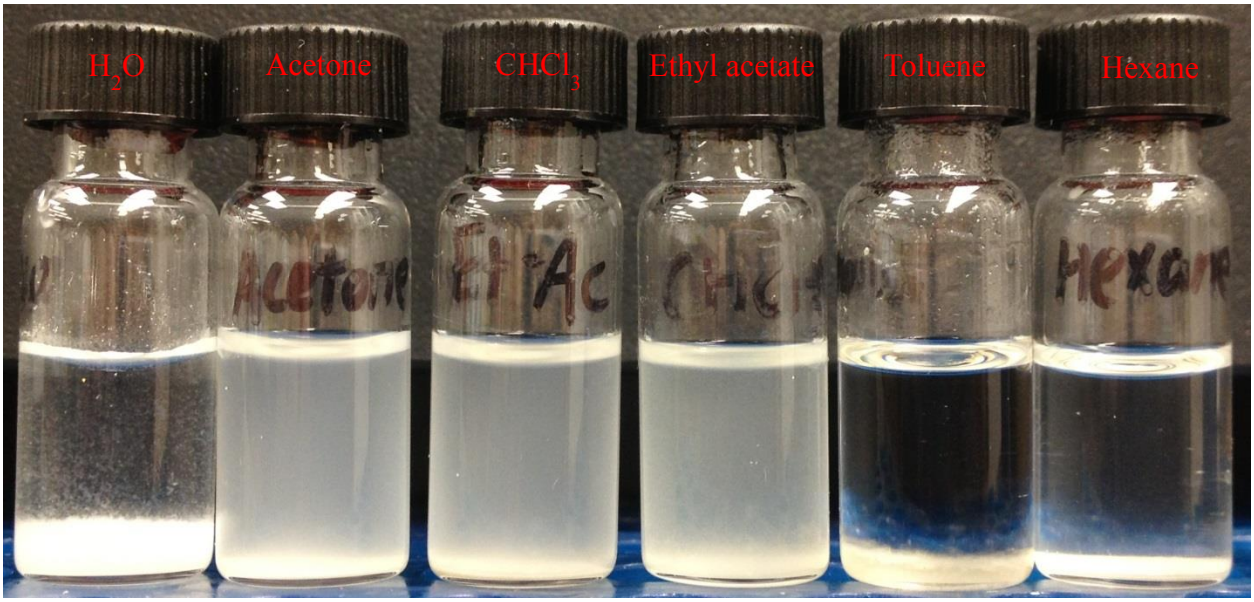

Figure 6-5. The dispersion of HCl-CNCs-PIBSA in solvents of different polarities.

6.3.4 Fluorescence labeling of HCl-CNCs

The reactions of synthesizing fluorescent dye 4-ABBP and HCl-CNCs fluorescence labeling were illustrated in **Figure 6-6**. The fluorescence of 4-nitrophthalimide was enhanced when $–NO_2$ group was replaced with $–NH_2$. In 4-ABBP, strong electron donating group $–NH_2$ and weakly activating butyl group work together to induce the delocalization of conjugated π-electrons on the benzene ring (Senesi et al. 1991). As a result, the fluorescence of 4-ABBP was

intensified in DAPI, FITC, and TRITC channels. The labeling reaction proceeded with nucleophilic attack on the alkyl branch by deprotonating cellulose hydroxyls. The bromide group leaves as KBr at the presence of K_2CO_3. HCl-CNCs-4-ABBP was purified and washed with ethanol to remove the unreacted 4-ABBP completely.

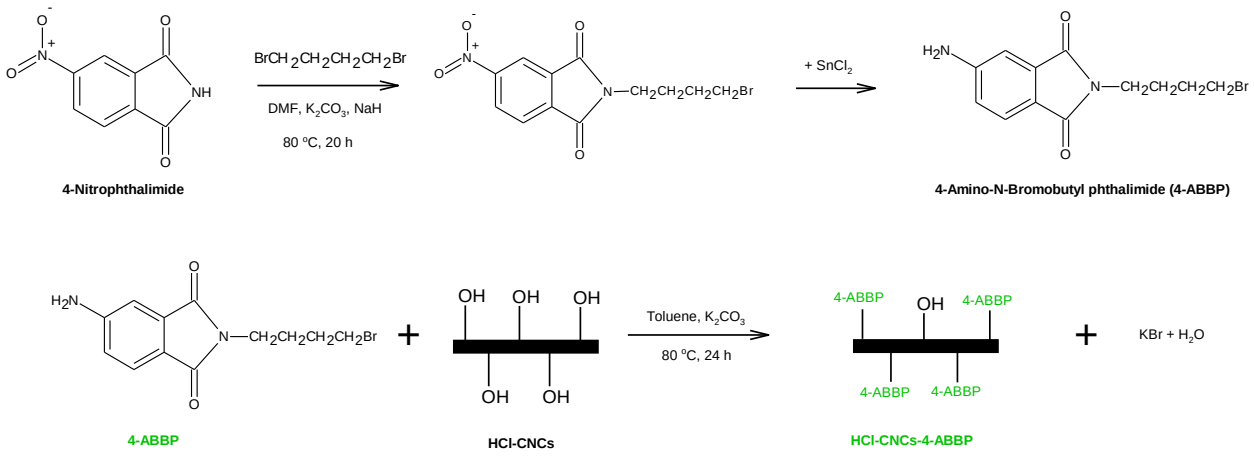

Figure 6-6. Synthesis of the dye (4-ABBP) and its labeling on HCl-CNCs.

The fluorescence of CNCs-4-ABBP was analyzed by fluorescence microscopy (**Figure 6-7**). The unlabeled HCl-CNCs and 4-ABBP-labled CNCs were compared in their fluorescence. Apparently, the HCl-CNCs-4-ABBP revealed much stronger fluorescent intensity suggesting a successful bonding with 4-ABBP viewed through DAPI, FITC, and TRITC.

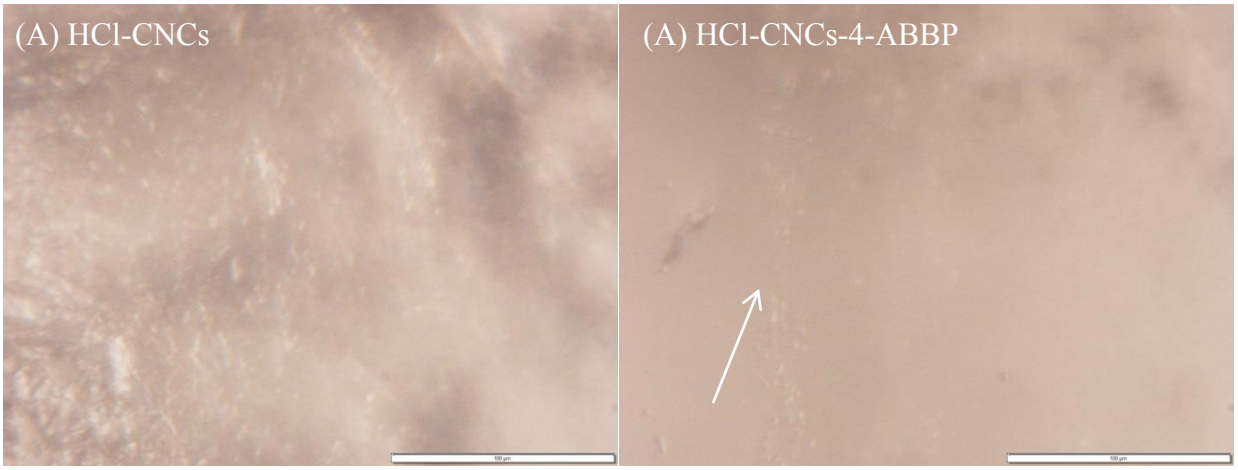

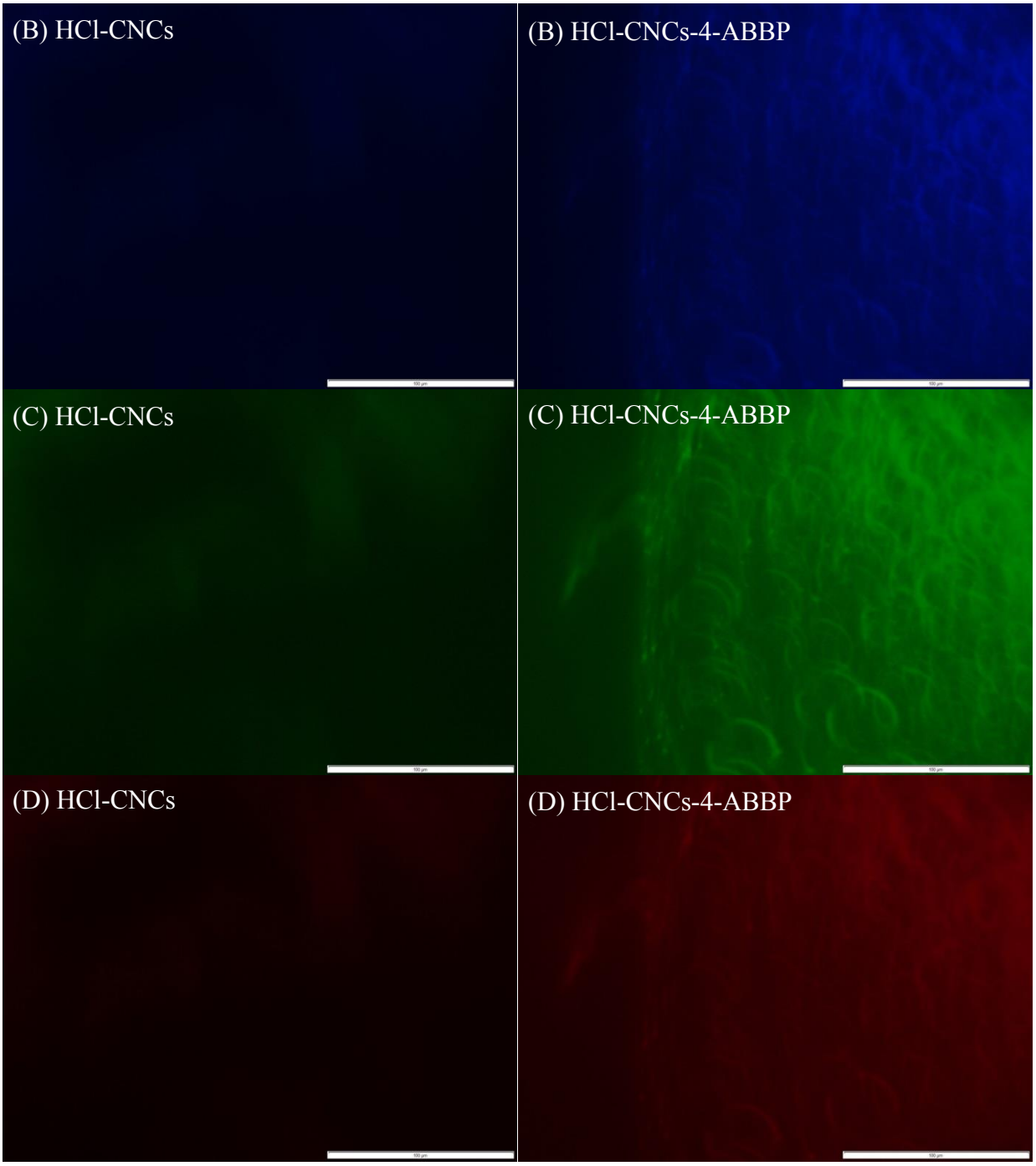

Figure 6-7. Fluorescence microscopy images of unlabeled and 4-ABBP-labeled HCl-CNCs under BF (A) and filters of DAPI (B), FITC (C), and TRITC (D) channel. The arrow indicates the edge of casted CNCs-4-ABBP on the slide.

6.3.5 FTIR analysis of modified HCl-CNCs

The FTIR spectra of HCl-CNCs and modified HCl-CNCs were compared in **Figure 6-8**. Majorly increased band at 1740 cm^{-1} was assigned for C=O stretching in a form of ester on HCl-CNCs. However, HCl-CNCs-PIBSA only showed a weak band at 1740 cm^{-1} probably due to low grafting efficiency. The other two primarily increased bands in HCl-CNCs-Ac were at 1370 and 1235 cm^{-1} corresponding to the groups of C-O and C-CH_3, respectively (Hurtubise 1962). A small peak occurred at 1642 cm^{-1} revealed the intro-bonded H_2O (Habibi et al. 2006). It should be pointed out that the degree of substitution was difficult to quantify only based on the IR spectra. Qualitatively, the overall enhanced intensity of typical absorption bands confirmed the esterification of HCl-CNCs.

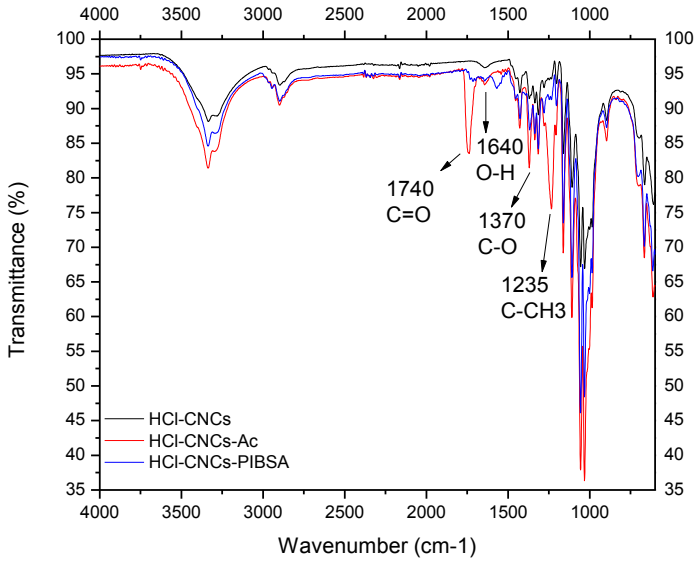

Figure 6-8. FTIR spectra of modified HCl-CNCs.

6.3.6 TEMPO-mediated carboxylation of CNCs

TEMPO-mediated oxidation of polysaccharides can convert primary hydroxyl group into carboxylate group through aldehyde as the intermediate (De Nooy et al. 1995; de Nooy et al. 1996; Isogai et al. 2011). Based on this method, the primary hydroxyl group on AGU was oxidized to carboxylate group by TEMPO/NaBr/NaClO at pH 10-11 (**Figure 6-9**). However, not all AGU were accessible as the repeating unit of cellobiose makes half of the $–CH_2OH$ groups buried inside the crystalline cellulose. The degree of oxidation could be controlled by the molar ratio of NaClO over AGU (Habibi et al. 2006).

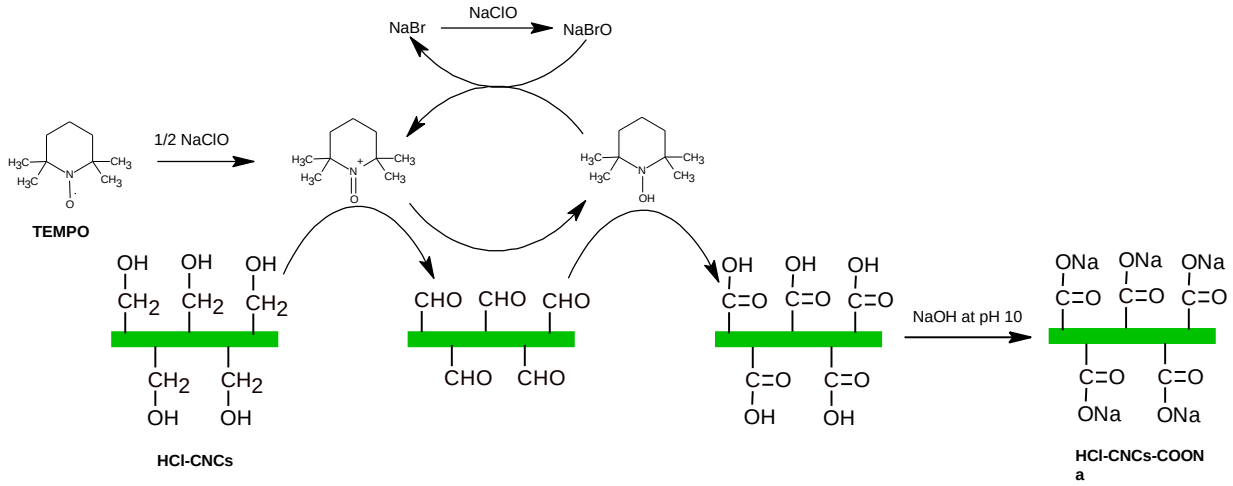

Figure 6-9. Oxidation of primary hydroxyls of HCl-CNCs to carboxylates by TEMPO/NaBr/NaClO in water at pH 10-11 (Isogai et al. 2011).

Oxidized HCl-CNCs, with change of molar ratio of NaClO over AGU (0, 0.05, 0.1, 0.5, 1, and 2) were tested and analyzed by FTIR (**Figure 6-10**). The detected peak with frequency at 1730 cm^{-1} corresponded to the stretching absorption of C=O in their acidic form (Habibi et al. 2006). Apparently, the oxidized HCl-CNCs with higher NaClO/AGU exhibited higher intensity at band 1730 cm^{-1}, suggesting more hydroxyl methyl groups were converted to carboxylate

groups. At low NaClO/AGU ratio (0.05 and 0.1), however, no band at this frequency was detected.

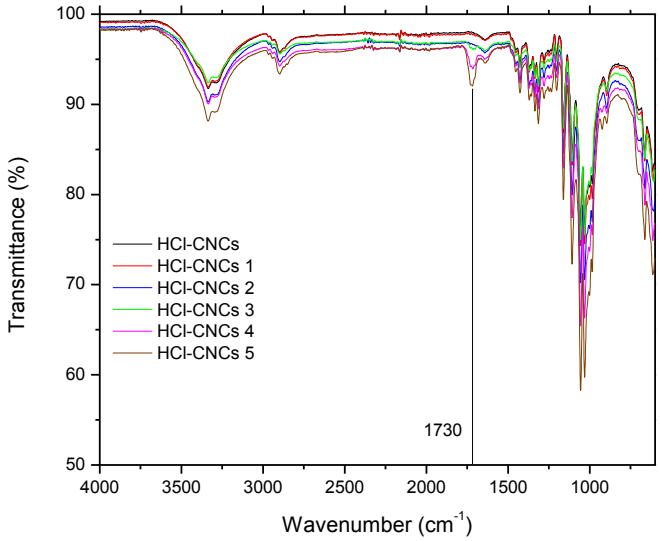

Figure 6-10. FTIR spectra of TEMPO-mediated HCl-CNCs oxidization with different NaClO/AGU molar ratio (1: 0.05, 2: 0.1, 3: 0.5, 4: 1.0, and 5: 2.0).

The oxidized cellulose was reported to be resistant to the hydrolysis by commercial crude cellulase (Kato et al. 2002). We studied the enzymatic hydrolyzability of oxidized HCl-CNCs by plotting the glucose released against incubation time (**Figure 6-11**). Oxidized HCl-CNCs by higher NaClO/AGU ratio were more resistant to the enzymatic hydrolysis by Novozyme 22C, which were consistent with the findings by others (Isogai et al. 2011; Kato et al. 2002). When the NaClO/AGU reached 1.0, the cellulolytic enzyme hardly hydrolyzed any substrate (less than 3% after 72 h incubation). It was found that the carboxyl groups appeared to be stronger on impeding enzymatic hydrolysis than sulfate groups (**Figure 6-11A** vs **Figure 5-11A**). Meanwhile, glucuronic acid, a product during the oxidation by converting the hydroxyl methyl groups into carboxylic groups, was released and identified. Higher oxidation degree gave rise to more

glucuronic acid released from the substrate (**Figure 6-11B**). The released glucuronic acid confirmed the oxidation degree and agreed with the results analyzed by FTIR (**Figure 6-10**).

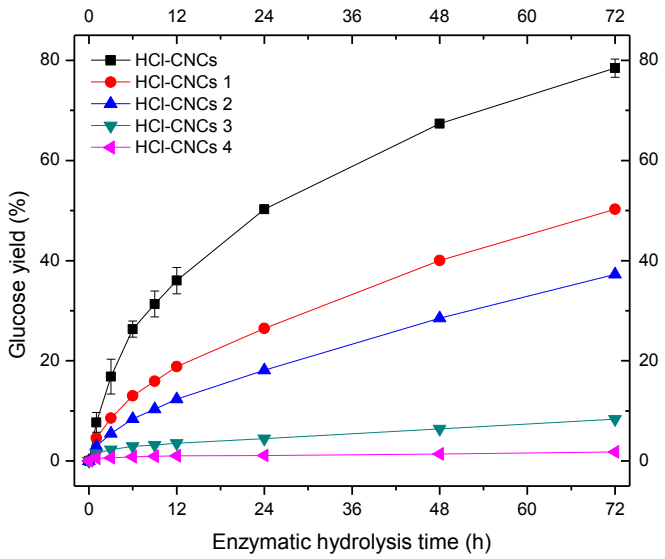

(A)

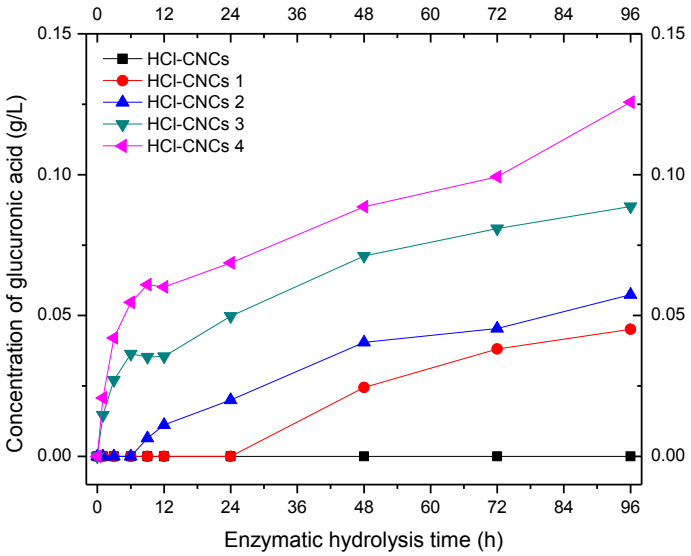

(B)

Figure 6-11. Enzymatic hydrolysis of oxidized HCl-CNCs by TEMPO/NaClO/NaBr with different oxidation degree.

Similar results were found when we hydrolyze oxidized H_2SO_4-CNCs (**Figure 6-12**). As expected, oxidized H_2SO_4-CNCs were only slightly hydrolyzed after 72 h incubation, about 10% for NaClO/AGU 0.05 and 0.1. When the NaClO/AGU was increased to 0.5, nearly no H_2SO_4-CNCs were hydrolyzed (glucose released less than 3%). Less hydrolyzability of oxidized H_2SO_4-CNCs than that of HCl-CNCs was perhaps due to the presence of both sulfate groups and carboxylate groups, which significantly retarded the enzyme recognition of hydrolyzable spots.

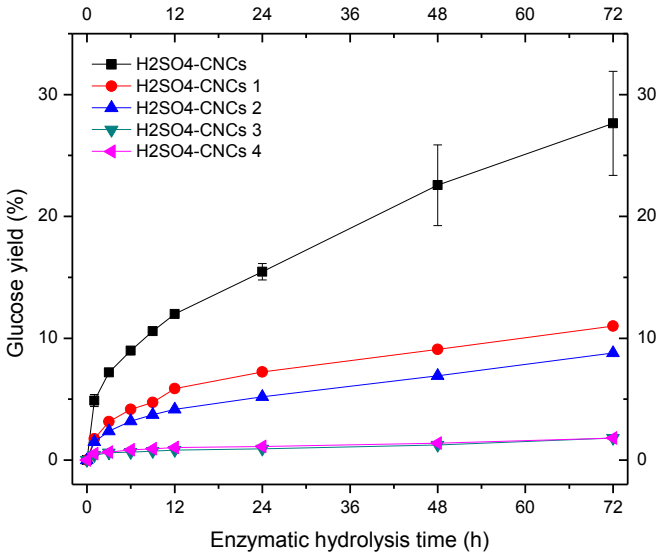

(A)

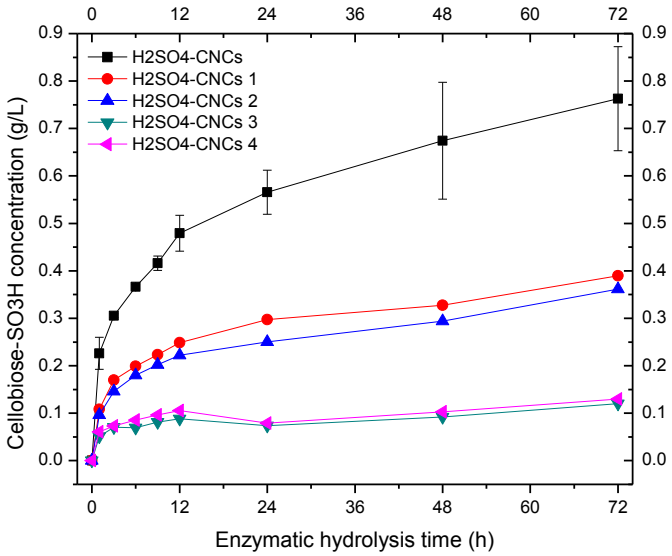

(B)

Figure 6-12. Enzymatic hydrolysis of oxidized H_2SO_4-CNCs by TEMPO/NaClO/NaBr with different oxidation degree.

6.3.7 Functionalization of H_2SO_4-CNCs with TSC

The reducing ends of CNCs were functionalized with thiol groups using reductive amination reaction in the aqueous medium (**Figure 6-13**). Environmentally benign reducing agent, 2-picoline−borane, was used for the reductive amination reaction. The anisotropic thiol modification at the reducing ends was characterized by SEM. It was found the thiolation of CNCs enabled significantly higher adsorption on gold substrate than unmodified CNCs (**Figure 6-14**). The H_2SO_4-CNCs was probably chemisorbed on the gold surface because the physical absorbed CNCs were washed out completely in the control. There was an issue in making CNCs brush on gold surface from the presence of aldehyde groups on the side of cellulose nano-rods. These side groups coupling with TSC cannot be avoided which will result in the chemisorption of CNCs on the gold from the side rather than from the end.

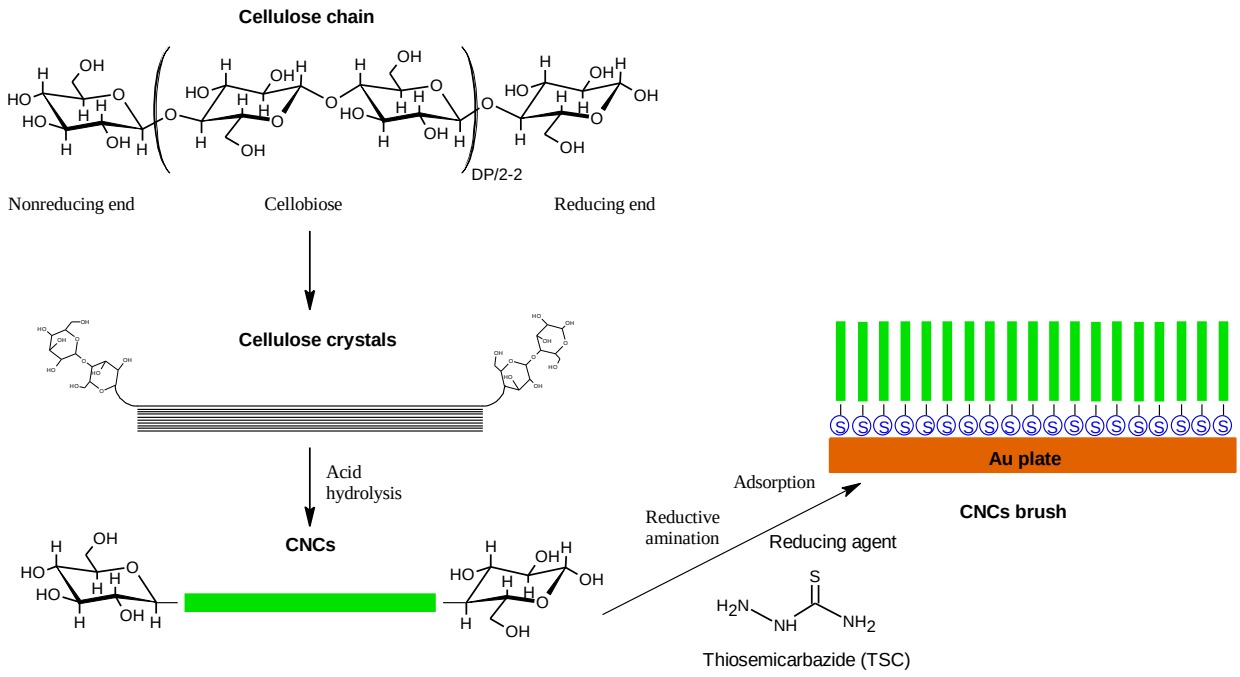

Figure 6-13. Schematic of thiosemicarbazide (TSC) functionalized CNCs-brush on gold nanolayer.

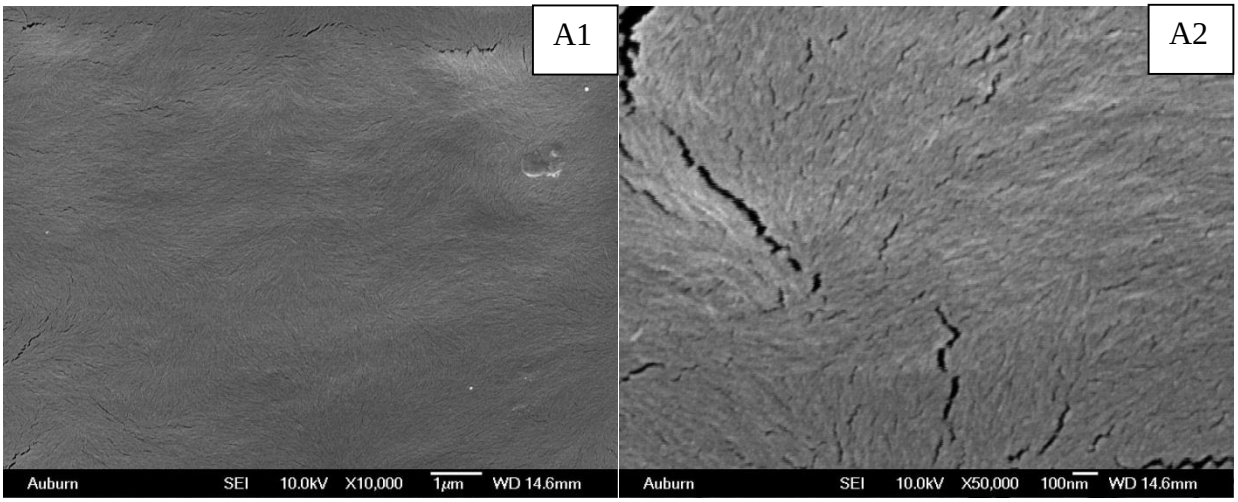

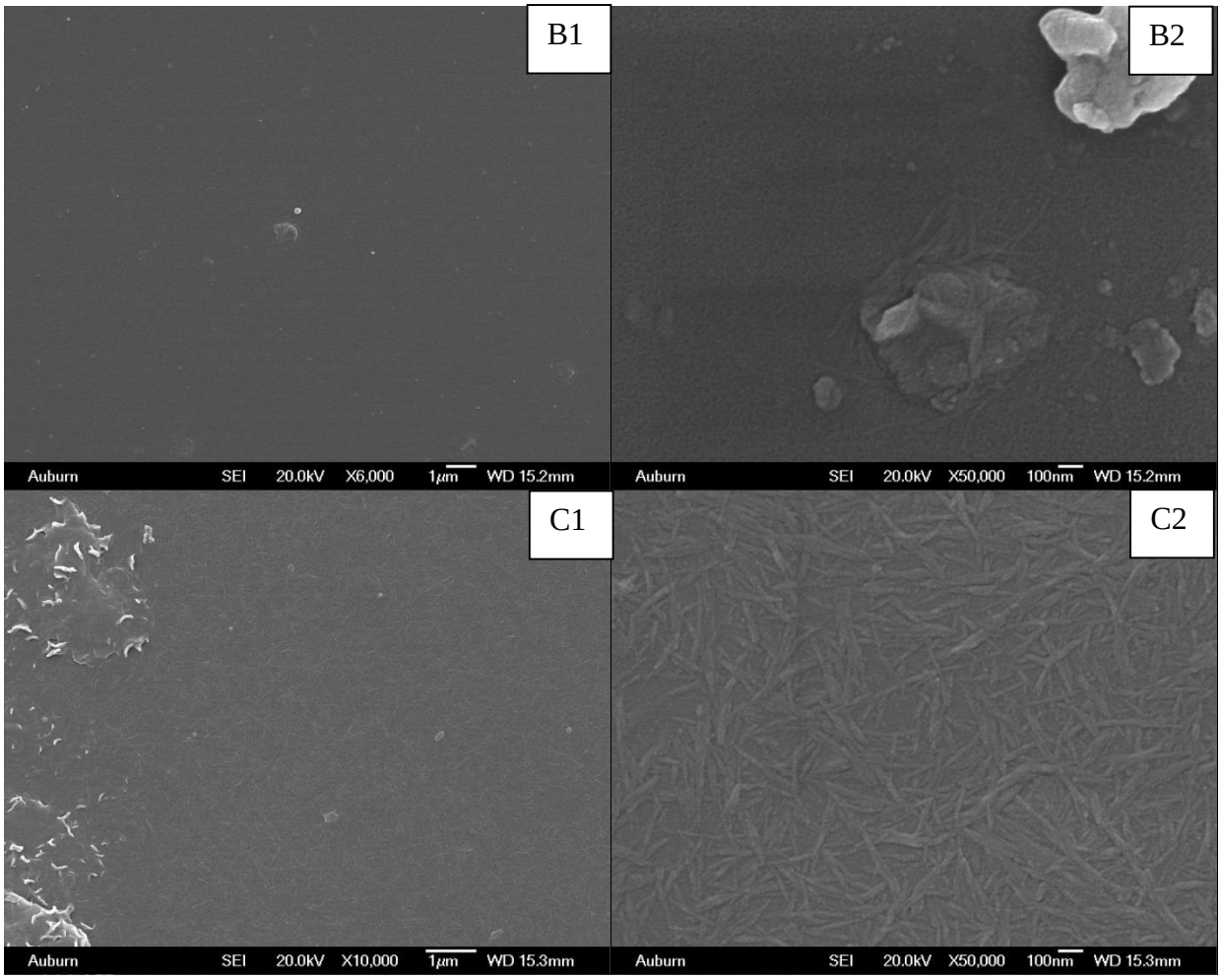

Figure 6-14. SEM images of S-labeled CNCs onto gold substrate (A: direct casted drop without washing; B: control without TSC added; C: CNCs-TSC).

6.4 Conclusion

The HCl-CNCs were chemically modified with acetic anhydride and PIBSA. The covalent bond was confirmed by the FTIR spectrum, which suggested the presence of carbonyl groups in the form of ester on HCl-CNCs. But carbonyl groups on the PIBSA grafted CNCs only presented weak carbonyl absorbance band indicating less modification efficiency. The films made from modified HCl-CNCs either with Ac_2O or PIBSA were more hydrophobic than unmodified HCl-CNCs film due to the increased water contact angle (from 0 to 112 ° and 134 °, respectively). The HCl-CNCs-PIBSA was well dispersed in solvents with medium polarity such

as acetone, chloroform, and ethyl acetate. The hydroxymethyl groups on HCl-CNCs were oxidized by NaClO/NaBr with the mediation of TEMPO. The presence of carboxyl groups added negative charges on the surface of CNCs reduced the enzymatic hydrolyzability. A lab-made fluorescent agent was grafted onto the HCl-CNCs for a potential application as nanocomposite marker. Finally, the TSC was successfully coupled to the reducing end of the H_2SO_4-CNCs confirmed by SEM images. The TSC modified CNCs showed a bright potential for the alignment of nano-rods on gold surface.

Future work

The mechanism of residual lignin and xylan limiting enzymatic hydrolysis has not been fully understood. What is the difference between non-productive binding and physical blocking in enzymatic hydrolysis restricted by residual lignin? Can we quantify the interaction between lignin and enzyme? What is the exact role of residual xylan in enzymatic hydrolysis? Does the xylan inhibit enzymatic hydrolysis or reduce the accessibility of cellulose to enzymes? What are the key functional groups of xylan or lignin affecting enzymatic hydrolysis? These questions should be further investigated and elaborated in order to enhance the hydrolysis efficiency for future biofuels and bioproducts production. How to generate biomass substrates with different xylan content while keeping other parameters constant? It will be important to further confirm the relationship between xylan content and initial hydrolysis rate. Furthermore, how to control the ethyl glucoside or xyloside formation in the organosolv process is important. The formation of ethyl xyloside in SSF process should be addressed as well to improve overall ethanol yield.

In the catalytic conversion of biomass sugars to value-added chemicals, we found different alkaline solution have remarkably influenced the yield of lactic acid. The $Ba(OH)_2$ increased the formation of lactic acid over other frequently used alkali. A step further, the mechanism of the divalent cation catalyzing the reaction toward lactic acid needs to be established. The improvement of pentose conversion to lactic acid by $Ba(OH)_2$ should be further explored. This may set the stage for using prehydrolysate stream, high in pentose, to produce lactic acid.

Finally, CNCs-derived new materials have showed great potential to be developed as engineered materials. To best utilize CNCs, more efficient chemical modification methods are

needed to introduce ionic, hydrophobic, or polymeric molecules onto their surfaces. We have characterized physiochemical properties of CNCs and modified CNCs. We have made progress on the alignment of CNCs by shearing and self-assembly. How to align CNCs effectively is critical and should be studied in the future.

References

Abitbol T, Kloser E, Gray DG. 2013a. Estimation of the surface sulfur content of cellulose nanocrystals prepared by sulfuric acid hydrolysis. Cellulose 20(2):785-794.

Abitbol T, Palermo A, Moran-Mirabal JM, Cranston ED. 2013b. Fluorescent Labeling and Characterization of Cellulose Nanocrystals with Varying Charge Contents. Biomacromolecules 14(9):3278-3284.

Adorjan I, Sjoberg J, Rosenau T, Hofinger A, Kosma P. 2004. Kinetic and chemical studies on the isomerization of monosaccharides in N-methylmorpholine-N-oxide (NMMO) under Lyocell conditions. Carbohydrate Research 339(11):1899-1906.

Agbor VB, Cicek N, Sparling R, Berlin A, Levin DB. 2011. Biomass pretreatment: fundamentals toward application. Biotechnology advances 29(6):675-685.

Alizadeh H, Teymouri F, Gilbert TI, Dale BE. 2005. Pretreatment of switchgrass by ammonia fiber explosion (AFEX). Applied biochemistry and biotechnology 124(1-3):1133-1141.

Allen SG, Kam LC, Zemann AJ, Antal MJ. 1996. Fractionation of sugar cane with hot, compressed, liquid water. Industrial & Engineering Chemistry Research 35(8):2709-2715.

Ameyama M. 1975. Gluconobacter oxydans subsp. sphaericus, new subspecies isolated from grapes. International Journal of Systematic Bacteriology 25(4):365-370.

Araki J, Wada M, Kuga S, Okano T. 1998. Flow properties of microcrystalline cellulose suspension prepared by acid treatment of native cellulose. Colloids and Surfaces A: Physicochemical and Engineering Aspects 142(1):75-82.

Araki J, Wada M, Kuga S, Okano T. 1999. Influence of surface charge on viscosity behavior of cellulose microcrystal suspension. Journal of wood science 45(3):258-261.

Arantes V, Saddler JN. 2011. Cellulose accessibility limits the effectiveness of minimum cellulase loading on the efficient hydrolysis of pretreated lignocellulosic substrates. Biotechnology for Biofuels 4.

Araque E, Parra C, Freer J, Contreras D, Rodr ́guez J, Mendon ̧a R, Baeza J. 2008. Evaluation of organosolv pretreatment for the conversion of< i> Pinus radiata</i> D. Don to ethanol. Enzyme and Microbial Technology 43(2):214-219.

Azzam AM. 1987. Saccharification of bagasse cellulose pretreated with ZnCl< sub> 2</sub> and HCl. Biomass 12(1):71-77.

Bai W, Holbery J, Li K. 2009. A technique for production of nanocrystalline cellulose with a narrow size distribution. Cellulose 16(3):455-465.

Balat M. 2011. Production of bioethanol from lignocellulosic materials via the biochemical pathway: A review. Energy conversion and management 52(2):858-875.

Ballesteros I, Negro MJ, Oliva JM, Cabañas A, Manzanares P, Ballesteros M. Ethanol production from steam-explosion pretreated wheat straw 2006. Springer. p 496-508.

Bamford CH, Bamford D, Collins JR. 1950. Kinetic Studies on Carbohydrates in Alkaline Conditions. 2. The Kinetics of the Rearrangements of Glucose and Fructose in Alkaline Solution. Proceedings of the Royal Society of London Series a-Mathematical and Physical Sciences 204(1076):85-98.

Bamford CH, Collins JR. 1955. Kinetics Studies on Carbohydrates in Alkaline Conditions. 3. Interconversion of Deuterium-glucose, Deuterium-fructose and Deuterium-mannose in Feebly Alkaline Solution. Proceedings of the Royal Society of London Series a-Mathematical and Physical Sciences 228(1172):100-119.

Banerjee S, Sen R, Pandey RA, Chakrabarti T, Satpute D, Giri BS, Mudliar S. 2009. Evaluation of wet air oxidation as a pretreatment strategy for bioethanol production from rice husk and process optimization. biomass and bioenergy 33(12):1680-1686.

Batzing BL, Claus GW. 1971. Biphasic growth of Acetobacter suboxydans on a glycerol-limiting medium. Journal of bacteriology 108(1):592-595.

Batzing BL, Claus GW. 1973. Fine structural changes of Acetobacter suboxydans during growth in a defined medium. Journal of bacteriology 113(3):1455-1461.

Beck-Candanedo S, Roman M, Gray DG. 2005. Effect of reaction conditions on the properties and behavior of wood cellulose nanocrystal suspensions. Biomacromolecules 6(2):1048-1054.

Bergman R, Cai Z, Carll CG, Clausen CA, Dietenberger MA, Falk RH, Frihart CR, Glass SV, Hunt CG, Ibach RE and others. 2010. Wood Handbook: Wood as an Engineering Material. Madison, WI: Forest Products Laboratory. 509 p.

Berlin A, Gilkes N, Kurabi A, Bura R, Tu MB, Kilburn D, Saddler J. 2005. Weak lignin-rinding enzymes - A novel approach to improve activity of cellulases for hydrolysis of lignocellulosics. Applied Biochemistry and Biotechnology 121:163-170.

Berlin A, Maximenko V, Gilkes N, Saddler J. 2007. Optimization of enzyme complexes for lignocellulose hydrolysis. Biotechnology and Bioengineering 97(2):287-296.

Berlioz S, Molina-Boisseau S, Nishiyama Y, Heux L. 2009. Gas-phase surface esterification of cellulose microfibrils and whiskers. Biomacromolecules 10(8):2144-2151.

Bicker M, Endres S, Ott L, Vogel H. 2005. Catalytical conversion of carbohydrates in subcritical water: A new chemical process for lactic acid production. Journal of Molecular Catalysis a-Chemical 239(1-2):151-157.

Bledzki AK, Mamun AA, Lucka-Gabor M, Gutowski VS. 2008. The effects of acetylation on properties of flax fibre and its polypropylene composites. Express Polym Lett 2(6):413-22.

Bondeson D, Mathew A, Oksman K. 2006. Optimization of the isolation of nanocrystals from microcrystalline cellulose by acid hydrolysis. Cellulose 13(2):171-180.

Bondeson D, Oksman K. 2007. Dispersion and characteristics of surfactant modified cellulose whiskers nanocomposites. Composite Interfaces 14(7-9):617-630.

Braun B, Dorgan JR. 2008. Single-step method for the isolation and surface functionalization of cellulosic nanowhiskers. Biomacromolecules 10(2):334-341.

Brink DL. 1993. Method of treating biomass material. Google Patents.

Brink DL. 1994. Method of treating biomass material. Google Patents.

Brodeur G, Yau E, Badal K, Collier J, Ramachandran KB, Ramakrishnan S. 2011. Chemical and physicochemical pretreatment of lignocellulosic biomass: a review. Enzyme research 2011.

Brownell HH, Yu EKC, Saddler JN. 1986. Steam-explosion pretreatment of wood: Effect of chip size, acid, moisture content and pressure drop. Biotechnology and bioengineering 28(6):792-801.

Brunauer S, Emmett PH, Teller E. 1938. Adsorption of gases in multimolecular layers. Journal of the American Chemical Society 60(2):309-319.

Brunner G. 2005. Supercritical fluids: technology and application to food processing. Journal of Food Engineering 67(1):21-33.

Buchert J, Puls J, Poutanen K. 1988. Comparison of Pseudomonas fragi and Gluconobacter oxydans for production of xylonic acid from hemicellulose hydrolyzates. Applied microbiology and biotechnology 28(4-5):367-372.

Buchert J, Viikari L. 1988a. Oxidative D-xylose metabolism of Gluconobacter oxydans. Applied microbiology and biotechnology 29(4):375-379.

Buchert J, Viikari L. 1988b. The role of xylonolactone in xylonic acid production by Pseudomonas fragi. Applied microbiology and biotechnology 27(4):333-336.

Bull T. 1999. Biomass in the energy picture. Science 285(5431):1209-1209.

Camarero Espinosa S, Kuhnt T, Foster EJ, Weder C. 2013. Isolation of thermally stable cellulose nanocrystals by phosphoric acid hydrolysis. Biomacromolecules 14(4):1223-1230.

Carrasco JE, S âz MC, Navarro A, Soriano P, Saez F, Martinez JM. 1994. Effects of dilute acid and steam explosion pretreatments on the cellulose structure and kinetics of cellulosic fraction hydrolysis by dilute acids in lignocellulosic materials. Applied biochemistry and biotechnology 45(1):23-34.

Chen XW, Shekiro J, Franden MA, Wang W, Zhang M, Kuhn E, Johnson DK, Tucker MP. 2012. The impacts of deacetylation prior to dilute acid pretreatment on the bioethanol process. Biotechnology for Biofuels 5.

Cheng Y-S, Zheng Y, Yu CW, Dooley TM, Jenkins BM, VanderGheynst JS. 2010. Evaluation of high solids alkaline pretreatment of rice straw. Applied biochemistry and biotechnology 162(6):1768-1784.

Cho M-J, Park B-D. 2011. Tensile and thermal properties of nanocellulose-reinforced poly (vinyl alcohol) nanocomposites. Journal of Industrial and Engineering Chemistry 17(1):36-40.

Chou Y-CT. 1987. Supercritical ammonia treatment of lignocellulosic materials. Google Patents.

Chum HL, Johnson DK, Black S, Baker J, Grohmann K, Sarkanen KV, Wallace K, Schroeder HA. 1988. Organosolv Pretreatment for Enzymatic-Hydrolysis of Poplars .1. Enzyme Hydrolysis of Cellulosic Residues. Biotechnology and Bioengineering 31(7):643-649.

Chun B-W, Dair B, Macuch PJ, Wiebe D, Porteneuve C, Jeknavorian A. The development of cement and concrete additive 2006. Springer. p 645-658.

Chundawat SPS, Venkatesh B, Dale BE. 2007. Effect of particle size based separation of milled corn stover on AFEX pretreatment and enzymatic digestibility. Biotechnology and bioengineering 96(2):219-231.

Coleman-Kammula S. 1989. Process for the preparation of hydrocarbyl-grafted cellulose fibers. Google Patents.

Dahman Y. 2012. Sustainable Biobutanol and Working towards the Green Gasoline of the Future. Ferment Technol 1:e111.

Datta R, Henry M. 2006. Lactic acid: recent advances in products, processes and technologies - a review. Journal of Chemical Technology and Biotechnology 81(7):1119-1129.

De Bruijn JM. 1986. Monosaccharides in alkaline medium: isomerization, degradation, oligomerization. Netherlands: Delft University of Technology. 163 p.

de Morais Teixeira E, Corrêa AC, Manzoli A, de Lima Leite F, de Oliveira CR, Mattoso LHC. 2010. Cellulose nanofibers from white and naturally colored cotton fibers. Cellulose 17(3):595-606.

De Nooy AEJ, Besemer AC, van Bekkum H. 1995. Highly selective nitroxyl radical-mediated oxidation of primary alcohol groups in water-soluble glucans. Carbohydrate research 269(1):89-98.

de Nooy AEJ, Besemer AC, van Bekkum H. 1996. On the use of stable organic nitroxyl radicals for the oxidation of primary and secondary alcohols. Synthesis 1996(10):1153-1176.

Debruijn JM, Kieboom APG, Vanbekkum H. 1987. Alkaline Degradation of Monosaccharides. 5. Kinetics of the Alkaline Isomerization and Degradation of Monosaccharides. Recueil Des Travaux Chimiques Des Pays-Bas-Journal of the Royal Netherlands Chemical Society 106(2):35-43.

Dien BS, Ximenes EA, O'Bryan PJ, Moniruzzaman M, Li XL, Balan V, Dale B, Cotta MA. 2008. Enzyme characterization for hydrolysis of AFEX and liquid hot-water pretreated distillers' grains and their conversion to ethanol. Bioresource Technology 99(12):5216-5225.

Digman MF, Shinners KJ, Casler MD, Dien BS, Hatfield RD, Jung H-JG, Muck RE, Weimer PJ. 2010. Optimizing on-farm pretreatment of perennial grasses for fuel ethanol production. Bioresource technology 101(14):5305-5314.

Dong XM, Gray DG. 1997. Effect of counterions on ordered phase formation in suspensions of charged rodlike cellulose crystallites. Langmuir 13(8):2404-2409.

Dong XM, Kimura T, Revol J-F, Gray DG. 1996. Effects of ionic strength on the isotropic-chiral nematic phase transition of suspensions of cellulose crystallites. Langmuir 12(8):2076-2082.

Dong XM, Revol J-f, Gray DG. 1998. Effect of microcrystallite preparation conditions on the formation of colloid crystals of cellulose. Cellulose 5(1):19-32.

Donohoe BS, Decker SR, Tucker MP, Himmel ME, Vinzant TB. 2008. Visualizing Lignin Coalescence and Migration Through Maize Cell Walls Following Thermochemical Pretreatment. Biotechnology and Bioengineering 101(5):913-925.

Duff SJB, Murray WD. 1996. Bioconversion of forest products industry waste cellulosics to fuel ethanol: a review. Bioresource Technology 55(1):1-33.

Dufresne A. 2013. Nanocellulose: a new ageless bionanomaterial. Materials Today 16(6):220-227.

Eichhorn SJ. 2011. Cellulose nanowhiskers: promising materials for advanced applications. Soft Matter 7(2):303-315.

Eichhorn SJ, Dufresne A, Aranguren M, Marcovich NE, Capadona JR, Rowan SJ, Weder C, Thielemans W, Roman M, Renneckar S. 2010. Review: current international research into cellulose nanofibres and nanocomposites. Journal of Materials Science 45(1):1-33.

Eklund R, Galbe M, Zacchi G. 1995. The influence of SO< sub> 2</sub> and H< sub> 2</sub> SO< sub> 4</sub> impregnation of willow prior to steam pretreatment. Bioresource technology 52(3):225-229.

Elder T, Houtman C. 2013. Time-domain NMR study of the drying of hemicellulose extracted aspen (Populus tremuloides Michx.). Holzforschung 67(4):405-411.

Eriksson T, Karlsson J, Tjerneld F. 2002. A model explaining declining rate in hydrolysis of lignocellulose substrates with cellobiohydrolase I (Cel7A) and endoglucanase I (Cel7B) of Trichoderma reesei. Applied biochemistry and biotechnology 101(1):41-60.

Ernest B. 1940. Bleaching of textiles. US Patent 2,202,332.

Esposito D, Antonietti M. 2013. Chemical Conversion of Sugars to Lactic Acid by Alkaline Hydrothermal Processes. Chemsuschem 6(6):989-992.

Evans WL. 1942. Some Less Familiar Aspects of Carbohydrate Chemistry. Chemical Reviews 31(3):537-560.

Ezeji T, Qureshi N, Blaschek HP. 2007. Butanol production from agricultural residues: Impact of degradation products on Clostridium beijerinckii growth and butanol fermentation. Biotechnology and Bioengineering 97(6):1460-1469.

Felby C, Thygesen LG, Kristensen JB, Jørgensen H, Elder T. 2008. Cellulose–water interactions during enzymatic hydrolysis as studied by time domain NMR. Cellulose 15(5):703-710.

Felix JM, Gatenholm P. 1991. The nature of adhesion in composites of modified cellulose fibers and polypropylene. Journal of Applied Polymer Science 42(3):609-620.

Fengel D, Wegener G. 1989. Wood : chemistry, ultrastructure, reactions. Berlin ; New York: W. de Gruyter. xiii, 613 p. p.

Frederick WJ, Lien SJ, Courchene CE, DeMartini NA, Ragauskas AJ, Iisa K. 2008. Co-production of ethanol and cellulose fiber from Southern Pine: A technical and economic assessment. Biomass & Bioenergy 32(12):1293-1302.

Freudenberg U, Zschoche S, Simon F, Janke A, Schmidt K, Behrens SH, Auweter H, Werner C. 2005. Covalent immobilization of cellulose layers onto maleic anhydride copolymer thin films. Biomacromolecules 6(3):1628-1634.

Gharpuray MM, Lee YH, Fan LT. 1983. Structural Modification of Lignocellulosics by Pretreatments to Enhance Enzymatic-Hydrolysis. Biotechnology and Bioengineering 25(1):157-172.

Gragson DE, McCarty BM, Richmond GL. 1996. Surfactant/water interactions at the air/water interface probed by vibrational sum frequency generation. The Journal of Physical Chemistry 100(34):14272-14275.

Greer L, Pemberton S, Tan JC. The structure and mechanical behaviour of wood. http://www.doitpoms.ac.uk/tlplib/wood/printall.php.

Grethlein HE. 1985. The Effect of Pore-Size Distribution on the Rate of Enzymatic-Hydrolysis of Cellulosic Substrates. Bio-Technology 3(2):155-160.

Grohmann K, Mitchell DJ, Himmel ME, Dale BE, Schroeder HA. 1989. The Role of Ester Groups in Resistance of Plant-Cell Wall Polysaccharides to Enzymatic-Hydrolysis. Applied Biochemistry and Biotechnology 20-1:45-61.

Grous WR, Converse AO, Grethlein HE. 1986. Effect of steam explosion pretreatment on pore size and enzymatic hydrolysis of poplar. Enzyme and Microbial Technology 8(5):274-280.

Grunert M, Winter WT. 2002. Nanocomposites of cellulose acetate butyrate reinforced with cellulose nanocrystals. Journal of Polymers and the Environment 10(1-2):27-30.

Gunasekaran P, Raj KC. 1999. Ethanol fermentation technology- Zymomonas mobilis. Current Science 77(1):56-68.

Habibi Y. 2014. Key advances in the chemical modification of nanocelluloses. Chemical Society Reviews.

Habibi Y, Chanzy H, Vignon MR. 2006. TEMPO-mediated surface oxidation of cellulose whiskers. Cellulose 13(6):679-687.

Habibi Y, Lucia L, Rojas O. 2010. Cellulose Nanocrystals: Chemistry, Self-Assembly, and Applications. Chemical Reviews 110(6):3479-3500.

Hamelinck CN, Hooijdonk Gv, Faaij APC. 2005. Ethanol from lignocellulosic biomass: techno-economic performance in short-, middle-and long-term. Biomass and bioenergy 28(4):384-410.

Han J, Zhou C, Wu Y, Liu F, Wu Q. 2013. Self-assembling behavior of cellulose nanoparticles during freeze-drying: Effect of suspension concentration, particle size, crystal structure, and surface charge. Biomacromolecules 14(5):1529-1540.

Harrisson S, Drisko GL, Malmström E, Hult A, Wooley KL. 2011. Hybrid rigid/soft and biologic/synthetic materials: polymers grafted onto cellulose microcrystals. Biomacromolecules 12(4):1214-1223.

Hasani M, Cranston ED, Westman G, Gray DG. 2008. Cationic surface functionalization of cellulose nanocrystals. Soft Matter 4(11):2238-2244.

Heux L, Chauve G, Bonini C. 2000. Nonflocculating and chiral-nematic self-ordering of cellulose microcrystals suspensions in nonpolar solvents. Langmuir 16(21):8210-8212.

Himmel M, Ding S, Johnson D, Adney W, Nimlos M, Brady J, Foust T. 2007a. Biomass recalcitrance: Engineering plants and enzymes for biofuels production. Science 315(5813):804-807.

Himmel ME, Ding SY, Johnson DK, Adney WS, Nimlos MR, Brady JW, Foust TD. 2007b. Biomass recalcitrance: Engineering plants and enzymes for biofuels production. Science 315(5813):804-807.

Hoekman SK. 2009. Biofuels in the US - Challenges and Opportunities. Renewable Energy 34(1):14-22.

Holm M, Saravanamurugan S, Taarning E. 2010. Conversion of Sugars to Lactic Acid Derivatives Using Heterogeneous Zeotype Catalysts. Science 328(5978):602-605.

Holt JG, Krieg NR, Sneath PHA, Staley JT, Williams ST. 1994. Bergey's manual of determinative bacteriology. Baltimore: Williams and Wilkins 75:121.

Hong J, Ye XH, Zhang YHP. 2007. Quantitative determination of cellulose accessibility to cellulase based on adsorption of a nonhydrolytic fusion protein containing CBM and GFP with its applications. Langmuir 23(25):12535-12540.

HSU T, LADISCH M, TSAO G. 1980. ALCOHOL FROM CELLULOSE. Chemtech 10(5):315-319.

Huber GW, Chheda JN, Barrett CJ, Dumesic JA. 2005. Production of liquid alkanes by aqueous-phase processing of biomass-derived carbohydrates. Science 308(5727):1446-1450.

Huber GW, Cortright RD, Dumesic JA. 2004. Renewable alkanes by aqueous-phase reforming of biomass-derived oxygenates. Angewandte Chemie-International Edition 43(12):1549-1551.

Hurtubise FG. 1962. The analytical and structural aspects of the infrared spectroscopy of cellulose acetate. Tappi 45(6).

Hörmeyer HF, Schwald W, Bonn G, Bobleter O. 1988. Hydrothermolysis of birch wood as pretreatment for enzymatic saccharification. Holzforschung-International Journal of the Biology, Chemistry, Physics and Technology of Wood 42(2):95-98.

Ibraheem O, Ndimba BK. 2013. Molecular adaptation mechanisms employed by ethanologenic bacteria in response to lignocellulose-derived inhibitory compounds. International journal of biological sciences 9(6):598.

Isbell HS, Frush HL, Wade CWR, Hunter CE. 1969. Transformation of Sugars in Alkaline Solutions. Carbohydrate Research 9(2):163-&.

Ishihara Y, Hirai K, Miyamoto M, Goto G. 1994. Central cholinergic agents. 6. Synthesis and evaluation of 3-[1-(phenylmethyl)-4-piperidinyl]-1-(2, 3, 4, 5-tetrahydro-1H-1-benzazepin-8-yl)-1-propanones and their analogs as central selective acetylcholinesterase inhibitors. Journal of medicinal chemistry 37(15):2292-2299.

Isogai A, Saito T, Fukuzumi H. 2011. TEMPO-oxidized cellulose nanofibers. Nanoscale 3(1):71-85.

Jonoobi M, Harun J, Mathew AP, Hussein MZB, Oksman K. 2010. Preparation of cellulose nanofibers with hydrophobic surface characteristics. Cellulose 17(2):299-307.

Jorgensen H, Kristensen J, Felby C. 2007. Enzymatic conversion of lignocellulose into fermentable sugars: challenges and opportunities. Biofuels Bioproducts & Biorefining-Biofpr 1(2):119-134.

Jung S, Foston M, Sullards MC, Ragauskas AJ. 2010. Surface Characterization of Dilute Acid Pretreated Populus deltoides by ToF-SIMS. Energy & Fuels 24:1347-1357.

Kato Y, Habu N, Yamaguchi J, Kobayashi Y, Shibata I, Isogai A, Samejima M. 2002. Biodegradation of β-1, 4-linked polyglucuronic acid (cellouronic acid). Cellulose 9(1):75-81.

Keshwani DR, Cheng JJ. 2009. Switchgrass for bioethanol and other value-added applications: a review. Bioresource technology 100(4):1515-1523.

Kim D-Y, Nishiyama Y, Kuga S. 2002. Surface acetylation of bacterial cellulose. Cellulose 9(3-4):361-367.

Kim D-Y, Nishiyama Y, Wada M, Kuga S. 2001. High-yield carbonization of cellulose by sulfuric acid impregnation. Cellulose 8(1):29-33.

Kim J, Montero G, Habibi Y, Hinestroza JP, Genzer J, Argyropoulos DS, Rojas OJ. 2009. Dispersion of cellulose crystallites by nonionic surfactants in a hydrophobic polymer matrix. Polymer Engineering & Science 49(10):2054-2061.

Kim KH, Hong J. 2001. Supercritical CO< sub> 2</sub> pretreatment of lignocellulose enhances enzymatic cellulose hydrolysis. Bioresource Technology 77(2):139-144.

Kim TH, Lee YY. 2005. Pretreatment and fractionation of corn stover by ammonia recycle percolation process. Bioresource technology 96(18):2007-2013.

Kim TH, Lee YY, Sunwoo C, Kim JS. 2006. Pretreatment of corn stover by low-liquid ammonia recycle percolation process. Applied Biochemistry and Biotechnology 133(1):41-57.

Klemm D, Heublein B, Fink HP, Bohn A. 2005. Cellulose: fascinating biopolymer and sustainable raw material. Angewandte Chemie International Edition 44(22):3358-3393.

Klemm D, Kramer F, Moritz S, Lindström T, Ankerfors M, Gray D, Dorris A. 2011. Nanocelluloses: A New Family of Nature-Based Materials. Angewandte Chemie International Edition 50(24):5438-5466.

Kocurek MJ. 1984. Pulp and Paper Chemistry and Chemical-Technology, 3rd Edition, Vol 1-4 - Casey,Jp. Chemical Engineering 91(9):103-104.

Kong L, Li G, Wang H, He W, Ling F. 2008. Hydrothermal catalytic conversion of biomass for lactic acid production. Journal of Chemical Technology and Biotechnology 83(3):383-388.

Kooyman C, Vellenga K, Dewilt HGJ. 1977. Isomerization of D-glucose into D-fructose in Aqueous Alkaline Solution. Carbohydrate Research 54(1):33-44.

Kristensen JB, Thygesen LG, Felby C, Jorgensen H, Elder T. 2008. Cell-wall structural changes in wheat straw pretreated for bioethanol production. Biotechnology for Biofuels 1.

Kumakura M, Kojima T, Kaetsu I. 1982. Pretreatment of lignocellulosic wastes by combination of irradiation and mechanical crushing. Biomass 2(4):299-308.

Kumar R, Wyman CE. 2009a. Access of Cellulase to Cellulose and Lignin for Poplar Solids Produced by Leading Pretreatment Technologies. Biotechnology Progress 25(3):807-819.

Kumar R, Wyman CE. 2009b. Cellulase Adsorption and Relationship to Features of Corn Stover Solids Produced by Leading Pretreatments. Biotechnology and Bioengineering 103(2):252-267.

Labbe N, Kline LM, Moens L, Kim K, Kim PC, Hayes DG. 2012. Activation of lignocellulosic biomass by ionic liquid for biorefinery fractionation. Bioresource Technology 104:701-707.

Lau MJ, Lau MW, Gunawan C, Dale BE. 2010. Ammonia Fiber Expansion (AFEX) Pretreatment, Enzymatic Hydrolysis, and Fermentation on Empty Palm Fruit Bunch Fiber (EPFBF) for Cellulosic Ethanol Production. Applied Biochemistry and Biotechnology 162(7):1847-1857.

Laureano-Perez L, Teymouri F, Alizadeh H, Dale BE. 2005. Understanding factors that limit enzymatic hydrolysis of biomass. Applied Biochemistry and Biotechnology 121:1081-1099.

Lee D, Yu AHC, Wong KKY, Saddler JN. 1994. Evaluation of the Enzymatic Susceptibility of Cellulosic Substrates Using Specific Hydrolysis Rates and Enzyme Adsorption. Applied Biochemistry and Biotechnology 45-6:407-415.

Lee JW, Rodrigues RCLB, Kim HJ, Choi IG, Jeffries TW. 2010. The roles of xylan and lignin in oxalic acid pretreated corncob during separate enzymatic hydrolysis and ethanol fermentation. Bioresource Technology 101(12):4379-4385.

Li M, Tu M, Cao D, Bass P, Adhikari S. 2013. Distinct Roles of Residual Xylan and Lignin in Limiting Enzymatic Hydrolysis of Organosolv Pretreated Loblolly Pine and Sweetgum. Journal of agricultural and food chemistry 61(3):646-654.

Linde M, Galbe M, Zacchi G. 2007. Simultaneous saccharification and fermentation of steam-pretreated barley straw at low enzyme loadings and low yeast concentration. Enzyme and microbial technology 40(5):1100-1107.

Liou T-H. 2004. Preparation and characterization of nano-structured silica from rice husk. Materials Science and Engineering: A 364(1):313-323.

Lokanathan AR, Nykänen A, Seitsonen J, Johansson L-S, Campbell J, Rojas OJ, Ikkala O, Laine J. 2013. Cilia-Mimetic hairy surfaces based on end-immobilized nanocellulose colloidal rods. Biomacromolecules 14(8):2807-2813.

Lu P, Hsieh Y-L. 2010. Preparation and properties of cellulose nanocrystals: rods, spheres, and network. Carbohydrate Polymers 82(2):329-336.

Luo W, Schardt J, Bommier C, Wang B, Razink J, Simonsen J, Ji X. 2013. Carbon nanofibers derived from cellulose nanofibers as a long-life anode material for rechargeable sodium-ion batteries. Journal of Materials Chemistry A 1(36):10662-10666.

Lynd L. 1996. Overview and evaluation of fuel ethanol from cellulosic biomass: Technology, economics, the environment, and policy. Annual Review of Energy and the Environment 21:403-465.

López F, Alfaro A, Jiménez L, Rodríguez A. 2006. Alcohols as organic solvents for the obtainment of cellulose pulp. Afinidad 63(523):174-182.

MacLaurin DJ, Green JW. 1969. Carbohydrates in alkaline systems. I. Kinetics of the transformation and degradation of d-glucose, d-fructose, and d-mannose in 1 M sodium hydroxide at 22 ° C. Canadian Journal of Chemistry 47(21):3947-3955.

Marchessault RH, Morehead FF, Koch MJ. 1961. Some hydrodynamic properties of neutral suspensions of cellulose crystallites as related to size and shape. Journal of Colloid Science 16(4):327-344.

Marchessault RH, Morehead FF, Walter NM. 1959. Liquid crystal systems from fibrillar polysaccharides.

Marzialetti T, Valenzuela Olarte MB, Sievers C, Hoskins TJC, Agrawal PK, Jones CW. 2008. Dilute acid hydrolysis of Loblolly pine: A comprehensive approach. Industrial & Engineering Chemistry Research 47(19):7131-7140.

McAndrew RP, Peralta-Yahya PP, DeGiovanni A, Pereira JH, Hadi MZ, Keesling JD, Adams PD. 2011. Structure of a Three-Domain Sesquiterpene Synthase: A Prospective Target for Advanced Biofuels Production. Structure 19(12):1876-1884.

McMillan JD. Pretreatment of lignocellulosic biomass 1994.

Medve J, Stahlberg J, Tjerneld F. 1994. Adsorption and Synergism of Cellobiohydrolase-I and Cellobiohydrolase-Ii of Trichoderma-Reesei during Hydrolysis of Microcrystalline Cellulose. Biotechnology and Bioengineering 44(9):1064-1073.

Milsom PE, Meers JL. 1985. Gluconic and itaconic acids. Comprehensive biotechnology: the principles, applications, and regulations of biotechnology in industry, agriculture, and medicine/editor-in-chief, Murray Moo-Young.

Mishima D, Tateda M, Ike M, Fujita M. 2006. Comparative study on chemical pretreatments to accelerate enzymatic hydrolysis of aquatic macrophyte biomass used in water purification processes. Bioresource technology 97(16):2166-2172.

Missoum K, Belgacem MN, Barnes J-P, Brochier-Salon M-C, Bras J. 2012. Nanofibrillated cellulose surface grafting in ionic liquid. Soft Matter 8(32):8338-8349.

Missoum K, Belgacem MN, Bras J. 2013. Nanofibrillated cellulose surface modification: A review. Materials 6(5):1745-1766.

Monica Ek GG, Gunnar Henriksson. 2009. Wood Chemistry and Wood Biotechnology. In: Monica Ek GG, Gunnar Henriksson, editor. Pulp and Paper Chemistry and Technology. Germany: DE GRUYTER.

Montanari S, Roumani M, Heux L, Vignon MR. 2005. Topochemistry of carboxylated cellulose nanocrystals resulting from TEMPO-mediated oxidation. Macromolecules 38(5):1665-1671.

Montgomery R. 1949. The chemical production of lactic acid from sugars. Sugar Research Foundation, Inc. New York: The Ohio State University. 27 p.

Moon RJ, Martini A, Nairn J, Simonsen J, Youngblood J. 2011. Cellulose nanomaterials review: structure, properties and nanocomposites. Chemical Society Reviews 40(7):3941-3994.

Mosier N, Wyman C, Dale B, Elander R, Lee Y, Holtzapple M, Ladisch M. 2005. Features of promising technologies for pretreatment of lignocellulosic biomass. Bioresource Technology 96(6):673-686.

Mukherjee T, Sani M, Kao N, Gupta RK, Quazi N, Bhattacharya S. 2013. Improved dispersion of cellulose microcrystals in polylactic acid (PLA) based composites applying surface acetylation. Chemical Engineering Science 101:655-662.

Negro MJ, Manzanares P, Ballesteros I, Oliva JM, Cabañas A, Ballesteros M. 2003. Hydrothermal pretreatment conditions to enhance ethanol production from poplar biomass. Biotechnology for Fuels and Chemicals: Springer. p 87-100.

Nieminen S, Heikkinen J, Räty J. 2013. Laser transillumination imaging for determining wood defects and grain angle. Measurement Science and Technology 24(12):125401.

Ohgren K, Bura R, Saddler J, Zacchi G. 2007. Effect of hemicellulose and lignin removal on enzymatic hydrolysis of steam pretreated corn stover. Bioresource Technology 98(13):2503-2510.

Olijve W, Kok JJ. 1979. Analysis of growth of Gluconobacter oxydans in glucose containing media. Archives of Microbiology 121(3):283-290.

Owens DK, Wendt RC. 1969. Estimation of the surface free energy of polymers. Journal of applied polymer science 13(8):1741-1747.

Pan XJ, Arato C, Gilkes N, Gregg D, Mabee W, Pye K, Xiao ZZ, Zhang X, Saddler J. 2005. Biorefining of softwoods using ethanol organosolv pulping: Preliminary evaluation of process streams for manufacture of fuel-grade ethanol and co-products. Biotechnology and Bioengineering 90(4):473-481.

Pan XJ, Gilkes N, Kadla J, Pye K, Saka S, Gregg D, Ehara K, Xie D, Lam D, Saddler J. 2006. Bioconversion of hybrid poplar to ethanol and co-products using an organosolv fractionation process: Optimization of process yields. Biotechnology and Bioengineering 94(5):851-861.

Park J-y, Shiroma R, Al-Haq MI, Zhang Y, Ike M, Arai-Sanoh Y, Ida A, Kondo M, Tokuyasu K. 2010a. A novel lime pretreatment for subsequent bioethanol production from rice straw–calcium capturing by carbonation (CaCCO) process. Bioresource technology 101(17):6805-6811.

Park S, Baker JO, Himmel ME, Parilla PA, Johnson DK. 2010b. Research cellulose crystallinity index: measurement techniques and their impact on interpreting cellulase performance. Biotechnol Biofuels 3(10).

Park S, Johnson DK, Ishizawa CI, Parilla PA, Davis MF. 2009. Measuring the crystallinity index of cellulose by solid state 13C nuclear magnetic resonance. Cellulose 16(4):641-647.

Peralta-Yahya PP, Ouellet M, Chan R, Mukhopadhyay A, Keasling JD, Lee TS. 2011. Identification and microbial production of a terpene-based advanced biofuel. Nature Communications 2.

Pettersen RC. 1984. The chemical composition of wood. The chemistry of solid wood 207:57-126.

Pienkos P, Zhang M. 2009. Role of pretreatment and conditioning processes on toxicity of lignocellulosic biomass hydrolysates. Cellulose 16(4):743-762.

Podsiadlo P, Choi S-Y, Shim B, Lee J, Cuddihy M, Kotov NA. 2005. Molecularly engineered nanocomposites: layer-by-layer assembly of cellulose nanocrystals. Biomacromolecules 6(6):2914-2918.

Purves WK, Orians GH, Heller HCR. 1994. Life: The Science of Biology: Sinauer Associates Inc.

Qing Q, Wyman CE. 2011. Supplementation with xylanase and beta-xylosidase to reduce xylo-oligomer and xylan inhibition of enzymatic hydrolysis of cellulose and pretreated corn stover. Biotechnology for Biofuels 4.

Qing Q, Yang B, Wyman CE. 2010. Impact of surfactants on pretreatment of corn stover. Bioresource Technology 101(15):5941-5951.

Qureshi N, Ezeji TC. 2008. Butanol,'a superior biofuel'production from agricultural residues (renewable biomass): recent progress in technology. Biofuels, Bioproducts and Biorefining 2(4):319-330.

Ragauskas AJ, Williams CK, Davison BH, Britovsek G, Cairney J, Eckert CA, Frederick WJ, Hallett JP, Leak DJ, Liotta CL. 2006. The path forward for biofuels and biomaterials. science 311(5760):484-489.

Ramachandran S, Fontanille P, Pandey A, Larroche C. 2006. Gluconic acid: Properties, applications and microbial production. Food Technology and Biotechnology 44(2):185-195.

Revol JF, Bradford H, Giasson J, Marchessault RH, Gray DG. 1992. Helicoidal self-ordering of cellulose microfibrils in aqueous suspension. International journal of biological macromolecules 14(3):170-172.

Roman M, Winter WT. 2004. Effect of sulfate groups from sulfuric acid hydrolysis on the thermal degradation behavior of bacterial cellulose. Biomacromolecules 5(5):1671-1677.

Rouquerol J, Rouquerol F, Llewellyn P, Maurin G, Sing KSW. 2013. Adsorption by powders and porous solids: principles, methodology and applications: Academic press.

Ruiz R, Ehrman T. 1996. Determination of Carbohydrates in Biomass by High Performance Liquid Chromatography.

Rácz I, Borsa J, Bodor G. 1996. Crystallinity and accessibility of fibrous carboxymethylcellulose by pad-roll technology. Journal of applied polymer science 62(12):2015-2024.

Sadeghifar H, Filpponen I, Clarke SP, Brougham DF, Argyropoulos DS. 2011. Production of cellulose nanocrystals using hydrobromic acid and click reactions on their surface. Journal of materials science 46(22):7344-7355.

Saha BC, Cotta MA. 2006. Ethanol production from alkaline peroxide pretreated enzymatically saccharified wheat straw. Biotechnology Progress 22(2):449-453.

Saha BC, Cotta MA. 2007. Enzymatic saccharification and fermentation of alkaline peroxide pretreated rice hulls to ethanol. Enzyme and Microbial Technology 41(4):528-532.

Sassi J-F, Chanzy H. 1995. Ultrastructural aspects of the acetylation of cellulose. Cellulose 2(2):111-127.

Sawan SP. 1998. Supercritical fluid cleaning: fundamentals, technology and applications: Elsevier.

Selig MJ, Vinzant TB, Himmel ME, Decker SR. 2009. The Effect of Lignin Removal by Alkaline Peroxide Pretreatment on the Susceptibility of Corn Stover to Purified Cellulolytic and Xylanolytic Enzymes. Applied Biochemistry and Biotechnology 155(1-3):397-406.

Senesi N, Miano TM, Provenzano MR, Brunetti G. 1991. Characterization, differentiation, and classification of humic substances by fluorescence spectroscopy. Soil Science 152(4):259-271.

Shaffer PA, Friedemann TE. 1930. Sugar activation by alkali: I. Formation of lactic acid and saccharinic acids. The Journal of Biological Chemistry 86:345-374.

Shafizadeh F. 1976. Thermal uses and properties of carbohydrates and lignins: Elsevier.

Sheehan JS, Himmel ME. 2001. Outlook for bioethanol production from lignocellulosic feedstocks: technology hurtles. Agro Food Industry Hi-Tech 12(5):54-57.

Sievers C, Marzialetti T, Hoskins TJC, Olarte MBV, Agrawal PK, Jones CW. 2009. Quantitative solid state NMR analysis of residues from acid hydrolysis of loblolly pine wood. Bioresource Technology 100(20):4758-4765.

Sluiter A, Hames B, Ruiz R, Scarlata C, Sluiter J, Templeton D, Crocker D. 2011. Determination of strucutral carbonhydrates and lignin in biomass. National Renewable Energy Laboratory.

Speck JC. 1958. The Lobry Debruyn-Alberda Vanekenstein Transformation. Advances in Carbohydrate Chemistry 13:63-103.

Sun F, Chen H. 2008. Organosolv pretreatment by crude glycerol from oleochemicals industry for enzymatic hydrolysis of wheat straw. Bioresource technology 99(13):5474-5479.

Sun R, Lawther JM, Banks WB. 1995. Influence of alkaline pre-treatments on the cell wall components of wheat straw. Industrial crops and products 4(2):127-145.

Sun Y, Cheng J. 2002. Hydrolysis of lignocellulosic materials for ethanol production: a review. Bioresource Technology 83(1):1-11.

Suryawati L, Wilkins MR, Bellmer DD, Huhnke RL, Maness NO, Banat IM. 2009. Effect of hydrothermolysis process conditions on pretreated switchgrass composition and ethanol yield by SSF with< i> Kluyveromyces marxianus</i> IMB4. Process Biochemistry 44(5):540-545.

Sèbe G, Ham-Pichavant F, Pecastaings G. 2013. Dispersibility and emulsion-stabilizing effect of cellulose nanowhiskers esterified by vinyl acetate and vinyl cinnamate. Biomacromolecules 14(8):2937-2944.

Taherzadeh MJ, Karimi K. 2007. ENZYME-BASED HYDROLYSIS PROCESSES FOR ETHANOL FROM LIGNOCELLULOSIC MATERIALS: A REVIEW. Bioresources 2(4):707-738.

Taherzadeh MJ, Karimi K. 2008. Pretreatment of lignocellulosic wastes to improve ethanol and biogas production: a review. International journal of molecular sciences 9(9):1621-1651.

Tahiri C, Vignon MR. 2000. TEMPO-oxidation of cellulose: Synthesis and characterisation of polyglucuronans. Cellulose 7(2):177-188.

Tarvainen M, Sutinen R, Peltonen S, Mikkonen H, Maunus J, Vähä-Heikkilä K, Lehto V-P, Paronen P. 2003. Enhanced film-forming properties for ethyl cellulose and starch acetate using< i> n</i>-alkenyl succinic anhydrides as novel plasticizers. European journal of pharmaceutical sciences 19(5):363-371.

Tengborg C, Galbe M, Zacchi G. 2001. Influence of enzyme loading and physical parameters on the enzymatic hydrolysis of steam-pretreated softwood. Biotechnology Progress 17(1):110-117.

Teymouri F, Laureano-Perez L, Alizadeh H, Dale BE. 2005. Optimization of the ammonia fiber explosion (AFEX) treatment parameters for enzymatic hydrolysis of corn stover. Bioresour Technol 96(18):2014-8.

Thring RW, Chornet E, Overend RP. 1990. Recovery of a solvolytic lignin: effects of spent liquor/acid volume ratio, acid concentration and temperature. Biomass 23(4):289-305.

Torstensen HH. 1939. A study of the action of benzyl trimethyl ammonium hydroxide, guanidium hydroxide, and trimethyl sulfonium hydroxide on d-glucose, d-mannose, d-fructose, and maltose: Ohio state university.

Tu MB, Chandra RP, Saddler JN. 2007a. Evaluating the distribution of cellulases and the recycling of free cellulases during the hydrolysis of lignocellulosic substrates. Biotechnology Progress 23(2):398-406.

Tu MB, Chandra RP, Saddler JN. 2007b. Recycling cellulases during the hydrolysis of steam exploded and ethanol pretreated lodgepole pine. Biotechnology Progress 23(5):1130-1137.

Tu MB, Zhang X, Paice M, McFarlane P, Saddler JN. 2009. Effect of Surfactants on Separate Hydrolysis Fermentation and Simultaneous Saccharification Fermentation of Pretreated Lodgepole Pine. Biotechnology Progress 25(4):1122-1129.

Ureña-Benavides EE, Ao G, Davis VA, Kitchens CL. 2011. Rheology and phase behavior of lyotropic cellulose nanocrystal suspensions. Macromolecules 44(22):8990-8998.

Vaccarino C, Lo Curto RB, Tripodo MM, Bellocco E, Laganà G, Patanè R. 1987. Effect of SO< sub> 2</sub>, NaOH and Na< sub> 2</sub> CO< sub> 3</sub> pretreatments on the degradability and cellulase digestibility of grape marc. Biological Wastes 20(2):79-88.

van Maris AJ, Abbott DA, Bellissimi E, van den Brink J, Kuyper M, Luttik MA, Wisselink HW, Scheffers WA, van Dijken JP, Pronk JT. 2006. Alcoholic fermentation of carbon sources in biomass hydrolysates by Saccharomyces cerevisiae: current status. Antonie Van Leeuwenhoek 90(4):391-418.

Väljamäe P, Kipper K, Pettersson G, Johansson G. 2003. Synergistic cellulose hydrolysis can be described in terms of fractal-like kinetics. Biotechnology and bioengineering 84(2):254-257.

Wada M, Heux L, Sugiyama J. 2004. Polymorphism of cellulose I family: reinvestigation of cellulose IVI. Biomacromolecules 5(4):1385-1391.

Walker L, Wilson D. 1991. Enzymatic hydrolysis of cellulose: an overview. Bioresource Technology 36(1):3-14.

Wang F, Wang Y, Ji M. 2005. Mechanisms and kinetics models for ultrasonic waste activated sludge disintegration. Journal of Hazardous Materials 123(1):145-150.

Wang H, Wang J, Fang Z, Wang X, Bu H. 2010. Enhanced bio-hydrogen production by anaerobic fermentation of apple pomace with enzyme hydrolysis. International Journal of Hydrogen Energy 35(15):8303-8309.

Wang N, Ding E, Cheng R. 2008. Preparation and liquid crystalline properties of spherical cellulose nanocrystals. Langmuir 24(1):5-8.

Wei L, Shrestha A, Tu M, Adhikari S. 2011. Effects of surfactant on biochemical and hydrothermal conversion of softwood hemicellulose to ethanol and furan derivatives. Process Biochemistry 46(9):1785-1792.

Weil J, Sarikaya A, Rau S-L, Goetz J, Ladisch CM, Brewer M, Hendrickson R, Ladisch MR. 1997. Pretreatment of yellow poplar sawdust by pressure cooking in water. Applied Biochemistry and Biotechnology 68(1-2):21-40.

Wyman C. 1996. Handbook on bioethanol: production and utilization: CRC press.

Wyman CE, Balan V, Dale BE, Elander RT, Falls M, Hames B, Holtzapple MT, Ladisch MR, Lee YY, Mosier N and others. 2011. Comparative data on effects of leading pretreatments and enzyme loadings and formulations on sugar yields from different switchgrass sources. Bioresource Technology 102(24):11052-11062.

Wyman CE, Dale BE, Elander RT, Holtzapple M, Ladisch MR, Lee Y. 2005. Comparative sugar recovery data from laboratory scale application of leading pretreatment technologies to corn stover. Bioresource technology 96(18):2026-2032.

Wyman CE, Dale BE, Elander RT, Holtzapple M, Ladisch MR, Lee YY, Mitchinson C, Saddler JN. 2009. Comparative sugar recovery and fermentation data following pretreatment of poplar wood by leading technologies. Biotechnology Progress 25(2):333-339.

Wågberg L, Decher G, Norgren M, Lindström T, Ankerfors M, Axnäs K. 2008. The build-up of polyelectrolyte multilayers of microfibrillated cellulose and cationic polyelectrolytes. Langmuir 24(3):784-795.

Xiao W, Clarkson WW. 1997. Acid solubilization of lignin and bioconversion of treated newsprint to methane. Biodegradation 8(1):61-66.

Xie R. 2014. Carbonyl inhibition and detoxification in microbial fermentation of biomass hydrolysates.

Xu J, Thomsen MH, Thomsen AB. 2009. Pretreatment on corn stover with low concentration of formic acid. Journal of microbiology and biotechnology 19(8):845-850.

Yan X, Jin F, Tohji K, Kishita A, Enomoto H. 2010. Hydrothermal Conversion of Carbohydrate Biomass to Lactic Acid. Aiche Journal 56(10):2727-2733.

Yan X, Jin F, Tohji K, Moriya T, Enomoto H. 2007. Production of lactic acid from glucose by alkaline hydrothermal reaction. Journal of Materials Science 42(24):9995-9999.

Yang B, Montgomery R. 1996a. Alkaline degradation of glucose: Effect of initial concentration of reactants. Carbohydrate Research 280(1):27-45.

Yang B, Wyman CE. 2004. Effect of xylan and lignin removal by batch and flowthrough pretreatment on the enzymatic digestibility of corn stover cellulose. Biotechnology and Bioengineering 86(1):88-95.

Yang BY, Montgomery R. 1996b. Alkaline degradation of fructofuranosides. Carbohydrate research 280(1):47-57.

Yokota S, Kitaoka T, Opietnik M, Rosenau T, Wariishi H. 2008. Synthesis of gold nanoparticles for in situ conjugation with structural carbohydrates. Angewandte Chemie International Edition 47(51):9866-9869.

Yu MR, Zhang YL, Tang IC, Yang ST. 2011. Metabolic engineering of Clostridium tyrobutyricum for n-butanol production. Metabolic Engineering 13(4):373-382.

Yuan H, Nishiyama Y, Wada M, Kuga S. 2006. Surface acylation of cellulose whiskers by drying aqueous emulsion. Biomacromolecules 7(3):696-700.

Zhang D. 2014. 2D NMR Characterization of Cellobiose Sulfate Hydrolyzed from Cellulose Nanocrystals.

Zhang J, Heiss C, Thorne PG, Bal C, Azadi P, Lynd LR. 2009. Formation of ethyl beta-xylopyranoside during simultaneous saccharification and co-fermentation of paper sludge. Enzyme and Microbial Technology 44(4):196-202.

Zhang JH, Siika-aho M, Tenkanen M, Viikari L. 2011. The role of acetyl xylan esterase in the solubilization of xylan and enzymatic hydrolysis of wheat straw and giant reed. Biotechnology for Biofuels 4.

Zhang YHP, Ding SY, Mielenz JR, Cui JB, Elander RT, Laser M, Himmel ME, McMillan JR, Lynd LR. 2007. Fractionating recalcitrant lignocellulose at modest reaction conditions. Biotechnology and Bioengineering 97(2):214-223.

Zhang YHP, Lynd LR. 2004. Toward an aggregated understanding of enzymatic hydrolysis of cellulose: Noncomplexed cellulase systems. Biotechnology and Bioengineering 88(7):797-824.

Zhao X, Cheng K, Liu D. 2009. Organosolv pretreatment of lignocellulosic biomass for enzymatic hydrolysis. Applied Microbiology and Biotechnology 82(5):815-827.

Zhu J, Pan X. 2010a. Woody biomass pretreatment for cellulosic ethanol production: technology and energy consumption evaluation. Bioresource technology 101(13):4992-5002.

Zhu JY, Pan XJ. 2010b. Woody biomass pretreatment for cellulosic ethanol production: Technology and energy consumption evaluation. Bioresource Technology 101(13):4992-5002.

Zhu L, O'Dwyer JP, Chang VS, Granda CB, Holtzapple MT. 2008. Structural features affecting biomass enzymatic digestibility. Bioresource Technology 99(9):3817-3828.

Zhu L, O'Dwyer JP, Chang VS, Granda CB, Holtzapple MT. 2010. Multiple linear regression model for predicting biomass digestibility from structural features. Bioresource Technology 101(13):4971-4979.

Zhu S, Wu Y, Chen Q, Yu Z, Wang C, Jin S, Ding Y, Wu G. 2006. Dissolution of cellulose with ionic liquids and its application: a mini-review. Green Chem. 8(4):325-327.